

INPE-5238-TAE/002

**PARAMETRIC MOTION TRASDUCER
FOR GRAVITATIONAL WAVE DETECTORS**

Odylio Denys de Aguiar

**INPE
São José dos Campos
Abril de 1991**

**SECRETARIA DA CIÊNCIA E TECNOLOGIA
INSTITUTO NACIONAL DE PESQUISAS ESPACIAIS**

INPE-5238-TAE/002

**PARAMETRIC MOTION TRANSDUCER
FOR GRAVITATIONAL WAVE DETECTORS**

Odylio Denys de Aguiar

Tese de Doutorado em Ciência Espacial/
orientada pelo Professor Warren Johnson,
Faculty of the Louisiana State University and
Agricultural and Mechanical College,
aprovada em dezembro de 1990.

**INPE
São José dos Campos
Abril de 1991**

CDU 530.145.6

Key Words: Gravitational waves; Transducers;
Gravitational waves: Superconductivity;
Parametric transducer

**PARAMETRIC MOTION TRANSDUCER
FOR GRAVITATIONAL WAVE DETECTORS**

A Dissertation

Submitted to the Graduate Faculty of the
Louisiana State University and
Agricultural and Mechanical College
in partial fulfillment of the
requirements for the degree of
Doctor of Philosophy

in

The Department of Physics and Astronomy

by

Odylio Denys de Aguiar

B.S., Instituto Tecnológico de Aeronáutica, S. J. dos Campos, SP, Brazil, 1978
M.S., Instituto Nacional de Pesquisas Espaciais, S. J. dos Campos, SP, Brazil, 1983
December 1990

DEDICATION

To the memory of my father and sister,
Gabriel and Gilda Gabriela

ACKNOWLEDGEMENTS

I would like to thank my thesis advisor, Professor Warren Johnson for having introduced me to the exciting business of parametric transducers, for showing me how to do a careful and detailed analyses of a problem, for all his technical assistance, and for his encouragement.

My thanks also goes to Professor Bill Hamilton who taught me the first steps on the road of Gravitational Wave Astronomy research. I gained plenty experimental expertise from him, from how a vacuum diffusion pump works to what is the best way to calibrate a transducer.

I also thank all the other members of the LSU Experimental Gravitation Group, including the undergraduate student workers, for their friendly collaboration in the various phases of this experiment. Norbert Solomonson, Brad Price, Bu-Xin Xu, Tony Mann, Kenny Geng, Zhu Ning, Stephen Merkwowitz, Chris Jensen, John Harper, Les Richoux, Freddie Landry, and Allen Sibley made room 65 look like home during my stay in Baton Rouge. Norb and Brad, especially, shared with me their experimental and computer expertise, and without Norbert's built "cooking machine" I would have had a hard time to anneal my niobium transducer.

Thanks to Phil Nurse, Ivan Shuff, Leo Jordan, and Allen Young I had all the cryogenic and additional machining support necessary to accomplish this work. They all contributed with their wise experience, skillfulness, and a sense of perfection.

I thank Randy Gould, Marcus Sen, and Brad Ellison for keeping my electronics alive and able to do "state of the art" measurements, and for all their "quick and clean" electronics support.

I thank Dee Hart for her always prompt assistance in all purchasing needed for my work. I also thank Dee Hart, Karla Tuley, and Linda Frazier for their secretarial support. They, together with my close friends, helped to keep my spirits up.

I would like to thank all other members of the faculty, staff, graduate student and undergraduate body that helped to enrich my doctoral education at LSU.

My thanks also goes to Mark Bocko, with whom I had interesting discussions about this work.

I also acknowledge the support of the National Science Foundation, Louisiana State University, the Brazilian Institute for Space Research and CNPq, the Brazilian NSF.

Finally, I would like to thank my wife Dorothy, my daughter Fernanda, and my mother Gilda for their patience and understanding, enduring difficulties during all these years with very great courage, in order to make it possible for me to obtain a Ph.D. in experimental gravitation. They, together with my brother Alberto and my other family members, made me feel that all this effort was meaningful and worthwhile.

ABSTRACT

We designed, constructed, and tested (using two different low phase noise electrical pump generators) a cryogenic double-resonant parabridge motion transducer made out of niobium, whose electrical output was amplified by a two stage MESFET cryogenic amplifier. Most of the experimental results agreed well with the theoretical models, and we successfully measured the mechanical Brownian motion of this transducer.

We were able to adjust the two electrical bridge resonant frequencies on top of each other at the pump frequency, allowing us to obtain an electromechanical coupling as high as 0.054. This high coupling, corresponding to an rms electric field strength of 1.79×10^5 V/m across the capacitor plates, is the highest measured so far for this class of transducers.

In one case, we observed a dip in the electrical noise spectrum near the mechanical resonant frequency due to destructive interference between this noise and its "reflection" from the mechanical resonator. At the bottom of this dip, we measured, for this transducer, an equivalent displacement noise of 4×10^{-16} m/ $\sqrt{\text{Hz}}$ with a systematic error of less than 10%.

This measured equivalent displacement noise allows this parametric transducer to detect accelerations of 1.4×10^{-8} m / s² at 929 Hz in a one Hz bandwidth. If coupled to the LSU gravitational wave antenna, a 2.3×10^3 kg aluminum

bar, this transducer resonator of 0.27 kg would detect gravitational wave strains (h) as small as 6×10^{-18} .

A large improvement can be achieved if we manage to obtain 50 V_{peak} across the transducer's capacitor plates with a 5 MHz crystal oscillator. In this case, we would reach an equivalent displacement noise of $2 \times 10^{-17} \text{ m} / \sqrt{\text{Hz}}$, corresponding to $h \sim 3 \times 10^{-19}$. Further improvement could be obtained by the use of a DC SQUID preamplifier.

TABLE OF CONTENTS

| | |
|--|------|
| DEDICATION..... | ii |
| ACKNOWLEDGEMENTS..... | iii |
| LIST OF TABLES | vii |
| LIST OF FIGURES | viii |
| ABSTRACT..... | x |
| CHAPTER 1 - THE DAWN OF GRAVITATIONAL WAVE ASTRONOMY..... | 1 |
| A) Gravitational Waves..... | 1 |
| B) Resonant-Mass Gravitational Wave Detectors..... | 7 |
| C) The LSU Resonant-Mass Bar Detector..... | 9 |
| D) Optimization of Resonant-Mass GW Detectors..... | 11 |
| E) Scientific Outcome of Gravitational Wave Astronomy..... | 14 |
| F) References..... | 16 |
| CHAPTER 2 - THE TRANSDUCER'S THEORETICAL EQUATIONS | 19 |
| A) Introduction..... | 19 |
| B) Circuit Analysis..... | 22 |
| C) Equations of Motion and Parametric Effect..... | 24 |
| D) Calibration..... | 28 |
| a) Electrical Output Signal | 28 |
| b) Generation of the Mechanical Input Signal..... | 29 |
| E) Noise Analysis | 33 |
| a) Mechanical Noise..... | 33 |
| b) Electrical Noise..... | 34 |
| F) References..... | 37 |

| | |
|--|----|
| CHAPTER 3 - DESIGN AND CONSTRUCTION OF A NIOBIUM CAPACITOR RF BRIDGE PARAMETRIC TRANSDUCER..... | 41 |
| A) Design..... | 41 |
| B) Construction..... | 48 |
| C) Test Cryostat..... | 55 |
| D) References..... | 59 |
| CHAPTER 4 - PERFORMANCE OF THE TRANSDUCER..... | 60 |
| A) Runs..... | 60 |
| B) Experimental Results..... | 65 |
| a) Parabridge Tuning and Balancing..... | 65 |
| b) Verification of the Parametric Feedback..... | 69 |
| c) Sensitivity and Noise..... | 76 |
| C) References..... | 84 |
| CHAPTER 5 - CONCLUSIONS..... | 86 |
| APPENDIX A..... | 92 |
| APPENDIX B..... | 97 |
| VITA..... | 98 |

LIST OF TABLES

| Table | Page |
|--|------|
| 3.1 Composition of niobium parts..... | 54 |
| 4.1 Transducer-amplifier total gain..... | 78 |
| 5.1 Fundamental parameters of the parabridge transducer..... | 86 |

LIST OF FIGURES

| Figure | Page |
|---|------|
| 1.1 Deformation of a square due to forces induced by pure h_+ or h_x waves..... | 6 |
| 1.2 The LSU Cryogenic Antenna..... | 10 |
| 2.1 Transducer-bridge electromechanical circuit..... | 21 |
| 2.2 Transducer Calibration..... | 30 |
| 3.1 Three-plate capacitor and shielding box..... | 43 |
| 3.2 Bridge shielding box..... | 45 |
| 3.3 Cryogenic amplifier..... | 47 |
| 3.4 Setup inside the cryostat's experimental space..... | 49 |
| 3.5 Hardware arrangement..... | 56 |
| 3.6 Vibration isolation performance (theoretical)..... | 58 |
| 4.1 Parabridge Resonances..... | 66 |
| 4.2 Balancing point inside the inner loop resonance..... | 68 |
| 4.3 Parabridge damping and anti-damping..... | 70 |
| 4.4 Parabridge damping and anti-damping as a function of the pump voltage and Q_{lr} | 72 |
| 4.5 Inverse mechanical decay time using high coupling..... | 74 |
| 4.6 Inverse mechanical decay time as a function of the pump frequency about 5 MHz..... | 75 |
| 4.7 Equivalent displacement noise of the transducer using the 5 MHz crystal oscillator..... | 81 |
| 4.8 Equivalent displacement noise of the transducer using a VDS-15 generator..... | 83 |

| | | |
|----|--|----|
| A1 | Quality factors for the 3502 Hz and 14716 Hz modes..... | 94 |
| A2 | Quality factors for the 1507 Hz, 1521 Hz, and 9995 Hz modes..... | 94 |
| A3 | Variation of the quality factor around the transition temperature for the 3502 Hz mode..... | 95 |

CHAPTER 1 - THE DAWN OF GRAVITATIONAL WAVE ASTRONOMY

A) Gravitational Waves

Shortly after the experimental confirmation of the existence of electromagnetic waves by H. Hertz in 1887, guesses were also made about the possible existence of gravitational waves (gw). Heaviside in 1893, Lorentz in 1900, and Poincaré in 1905 are examples of such scientists making suggestions.¹ However, a mathematical derivation of gravitational waves was only possible after the General Relativity theory had been formulated. Einstein himself derived them as a radiative solution of the vacuum equations of general relativity in 1916, and in a more detailed work two years later.² A modified version of this derivation can be found elsewhere^{3,4} and it is summarized below.

The Einstein field equations are (neglecting the cosmological constant):

$$R_{\mu\nu} - \frac{1}{2} g_{\mu\nu} R = 8 \pi \frac{G}{c^4} T_{\mu\nu} \quad (1.1)$$

where $c=2.99792458 \times 10^8$ m sec⁻¹, and $G=6.67259(85) \times 10^{-11}$ m³ kg⁻¹ sec⁻¹.

The left-hand side of these equations involves second order partial differential operations for the calculation of the components of the metric tensor. Because these equations are non-linear, the computation in GR theory is sometimes very complicated. This non-linearity of gravity also implies that the principle of superposition is no longer valid. Nevertheless, if the masses in the vicinity of a region of interest are much smaller than their radius multiplied by c^2 / G , the gravitational

field is weak and many linearizations can be assumed. The spacetime curvature is nearly flat and the metric can be written as

$$g_{\mu\nu} = \eta_{\mu\nu} + h_{\mu\nu} \quad (1.2)$$

where $\eta_{\mu\nu}$ is the Minkowski metric tensor and $h_{\mu\nu} \ll 1$. This simplifies the calculation of the Riemann tensor, which now can be expressed as:

$$R_{\alpha\beta\mu\nu} = \frac{1}{2} (h_{\alpha\nu, \beta\mu} + h_{\beta\mu, \nu\alpha} - h_{\beta\nu, \alpha\mu} - h_{\alpha\mu, \beta\nu}) \quad (1.3)$$

where $h_{\alpha\beta, \mu\nu} = \frac{\partial h_{\alpha\beta}}{\partial x_\mu \partial x_\nu}$ if terms of order h^2 are ignored. The Ricci and scalar tensors

can now be computed and substituted into the field equations.

Because the field equations contain the $g_{\mu\nu} / 2$ term, we simplify them if we

define

$$\bar{h}_{\mu\nu} \equiv h_{\mu\nu} - \frac{1}{2} \eta_{\mu\nu} h \quad (1.4)$$

where $h \equiv h_\alpha{}^\alpha \equiv \eta^{\alpha\beta} h_{\alpha\beta}$.

In addition to that, to obtain an even more compact form for the field equations, we choose a convenient gauge (the "Lorentz gauge") in which:

$$\bar{h}^{\mu\alpha}{}_{, \alpha} = 0 \quad (1.5)$$

The field equations then assume the form

$$\square^2 \bar{h}_{\mu\nu} \equiv \left(-\frac{1}{c^2} \frac{\partial^2}{\partial t^2} + \nabla^2 \right) \bar{h}_{\mu\nu} \equiv \bar{h}_{\mu\nu, \alpha\beta} \eta^{\alpha\beta} = -16 \pi \frac{G}{c^4} T_{\mu\nu} \quad (1.6)$$

In vacuum $T_{\mu\nu} = 0$, and we have a tensor wave equation with solutions of the form

$$\bar{h}_{\mu\nu} = A_{\mu\nu} e^{[ik(z-ct)]}, \quad (1.7)$$

which represents a monochromatic wave of spacetime geometry⁵ propagating along the +z direction with speed c and frequency kc. These waves, ripples in the curvature of spacetime, are so called gravitational waves.

In comparison to the electromagnetic waves, which are generated by the acceleration of charges, gravitational waves are produced by acceleration of masses. But there are some major differences between the two kinds of waves. The conservation of momentum in a system, plus the fact that mass comes with only one sign, positive, prevents an oscillating (or accelerating) mass dipole from radiating gravitational waves.⁶ Only accelerated mass quadrupole or higher multipole moments can produce gravitational waves. In other words, the source of gravitational waves must contain more components than a dipole (vector) to stimulate them; it must be as complicated as two vectors.⁷ Unlike electromagnetic waves, which can be generated by a single accelerating charge, gravitational waves need at least two masses accelerating in opposite directions. Another difference is that the gravitational force in nature is about 36 orders of magnitude weaker than the electromagnetic force

$$\left(\frac{G m_p^2}{\left(\frac{1}{4 \pi \epsilon_0} \right) e^2} \approx 10^{-36}, \text{ where } m_p \text{ is the proton mass and } e \text{ its charge} \right).$$

This fact added to the impossibility of emission of dipole gravitational radiation, makes the generation of gravitational waves in nature only potentially significant for dynamically evolving systems where $GM / c^2 R \sim 1$.⁷ Therefore, only compact stars, the center of galaxies, the Big Bang event and some bizarre bodies would be able to eventually produce gravitational waves in large intensities.

This weak coupling between mass and gravitational waves is reciprocal. Gravitational waves, as it would be expected, also couple very weakly with matter. This is good in one sense: gravitational waves can bring information from the dense cores of some astrophysical objects without being significantly attenuated by crossing the outside layers of matter, something electromagnetic waves are unable to do. But it is bad in another sense: this weak coupling of gw with matter makes it extremely

difficult for the experimentalist to detect them. Actually, since its mathematical prediction in 1916, no single gravitational radiation pulse has ever been detected directly. The only experimental confirmation of the existence of such radiation comes from the observed decrease in the orbital period of two compact objects (1.44 and 1.38 solar masses, respectively⁸) separated by one solar radius and some 5 kpc away from Earth at the binary pulsar PSR 1913+16 system discovered by Hulse and Taylor⁹ in 1974. After ruling out other mechanisms possible to explain the observed change of orbital period, gravitational radiation damping is left as the only probable cause. The GR theory prediction for this orbital period decrease due to the loss of energy by gravitational waves agrees within one standard deviation from the observed value of 76 ± 2 millionths of a second per year¹⁰.

In order to understand the interaction with matter of a locally plane gravitational wave in this linearized theory, we change the gauge, once more, to one that is transverse and traceless. In this gauge only spatial components of $h_{\mu\nu}$ are nonzero ($h_{\mu 0} = 0$), and they are transverse to the direction of propagation. Furthermore, these components are divergence-free ($h_{kj,j} = 0$) and trace-free ($h_{kk} = 0$). And since $h \equiv h_{\alpha}^{\alpha} = h_{kk} = 0$, we can conclude that

$$\bar{h}_{\mu\nu} = h_{\mu\nu} = h_{\mu\nu}^{\text{TT}} \quad (1.8)$$

This gauge is called a TT or transverse-traceless gauge.³ Here, the Riemann curvature tensor assumes the simple form

$$R_{j0k0} = -\frac{1}{2} h_{jk,00}^{\text{TT}} \quad (1.9)$$

and in particular¹¹

$$R_{x0x0} = -R_{y0y0} = -\frac{1}{2} \ddot{h}_+ \left(t - \frac{z}{c} \right) \quad \text{and} \quad R_{x0y0} = R_{y0x0} = -\frac{1}{2} \ddot{h}_\times \left(t - \frac{z}{c} \right) \quad (1.10)$$

where¹²

$$h_+ \equiv h_{xx}^{\text{TT}} = -h_{yy}^{\text{TT}} = \mathbf{R} \left\{ A_+ e^{-i[\omega(t-z/c) + \phi_+]} \right\} \quad (1.11)$$

and

$$h_x \equiv h_{xy}^{TT} = h_{yx}^{TT} = R \left\{ A_x e^{-i[\omega(t-z/c) + \phi_x]} \right\} \quad (1.12)$$

and A_+ together with A_x are the amplitudes of the two independent modes of polarization (+ and x). Then, the gravitational wave driving force acting on each element of mass m_i of a material body can be derived as

$$F_j = \frac{1}{2} m_i \ddot{h}_{jk}^{TT} k, \quad \text{where } j, k = x \text{ or } y, \quad (1.13)$$

and the total force ($= F_x e_x + F_y e_y$) becomes

$$\vec{F} = \frac{1}{2} m_i \left\{ \left(\ddot{h}_+ x + \ddot{h}_x y \right) e_x + \left(\ddot{h}_x x - \ddot{h}_+ y \right) e_y \right\} \quad (1.14)$$

From equations 1.11 and 1.12: if $\phi_+ = \phi_x$, the resultant force is linearly polarized; if $\phi_+ = \phi_x \pm 90^\circ$ and the magnitudes A_+ and A_x are equal, the resultant force is circularly polarized; otherwise it is elliptically polarized.

Forces induced by gravitational waves are strictly transverse, as in Fig. 1.1, which shows the effect of pure h_+ or h_x plane gravitational waves arriving perpendicular to the plane of a square array of test particles (the amplitudes are exaggerated). It is apparent that gw not only change distances, but also angles. The orthogonality between h_+ or h_x can be appreciated if we imagine deformations for very small amplitudes; a material segment forming an angle $\phi = 0^\circ, 90^\circ, 180^\circ,$ and 270° with the x axis will change length due to h_+ and rotate due to h_x and vice versa if $\phi = 45^\circ, 135^\circ, 225^\circ,$ and 315° . It is the Principle of Equivalence that causes the acceleration, as well as the force, to be locally undetectable ($\xi_k = 0$). Only the relative acceleration or the "relative force" can be observed.

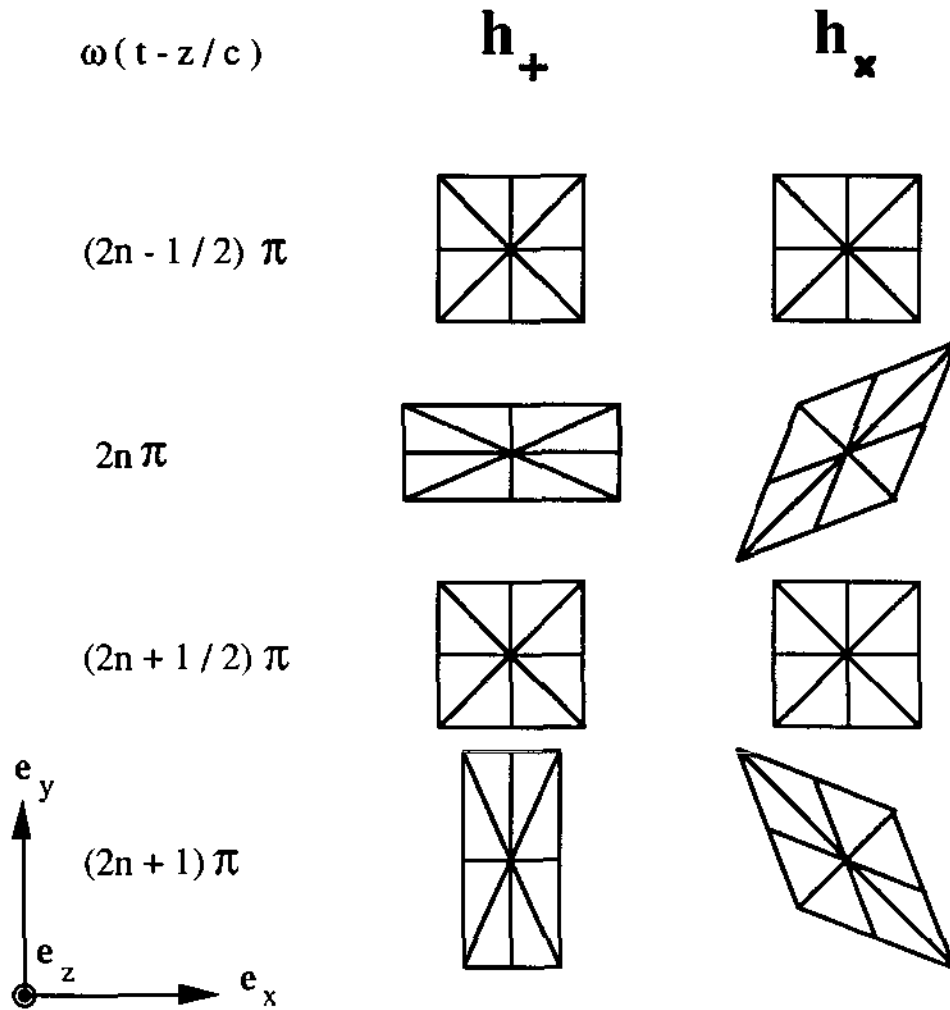


Fig. 1.1 - Deformation of a square due to forces induced by pure h_+ or h_x waves.

It is possible to envision various schemes of detection of gravitational waves.³ The two principles of detection mostly explored are the monitoring of the distance between two or more points and the measurement of the oscillations driven on a solid "antenna" by stress.¹³ The first principle of detection can be performed with a laser interferometer, or a doppler tracking array. The second principle can be realized with a resonant-mass "antenna" or a non-resonant-mass "antenna" coupled to an electromechanical transducer of some kind.

The subject of this dissertation is the study and development of one particular type of electromagnetic transducer. This transducer is intended to be integrated to a 900Hz-resonant-mass "antenna" in the near future as part of the effort to improve the detector sensitivity towards the realization of gravitational wave astronomy.

B) Resonant-Mass Gravitational Wave Detectors

The first experiment to detect gravitational waves was done during the sixties by Weber.¹⁴ Around January of 1965 the first high-frequency detector, designed and constructed by Weber, was in operation.¹⁵ Since that year he has claimed the detection of events attributed to gravitational radiation.¹⁶ During the seventies there was a worldwide effort to repeat Weber's experiment with higher sensitivity. Unfortunately, to date there is no conclusive confirmation of such events, and theoretical estimates of local fluxes done so far also reinforce this position. By these estimates the best detectors today are only able to register the presence of gravitons that come from strong bursts in our Milky Way ($d < 30$ kpc). The rate of such events is calculated to be ~ 0.1 per year,¹⁷ and its detection requires the simultaneous operation of three or more detectors. Taking into account how hard it is to operate a single detector for more than six months, the chances for detection with present sensitivities are dim. Fortunately, however, there is a strong possibility of developing better sensitivities in the not too distant future. Strain sensitivities as low as $h = 10^{-21}$ are feasible in resonant-mass detectors with technology already achieved in some other physics experiments. This represents three orders of magnitude better than current sensitivities in strain, and more than we have improved since 1970, when

Weber¹⁸ measured $h = 10^{-16}$. Details of these optimistic calculations are discussed later in this chapter.

As we have mentioned, resonant-mass "antenna" is one of the techniques used for detection of gravitational waves, actually the most employed one. They were designed after the pioneering work of Weber, who designed the first aluminum bar antenna to operate with piezoelectric crystal sensors at room temperature. Nowadays, the bar detectors in operation belong to the so-called "second generation" detectors which originated in the laboratories of William Fairbank and William Hamilton. Each detector consists of a cryogenic antenna coupled to an electromechanical transducer that has its electrical output signal pre-amplified by a very low noise cryogenic amplifier. This pre-amplified signal is recorded on magnetic tape, after passing a lock-in amplifier and an analog-digital converter, for later digital filtering and computational analysis. The cryogenic antenna is made of a high mechanical Q material, kept in vacuum and at 4.2 K (liquid helium's boiling point), and isolated as much as possible from floor or sound vibrations. Piezoelectric crystals were the first transducer during the first generation (room temperature) of antennas. They were replaced around the mid-seventies by a superconducting tunable-diaphragm with an inductive pick-up transducer, designed and constructed by Ho Jung Paik.¹⁹

These cryogenic mass-resonant antennas are usually made from a high mechanical Q aluminum-alloy bar that has its first longitudinal vibrational mode (which is sensitive to a quadrupolar gravitational wave) around 1kHz. Because theoretical models estimate that collapsing and bouncing cores of supernovas, as well as corequakes and star collisions, produce large intensities of gravitational radiation in the vicinity of 1kHz,²⁰ these events are likely to be observed by mass-resonant detectors.

The strain expected to reach a bar detector coming from one of the burst sources mentioned above is highly uncertain. Thorne¹² gives the expression:

$$h = 2.7 \times 10^{-20} \left[\frac{\Delta E_{GW}}{M_{\odot} c^2} \right]^{1/2} \left[\frac{1 \text{ kHz}}{f} \right]^{1/2} \left[\frac{10 \text{ Mpc}}{d} \right] \quad (1.15)$$

where ΔE_{GW} is the energy converted to gw, M_{\odot} is the solar mass, f is the characteristic frequency of the burst, and d its distance from us (10 Mpc is the distance to the center of the Virgo Cluster of galaxies for a Hubble constant of 100 km/ sec / Mpc). The fraction of energy converted to gravitational radiation depends on the asymmetry of the event. For perfectly symmetrical events that fraction is zero, since there is no variation of the quadrupole moment. A fairly optimistic value for supernova events is an energy fraction around 10^{-2} , which gives a strain close to $h = 3 \times 10^{-18}$ if the supernova occurs in the center of our galaxy (10 kpc away). This strain was in the range of detection during the 7-month LSU 1988 run.²¹ On the other hand, SN 1987A would have not be seen even with 1988 sensitivities unless the fraction of energy converted to gw in that event was higher than a quarter of the sun's total mass.

C) The LSU Resonant-Mass Bar Detector

A schematic drawing of the LSU detector is shown in Fig. 1.2. The antenna is balanced on a titanium cable which is attached to the intermediate mass, an X-shape, 2.5-ton bronze casting supported by titanium rods that hang from vibration isolation stacks. These stacks are kept in vacuum chambers which are connected to the 2^o shell space. To avoid overloading the schematic, the aluminum frame and pneumatic air

springs on which the stacks rest were omitted from the drawing. The transducer is bolted to one of the bar ends, and a calibrator capacitor is bolted to the other end. All the wiring attached to the transducer passes through small intermediate brass discs connected to each other by fine titanium wires. This array of discs is named a "Taber isolation" stack after its inventor, and its function is to guarantee vibration isolation to the antenna-transducer system. The bronze X mass, the vibration isolation on top, and the "Taber isolation" stack work together to reflect the external mechanical excitation by the principle of mechanical impedance mismatching.

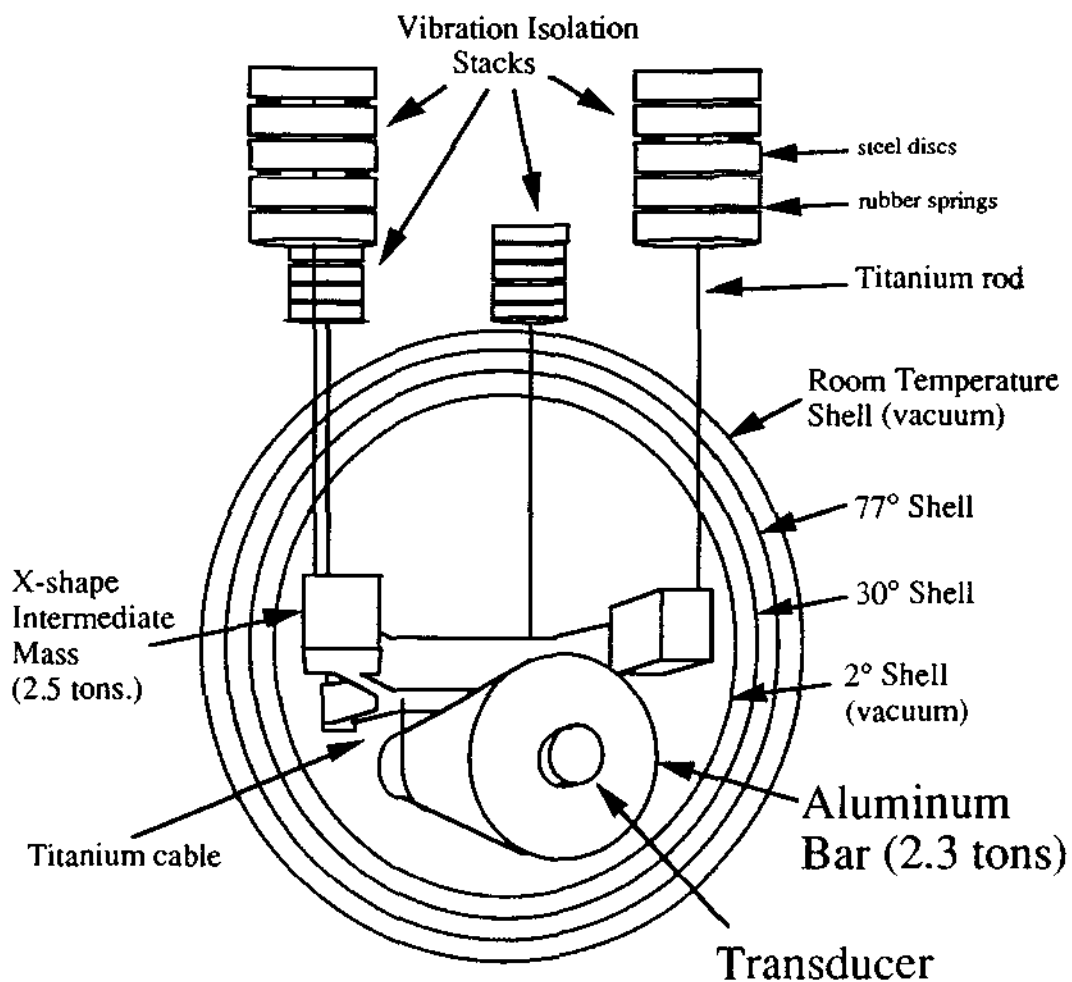


Figure 1.2 - The LSU Cryogenic Antenna.

The principle of detection is very simple. When gravitational waves strike the aluminum bar antenna, it is driven into oscillation. A major part of the energy received from the gw is coupled to the bar's first longitudinal mode which has a node about the titanium cable section and anti-nodes at both bar ends. The transducer attached to one of the ends is, therefore, set into oscillation. Because the transducer mechanical resonance is at the same frequency f_0 as the bar resonance frequency, there is a beating between the two oscillations with beat frequency equal to $f_0/2$ times the square root of the ratio: transducer effective mass / antenna effective mass. The amplitude of the transducer harmonic oscillator increases until almost all the energy from the bar's first longitudinal mode has been transferred to the transducer oscillation mode. This method obtains an amplitude gain equal to the square root of the inverse ratio mentioned above, and an increase in frequency bandwidth above noise level. The transducer then converts part of this energy into an electrical signal which is pre-amplified by a very low noise cryogenic amplifier. Finally, this amplified signal, as mentioned before, is recorded on magnetic tape for later analysis.

D) Optimization of Resonant-Mass GW Detectors

Gravitational radiation research has not yet received the level of support that other branches of astronomy -- for example, radioastronomy -- received during their development. This is partially due to a lack of interest from engineers and politicians. From the engineering point of view, "gravitational wave telecommunications" is rather science fiction now, and will probably remain so for the next few centuries. It is even less feasible to use them for "radar" purposes. From the political point of view, it is

difficult to find a military application for gravitational radiation research, at least for the kind developed with resonant-bar techniques. Of course, there is some technical outcome from this kind of research, but it is basically the same as that from any other experimental physics research. The scientific outcome, however, is the most important one. Unfortunately, although these scientific discoveries may bear tremendous fruit in the future even from the engineering and political points of view, no one can clearly see those benefits now. Because of the lack of support for gravitational radiation research, its development has been slow, and many things remain to be done. Let us examine some of the them.

As we have mentioned, gravitational waves have a very weak interaction with

matter. If we calculate the integrated cross section $\left(\int_0^\infty \sigma_n(v) dv \right)$ of a bar antenna of

mass M , length L , radius R , and Poisson ratio σ , for a sinusoidal gravitational wave with optimum polarization the result is²²

$$\int_0^\infty \sigma_n(v) dv = \left(\frac{8}{\pi} \right) \left(\frac{M}{n^2} \right) \left(\frac{G}{c} \right) \left(\frac{v}{c} \right)^2 \sin^4 \theta_i \left[1 + \frac{\sigma (1 - 2\sigma)}{2} \left(\frac{n \pi R}{L} \right)^2 \right] \quad (1.16)$$

where n is the longitudinal mode number, v is the material sound speed, and θ_i is the angle the wave propagation vector forms with the bar axis. For the first longitudinal mode ($n=1$) of the LSU antenna ($M=2300$ kg, $L=3$ m, $R=0.6$ m, $v=5.4$ km/sec, and $\sigma=.345$) and $\theta_i = 90^\circ$, this equation gives 4×10^{-25} m² or 4 kbarns, which is 4.5×10^{24} times smaller than the bar's physical cross section area.

This equation tells us that we can increase the cross section if we use higher density materials or a material with a higher sound velocity. If we include a transducer resonant at the same frequency as the bar antenna, the equation changes a little

because the mechanical system is no longer a single harmonic oscillator, but now has two normal modes. However, the integrated cross section continues to be dependent on the first power of M and the second power of v . But a more stringent equation is obtained if we take into account the noise involved in the process. We can define a noise temperature T_N which, when multiplied by the Boltzmann constant, is equal to the minimum energy deposited in the antenna by the gw pulse that can give a signal to noise ratio equal to one after optimum filtering. The rms conventional gravitational wave strain amplitude for the bar antenna as a function of this noise temperature can be found to be, at $f=915$ Hz for the LSU antenna, equal to²¹

$$h = \frac{\pi}{4} \frac{1}{L} \sqrt{\frac{4 k_B T_N}{M \omega^2}} = 10^{-18} \sqrt{\frac{T_N}{20 \text{ mK}}} \quad (1.17)$$

This means that by decreasing the noise temperature or by increasing the mass one achieves a smaller h .

The noise temperature could be lowered by increasing the mechanical Q of the antenna, or by cooling the antenna with a He³-He⁴ dilution refrigerator down to 0.1-0.01 K together with the use of less noisy transducers and amplifiers. A less noisy transducer can be obtained by increasing its mechanical and electrical Q 's, and a less noisy amplification can be achieved by the use of a D.C. SQUID preamplifier. The present state of the art SQUIDs can reach $\sim 2 \text{ } \Phi_0$ of energy sensitivity²³ in units of J Hz⁻¹. The bandwidth can be expanded by the use of a transducer with more stages²⁴ (bandwidth = $2 f_0 \sqrt{\mu}$, where μ is the ratio between two consecutive masses). The mass can be increased by a factor of 15 by the use of a spherical antenna. This also has the advantage of being omnidirectional, of measuring all the gw polarizations, and of determining the direction from which the wave arrives.^{25,26} Noise temperatures below the "standard Heisenberg quantum limit" for a 1 kHz resonant-mass bar detector ($T_N = \Phi_0 \omega / k_B = 0.05 \text{ } \mu\text{K}$) could be achieved by circumventing techniques that

perform quantum non-demolition measurements.²⁷ These implementations would require millions of dollars at 1990 prices, but would probably be able to measure one gw event per month from the Virgo cluster of galaxies.

E) Scientific Outcome of Gravitational Wave Astronomy

Since the formulation of the theory of General Relativity in 1915, it has only been possible to test it a few times. Rare experiments that successfully confirm, within their observed uncertainties, General Relativity are: the bending of starlight by the Sun, Mercury's perihelion shift, the time delay imparted to electromagnetic waves by the Sun's gravity, the Nordtvedt effect, and the indirect confirmation of gravitational radiation emission from the PSP-1913+16 binary pulsar system. The direct detection of gravitational waves, if performed, would add an important new test for General Relativity. Furthermore, many areas of science would receive direct impact from gravitational radiation astronomy: astrophysics, astronomy, nuclear physics, particle physics, and cosmology.²⁸

Theories of gravitation, including, of course, General Relativity, would be tested after the speed and polarity of the oncoming waves was determined. General Relativity, for example, predicts that the graviton -- the fundamental particle associated with gw -- has zero mass, and spin 2; therefore gravitons travel at the speed of light, carry energy ($E = \hbar\omega$) and momentum ($p = E/c$), and produce on matter the tensorial forces discussed at beginning of this chapter. General Relativity also predicts a very nonlinear gravity at vicinities of high density matter (strong field), a

phenomenon which could be confirmed by the detection of black hole coalescing binaries.

Astrophysics and astronomy will receive a strong boost from this "new window" of observation which can bring valuable information from an area on which electromagnetic waves are unable to provide data: from the dense core of some astrophysical objects. Gravitational Wave *telesensors* rather than electromagnetic telescopes will "feel" the mass dynamics of a compact object's interior. We may learn from gravitational collapses:

- the fraction of supernovas that are not visible;
- the effect of rotation in a supernova;
- the ratio of (neutron stars) / (black holes);
- their masses, and angular momentum;
- the timescale of collapse and rebound;
- the mass upper limit for neutron stars; and
- the distribution of pulsars, neutron stars, and black holes.

From coalescing binaries we may examine:

- neutron star masses and matter viscosity,
- the distribution of compact binary systems, and
- the dark matter distribution.

Cosmology will gain from the detection of compact coalescing binaries the knowledge:

- to determine Hubble's constant (and the age of the Universe), and
- to map the cosmological structure in order to discover the homogeneity and isotropy of the Universe.

And from the stochastic background of gravitational radiation we may learn about:

- the early Universe and

- galaxy formation.

Furthermore, we will also be able to:

- test string theories of galaxy formation and
- test inflationary theories (phase transitions).

From supernovas, Nuclear Physics will receive data that is not possible to obtain in laboratory experiments. Particle Physics will learn from observations of the early Universe (stochastic background); and gw from supernovas will establish a new upper limit for the neutrino mass, if gravitons are assumed to be massless. Proposed schemes of unified field theories will be tested, and new physics will be discovered that may cause a revolution in our understanding of the universe.

All this knowledge will be useful to other branches of science, one way or the other, and, eventually, some of it will help develop new technologies to improve the quality of life.

F) References

¹ E. Amaldi, in *Cosmic Gamma-Rays and Related Astrophysics*, eds. M.M. Shapiro and J.P. Wefel, NATO ASI Series C, Dordrecht, 1989, D. Reidel and Co., pp 563-607.

² A. Einstein, "Näherungsweise Integration der Feld gleichungen der Gravitation," *Sitzungsberichte der Königlich Preussischen Akad. der Wissenschaften*, Erster Halbband, Berlin , 688-696 (1916); "Über Gravitationswellen," *Sitzungsberichte der Königlich Preussischen Akad. der Wissenschaften*, Erster Halbband, Berlin , 154-167 (1918).

³ MTW - C. W. Misner, K. S. Thorne, and J. A. Wheeler, *Gravitation* (W. H. Freeman & Co., San Francisco, 1973).

- ⁴ J. Weber, *General Relativity and Gravitational Waves* (Interscience, New York, 1961).
- ⁵ R. H. Price, "General Relativity Primer," *Am. J. Phys.*, **50**, 300 (1982).
- ⁶ R. L. Forward, "General Relativity for the Experimentalist," *Proceedings of the IRE*, **49**, 892, (1961).
- ⁷ P. C. W. Davies, *The Search for Gravity Waves* (Cambridge Univ. Press, Cambridge, 1980).
- ⁸ J. H. Taylor, "Astronomical and Space Experiments to Test Relativity," in *Proc. of the 11th Intern. Conf. on General Relativity and Gravitation*, ed. M. A.H. MacCallum (Cambridge Univ. Press, Cambridge, 1987), pp 209-222.
- ⁹ J. H. Taylor et al., "Further Observations of the Binary Pulsar PSR 1913+16," *Astrophys. J. (Letters)*, **206**, L53 (1976).
- ¹⁰ C. M. Will, *Was Einstein Right ?* (Basic Books, New York, 1986).
- ¹¹ W. H. Press and K. S. Thorne, "Gravitational-Wave Astronomy," in *Annual Review of Astronomy and Astrophysics*, Ed. L. Goldberg, Palo Alto (1972).
- ¹² K. Thorne, "Gravitational Radiation," in *300 Years of Gravitation*, ed. S. W. Hawking and W. Israel (Cambridge Univ. Press, Cambridge, 1987), pp. 330-458.
- ¹³ Among other principles of operation which have not been pursued are: direct interaction between gw and ew, superfluid movements driven by gw, sharp phase transitions induced by gw, plasma antennas.
- ¹⁴ J. Weber, "Detection and Generation of Gravitational Waves," *Physical Review*, **117**, 306 (1960).
- ¹⁵ J. Weber, "Gravitational Radiation," *Physical Review Letters*, **18**, 498, (1967).
- ¹⁶ J. Weber, "Evidence for Discovery of Gravitational Radiation," *Physical Review Letters*, **22**, 1320 (1969).
- ¹⁷ J. N. Bahcall and T. Piran, "Stellar Collapses in the Galaxy," *The Astrophysical Journal*, **267**, L77 (1983).
- ¹⁸ J. Weber, "Gravitational Radiation from the Pulsars," *Physical Review Letters*, **21**, 395 (1968).
- ¹⁹ H.J. Paik, "Analysis and Development of a Very Sensitive Low Temperature Gravitational Radiation Detector," Ph. D. dissertation, Stanford University, Nov. 1974.

- ²⁰ The mean frequency for these events (ref. 3) is $\omega \sim (GM/R^3)^{1/2} = (4\pi G\rho/3)^{1/2}$, for densities at the instant of the core bounce ($\rho \sim 8 \times 10^{17} \text{ kg/m}^3$) this mean frequency is calculated to be around 1-3 kHz.
- ²¹ B.X. Xu, W. O. Hamilton, W. W. Johnson, N. D. Solomonson, and O. D. Aguiar, "Numerical Analysis of the performance of a Resonant Gravity-Wave Detector," *Physical Review*, **40D**, 1741 (1989).
- ²² H. J. Paik and R. V. Wagoner, "Calculations of the absorption cross section of a cylindrical gravitational-wave antenna," *Physical Review*, **13D**, 2694 (1976).
- ²³ D. D. Awschalom, J. Warnock, J. M. Hong, L. L. Chang, M. B. Ketchen, and W. J. Gallagher, "Magnetic Manifestation of Carrier Confinement in Quantum Wells," *Physical Review Letters*, **62**, 199 (1989).
- ²⁴ J.P. Richard, "Wide-Band Bar Detectors of Gravitational Radiation," *Physical Review Letters*, **52**, 165 (1984).
- ²⁵ R. L. Forward, "Multidirectional, Multipolarization Antennas for Scalar and Tensor Gravitational Radiation," *General Relativity and Gravitation*, **2**, 149 (1971).
- ²⁶ W. W. Johnson, *Review of Modern Physics*, to be published.
- ²⁷ K. S. Thorne, C. M. Caves, V. D. Sandberg, M. Zimmermann, and R. W. P. Drever, "The Quantum Limit for Gravitational-Wave Detectors and Methods of Circumventing It," in *Sources of Gravitational Radiation*, ed. L. L. Smarr (Cambridge Univ. Press, Cambridge, 1979), pp.49-68.
- ²⁸ J. Hough, B. J. Meers, G. P. Newion, N. A. Robertson, H. Ward, G. Leuchs, T. M. Niebauer, A. Rüdinger, R. Schilling, L. Schnupp, H. Walther, W. Winkler, B. F. Schutz, J. Ehlers, P. Kafka, G. Schäfer, M. W. Hamilton, I. Schütz, H. Welling, J. R. J. Bennett, I. F. Corbett, B. W. H. Edwards, R. J. S. Greenhalgh, and V. Kose, "Proposal for a Joint German-British Interferometric Gravitational Wave Detector," Max-Planck-Institut für Quantenoptik, MPQ 147, GWD/137/JH(89), Sept. 1989.

CHAPTER 2 - THE TRANSDUCER'S THEORETICAL EQUATIONS

In this chapter we present the theory that was developed to explain the experimental results of Chapter 4.

A) Introduction

Even though, in principle, we are able to detect gravitational waves coming from the cosmos,¹ we still have to improve our sensitivity another five orders of magnitude to increase the statistical rate of such events to one per month or so. A third generation of resonant-mass gravitational wave detectors is being built to accomplish this task.² This effort requires the construction of much better motion transducers, and a promising design relies on active transducer models, also called parametric transducers. These transducers have the capability to perform "back action evasion" and will likely surpass the standard quantum limit of a vibration amplitude measurement by carrying out a "quantum non-demolition measurement".³ It is this kind of transducer that we have designed, built, and experimentally tested, the results of which are reported here.

Parametric transducers for use in gravitational wave detectors have been designed since the mid seventies.^{4,5,6,7,8} The development of these transducers was intensified^{9,10,11,12} after the first schemes of "quantum non-demolition measurements" were proposed.¹³ These designs used either high-Q niobium cavities^{14,15,16,17} or an electrical parabrige circuit with lead-coated sapphire capacitors.^{18,19} The present design uses a niobium parabrige circuit with a niobium capacitor as a mechanical resonator; this capacitor is pumped at 5 MHz by an oscillator which had more than

three orders of magnitude smaller phase noise than the oscillators used in previous designs. We also built an very effective vibration isolation system that gave us the capability to measure the mechanical resonator's Brownian motion for this transducer.

The transducer-bridge electromechanical circuit is shown in Fig. 2.1. The middle plate of the three-plate capacitor is the mechanical resonator of this parametric transducer. The outer loop of the bridge is "pumped" at $f_p = 5$ MHz, and its resonance frequency f_{olr} is adjusted to a value as close as possible to f_p in order to enhance the pump signal across the capacitor plates. Impedance balancing guarantees a very small current in the middle branch for a motionless three-plate capacitor, to avoid saturating the amplifier chain with a signal at the pump frequency, and to minimize the presence of phase noise from the pump signal at the transducer output. In the presence of acceleration on the three-plate capacitor, the middle plate oscillates back and forth, changing both capacitances to the side plates. A current flows in the middle branch proportional to the middle plate displacement. This current is proportional to the time derivative of the product between the voltage across the capacitor plates and its capacitance; therefore, it has two components (that we will call idler signals) at frequencies that are equal to the sum ($f_+ = f_p + f_m$) and difference ($f_- = f_p - f_m$) of the mechanical frequency and pump frequency. Each of these idler signals is enhanced if the inner loop resonant frequency f_{ilr} is such that $|f_{ilr} - f_{\pm}| < (f_{ilr} / Q_{ilr})$. The voltage generated across the idler (or read-out) inductor by these currents is amplified by a two stage MESFET cryogenic pre-amplifier and a set of two amplifiers at room temperature. This voltage is demodulated and measured.

Bridge balancing was achieved by adjusting the side inductances (L'_1 and L'_r) and resistances (R_1 and R_r). These inductances, together with the idler (read-out) inductance (L_i), also could change the outer and inner loop resonant frequencies. We

were able to vary the inductances by moving, with the help of motors, a niobium rod inside each of them. The resistive balancing was adjusted by controlling with MESFET transistors the resistances of two external loops coupled to each side branch. There was no capacitive adjustment, so a perfect balance could be achieved only at one frequency at a time. C_a is a fixed value additional capacitance to decrease the capacitive imbalance between C_l and C_r . L_{cl} , L_{cm} , and L_{cr} are cable inductances.

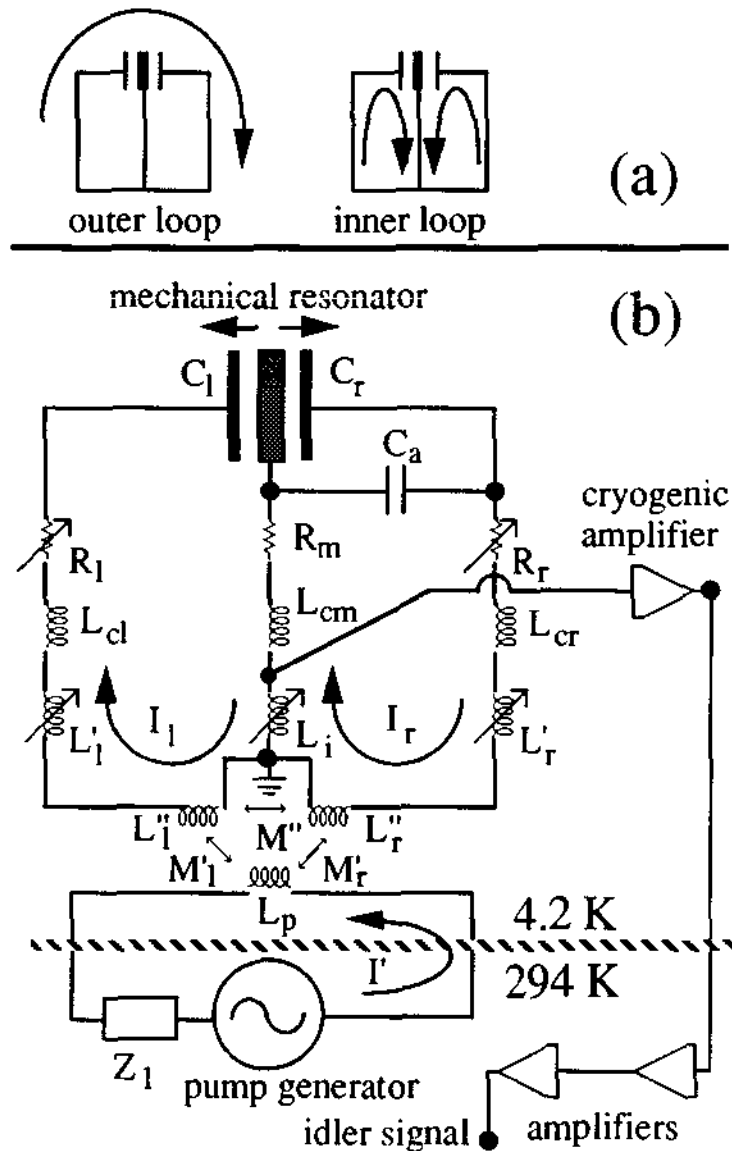


Fig. 2.1 - Transducer-bridge electromechanical circuit

B) Circuit Analysis

The two loop equations²⁰ of the electrical circuit in Fig. 2.1 when the primary loop is open circuit can be written as:

$$\begin{bmatrix} Z_{11} & Z_{12} \\ Z_{21} & Z_{22} \end{bmatrix} \begin{bmatrix} I_1 \\ I_r \end{bmatrix} = \begin{bmatrix} 0 \\ 0 \end{bmatrix}, \text{ where} \quad (2.1)$$

$$Z_{11} = L''_1 + L'_1 + L_{cl} + L_{cm} + L_i - 1/\omega^2 C_1,$$

$$Z_{12} = -(L_{cm} + L_i - M'' \sqrt{L''_r/L''_1}),$$

$$Z_{21} = -(L_{cm} + L_i - M'' \sqrt{L''_1/L''_r}), \text{ and}$$

$$Z_{22} = L''_r + L'_r + L_{cr} + L_{cm} + L_i - 1/\omega^2 C_r.$$

The two resonant frequencies that can be found by making $\det [Z(\omega)] = 0$ are:

$$\begin{aligned} \omega_{or}^2 &= \frac{-b + \sqrt{b^2 - 4ac}}{2a} \quad (\text{outer loop resonance}), \text{ and} \\ \omega_{ir}^2 &= \frac{-b - \sqrt{b^2 - 4ac}}{2a} \quad (\text{inner loop resonance}) \end{aligned} \quad (2.2)$$

where

$$a = C_r C_1 [(L''_1 + L'_1 + L_{cl} + L_{cm} + L_i) (L''_r + L'_r + L_{cr} + L_{cm} + L_i) - (L_{cm} + L_i - k L''_r) (L_{cm} + L_i - k L''_1)],$$

$$b = -[C_1 (L''_1 + L'_1 + L_{cl} + L_{cm} + L_i) + C_r (L''_r + L'_r + L_{cr} + L_{cm} + L_i)], \text{ and}$$

$$c = 1.$$

We can derive the voltage across the read-out inductor (V_{Li}) as a function of the generator loop current (I'). First we write the expressions for the voltages across L''_1 and L''_r :

$$V_1 = -j \omega L''_1 I_1 - j \omega M'' I_r - j \omega M'_1 I', \text{ and}$$

$$V_r = j \omega L''_r I_r + j \omega M'' I_1 + j \omega M'_r I', \text{ respectively.}$$

The two equalities relating these voltages and the voltage across the middle branch with the two loop currents are:

$$I_l = (V_l - V_m) / (Z_l - j \omega L''_l) \text{ and } I_r = (V_m - V_r) / (Z_r - j \omega L''_r), \text{ where}$$

$$Z_r = R_r + j \omega (L'_r + L_{cr} + L''_r) - j / \omega C_r \text{ and}$$

$$Z_l = R_l + j \omega (L'_l + L_{cl} + L''_l) - j / \omega C_l .$$

Solving for these loop currents we easily find the unbalanced current through the middle branch $I_m = I_l - I_r$. Then, the voltage across the read-out inductor is:

$$V_{Li} = [R_m L_i / (L_{cm} + L_i) + j \omega L_i] I_m,$$

if we suppose the middle branch resistance is proportionally spread between the coaxial cable inductance and the idler (read-out) inductance. Finally, the ratio V_{Li} / I' can be found as:

$$\frac{V_{Li}}{I'} = \frac{j \omega L_i}{R_m + j \omega (L_{cm} + L_i)} \times \frac{\omega^2 (L_{cm} + L_i) [A + j \omega B] + R_m \omega [\omega B - j A]}{(Z_l Z_r + \omega^2 M''^2) - (L_{cm} + L_i) \omega [2 \omega M'' - j (Z_l + Z_r)] + R_m [(Z_l + Z_r) + j 2 \omega M'']}, \quad (2.3)$$

where

$$A = M'_l Z_r - M'_r Z_l, \text{ and}$$

$$B = M'' (M'_l - M'_r).$$

On the other hand, the ratio V_{cap} / I' can be found by multiplying the average current through the outer loop $I'' = (I_l + I_r) / 2$ by the impedance of one side of the capacitor. As a result, we have:

$$\frac{V_{cap}}{I'} = \frac{-M'}{C \{R + j \omega [L' + L_c + L'' (1 + M'' / \sqrt{L''_l L''_r})] - j / \omega C\}}, \quad (2.4)$$

where $C = (C_l + C_r) / 2$, $L' = (L'_l + L'_r) / 2$, $L_c = (L_{cl} + L_{cr}) / 2$, $R = (R_l + R_r) / 2$.

Finally, reflecting the total outer loop impedance to the generator loop, we also can find the ratio V_{gen} / I' (the total generator loop impedance):

$$\frac{V_{gen}}{I'} = Z_1 + j \omega L_p + \frac{[\omega (M'_1 + M'_r)]^2}{Z_1 + Z_r + j 2\omega M''} \quad (2.5)$$

C) Equations of Motion and Parametric Effect

One of the characteristics of a parametric transducer is its ability to convert pump energy into energy of an electrical signal at an "idler" frequency equal to the sum or difference of the pump and mechanical frequencies. This "idler" signal carries the information of the mechanical oscillation motion. This phenomena of power transfer from one frequency to another is called the parametric effect. Although it was first discussed in 1831 by Faraday and has been studied by him and other eminent physicists such as Melde and Lord Rayleigh,²¹ it was not before the middle of the 1950's that Manley and Rowe derived the relations governing the parametric feedback.²²

The Manley and Rowe power relations for a parametric system with four frequencies such as one low frequency mechanical signal, one high frequency electrical pump signal, and two electrical sidebands $\omega_{pump} + \omega_m$ and $\omega_{pump} - \omega_m$ are:

$$-\frac{P_p^{(-)}}{\omega_p} = \frac{P_{p-m}}{\omega_p - \omega_m} \quad \text{and} \quad \frac{P_m^{(-)}}{\omega_m} = \frac{P_{p-m}}{\omega_p - \omega_m} \quad \text{for the } (-) \text{ interaction,}^{23} \quad \text{and} \quad (2.6)$$

$$-\frac{P_p^{(+)}}{\omega_p} = \frac{P_{p+m}}{\omega_p + \omega_m} \quad \text{and} \quad -\frac{P_m^{(+)}}{\omega_m} = \frac{P_{p+m}}{\omega_p + \omega_m} \quad \text{for the } (+) \text{ interaction.} \quad (2.7)$$

where $P_i^{(\pm)}$ is the power flowing into or out of the mode i due to the parametric interaction (\pm).

These equations also imply that:

$$P_p^{(-)} - P_m^{(-)} = P_{p-m} \text{ and } P_p^{(+)} + P_m^{(+)} = P_{p+m} .$$

Therefore, the sidebands always receive a net power. In the minus interaction the minus sideband receives power only from the pump mode, and in the plus interaction it receives power from both pump and mechanical modes. Also, in the minus interaction the net power received by the mechanical mode due to the parametric coupling is supplied by the pump mode. When the net power received by the plus sideband equals the power received by the minus sideband times the ratio of their frequencies ($\omega^{(+)} / \omega^{(-)}$), the mechanical mode does not receive or lose power due to the parametric interaction. We say in this case that the "loaded" Q (the effective Q when the interaction is turned on) of the mechanical mode has the same value as its "unloaded" Q. Otherwise, the "loaded" Q assumes different values, higher or lower than the "unloaded" Q depending, respectively, whether the (-) or (+) sideband dominates.

The parametrically coupled equations of motion for this transducer are approximately:³

$$\ddot{x}(t) + \frac{\omega_m}{Q_m} \dot{x}(t) + \omega_m^2 x(t) = \frac{F_m(t)}{M} + \frac{F_{vib}(t)}{M} + \frac{F_B(t)}{M} - \frac{V_{cap}(t)}{D M} q(t) , \quad (2.8)$$

and

$$\ddot{q}(t) + \frac{\omega_{ilr}}{Q_{ilr}} \dot{q}(t) + \omega_{ilr}^2 q(t) = - \frac{V_{cap}(t)}{L_{il}} \left(\frac{x(t)}{D} \right) + \frac{V_n(t)}{L_{il}} + \frac{I_n(t)}{L_{il}} \omega_{ilr} L_i , \quad (2.9)$$

where x and q are the displacement and charge of the middle plate;

ω_m , ω_{ilr} , Q_m and Q_{ilr} are the angular frequencies and figures of merit for the mechanical and inner loop resonances respectively; $F_m(t)$, $F_{vib}(t)$ and $F_B(t)$ are the forces of the mechanical signal, mechanical vibration noise, and Brownian noise (Langevin force)²⁴; M is the reduced mass of the transducer; D is the average capacitance gap; L_{il} is the total inner loop inductance ($\equiv 1 / [(C_1 + C_r) \omega_{ilr}^2]$), L_i is the

idler or read-out inductance, V_n is the Johnson noise²⁵ of the inner loop resistance, and I_n is the amplifier current noise. The last term in Equation 2.8 is the most important "back action" force term. The complete expression of the "back action" force is

$$F_{BA} = A_{cap} \frac{\epsilon_0}{2} \left\{ \left[\frac{V_{cap}(t) - V}{D - x(t)} \right]^2 - \left[\frac{V_{cap}(t) + V}{D + x(t)} \right]^2 \right\}$$

where V is the potential on the center plate, A_{cap} is the capacitor area, D is its gap.

From these motion equations we can derive the expression for the "loaded" relaxation time of the mechanical resonator,¹⁹ which is equal to:

$$\frac{1}{\tau_L} = \frac{1}{2} \left[\left(\frac{1}{\tau_{ilr}} + \frac{1}{\tau_m} \right) - \sqrt{\left(\frac{1}{\tau_{ilr}} - \frac{1}{\tau_m} \right)^2 - f \beta \omega_m^2} \right], \quad (2.10)$$

where $\beta = (V_{co}/D)^2 (\omega_{ilr}/\omega_m) (C/M\omega_m^2)$ is a dimensionless measure of the strength of the coupling between the mechanical and electrical modes,

$V_{co} = \sqrt{2} V_{cap}$, $\tau_m = Q_m/\omega_m$, $\tau_{ilr} = Q_{ilr}/\omega_{ilr}$, $C = (C_l + C_r) / 2$; and f is a factor that gives the measure of the net parametric feedback. When f has a positive value, the "loaded" mechanical relaxation time decreases as β is increased; and when f is negative the "loaded" mechanical relaxation time increases as β is increased.

However, our experiment has one important distinction from that of Bocko and Johnson. In their work, the transducer had two pump signals, and the idler signal was localized only on the top of the inner loop resonance; here our transducer had a single pump signal and two idler signals at the pump frequency plus and minus the mechanical frequency rather than on the top of the resonance. Therefore, we had to introduce some changes in the original result.

In Bocko and Johnson's work, f could only assume three possible values: -1, 0 or 1; here we should allow f to vary continuously according to where the pump is

localized relative to the top of the inner loop resonance. In order to accomplish this task, we first recognized the presence of two distinct parametric interactions, each of them associated with one idler signal, and each acting against the other. In the first of these parametric interactions, a (+) interaction according to the Manley-Rowe relations, the mechanical motion suffers damping. In the second, a (-) interaction, the mechanical oscillations suffer anti-damping. Next, we calculated the correction necessary to introduce the effect of each of these individual interactions.

According to the Manley-Rowe relations, the power received from or given to the mechanical mode is directly proportional to the power received by the idler mode. In the bridge circuit, the power received by the idler mode is proportional to the square of the steady state idler mode current. This current is given by the square of the magnitude of an universal resonance curve²⁶ at the idler frequency times the square of the current at the inner loop resonant frequency.²⁷ Therefore, if we want to consider the effect of having our idler signal at some frequency other than the exact resonant frequency, we should multiply the β factor -- which is directly proportional to the power received by the idler mode when at resonance -- by the square of the magnitude of an universal resonance curve at the new idler frequency. Because we have two idler signals, we have two products, or two new β 's:

$$\beta_{\pm} = (\text{abs}(f_{\pm}) V_{co}/D)^2 (\omega_{ilr}/\omega_m) (C/M\omega_m^2), \text{ where}$$

$$f_{\pm} = \left[\frac{1}{1 + j 2 Q_{ilr} \delta_{\pm}} \right], \quad (\text{universal resonance curve})$$

$$\delta_{\pm} = \frac{\omega_{\pm} - \omega_{ilr}}{\omega_{ilr}}, \text{ and}$$

$$\omega_{\pm} = \omega_p \pm \omega_m .$$

The final β becomes the difference β_+ minus β_- , or, similarly, f times β , where now

$$f = (\text{abs}(f_+))^2 - (\text{abs}(f_-))^2 \quad (2.11)$$

(curiously, by a property of universal resonance curves, f also can be represented by the real part of $f_+ - f_-$). Now, f takes into account the parametric feedback in the presence of the plus and minus sidebands. This is especially important when the inner loop bandwidth is larger than twice the mechanical resonant frequency, which is true in the present experiment.

D) Calibration

a) Electrical Output Signal

If the mechanical resonator does not oscillate, the voltage across the read-out inductor is given by equation 2.3 with the same frequency as the current running in the outer loop. If, on the other hand, we suppose the mechanical resonator with a motion described by $x(t) = x_0 \cos \omega_m t$ and a voltage $V_{\text{cap}}(t) = V_{\text{co}} \sin \omega_p t$ across one side of the capacitor, where ω_p is the pump frequency, there will be two output idler signals at the sum and difference frequencies. This is a straightforward result obtained from equation 2.9 if we neglect the noise terms. In this case, the steady state voltage across the idler (read-out) inductor is found to be:

$$V_{\text{Li}}(t) = \frac{x_0}{2} \frac{L_i}{L_{\text{il}}} \frac{V_{\text{co}}}{D} Q_{\text{ilr}} \times \left\{ \begin{array}{l} \frac{\sin(\omega_- t + \phi_-)}{\sqrt{Q_{\text{ilr}}^2 [(\omega_{\text{ilr}}/\omega_-)^2 - 1]^2 + (\omega_{\text{ilr}}/\omega_-)^2}} \\ + \frac{\sin(\omega_+ t + \phi_+)}{\sqrt{Q_{\text{ilr}}^2 [(\omega_{\text{ilr}}/\omega_+)^2 - 1]^2 + (\omega_{\text{ilr}}/\omega_+)^2}} \end{array} \right\}, \quad (2.12)$$

where

$$\phi_{\pm} = -\tan^{-1} \left\{ \omega_{\pm} \omega_{\text{ilr}} / [Q_{\text{ilr}} (\omega_{\text{ilr}}^2 - \omega_{\pm}^2)] \right\} \quad (2.13)$$

is the phase shift introduced due to the position of the idler relative to the inner loop resonant frequency. (V_{co}/D) is the peak electrostatic field strength across the

capacitor plates, x_o and ω_m are the amplitude and frequency of the mechanical oscillations, ω_+ and ω_- are the sideband frequencies, and Q_{ilr} is the inner loop resonance quality factor.

This two-sideband signal is amplified and goes to a mixer where it is demodulated by an RF local oscillator signal $V_{LO}(t) = V_{LO0} \sin(\omega_p t + \phi_{LO})$ that is supposed to have a constant phase difference ϕ_{LO} with respect to the generator signal. Then the final expression of the voltage at output of the mixer becomes:

$$V_{\text{mixer output}} = \frac{\sqrt{2}}{4} \frac{L_i}{L_{il}} \frac{V_{\text{cap}}}{D} Q_{ilr} \times x_o \left[\frac{\cos[\omega_m t - (\phi_- - \phi_{LO})]}{\sqrt{Q_{ilr}^2 [(\omega_{ilr} / \omega_-)^2 - 1]^2 + (\omega_{ilr} / \omega_-)^2}} + \frac{\cos[\omega_m t + (\phi_+ - \phi_{LO})]}{\sqrt{Q_{ilr}^2 [(\omega_{ilr} / \omega_+)^2 - 1]^2 + (\omega_{ilr} / \omega_+)^2}} \right] \quad (2.14)$$

b) Generation of the Mechanical Input Signal

Fig. 2.2 shows (a) the mechanism used to produce known amplitudes of oscillation on the mechanical resonator, (b) its mechanical schematic, and (c) the Voigt model²⁸ electrical equivalent. The masses of the resonator, transducer box, aluminum ring, brass vibration isolation stage, and aluminum plate are $m_1=0.27$ kg, $m_2=8.2$ kg, $m_3=0.3$ kg, $m_4=2.03$ kg, and $m_5=0.065$ kg, respectively. The spring constants are: $k_1=8.9$ MN/m, $k_2=0.353$ MN/m, $k_3=1.17$ MN/m, $k_4=0.217$ MN/m, and $k_{ext}=1.59$ MN/m. An a.c. voltage at half the mechanical resonant frequency is applied between the aluminum plate and the transducer box. This voltage generates a force acting on the box at the resonant frequency, making both box and resonator oscillate.

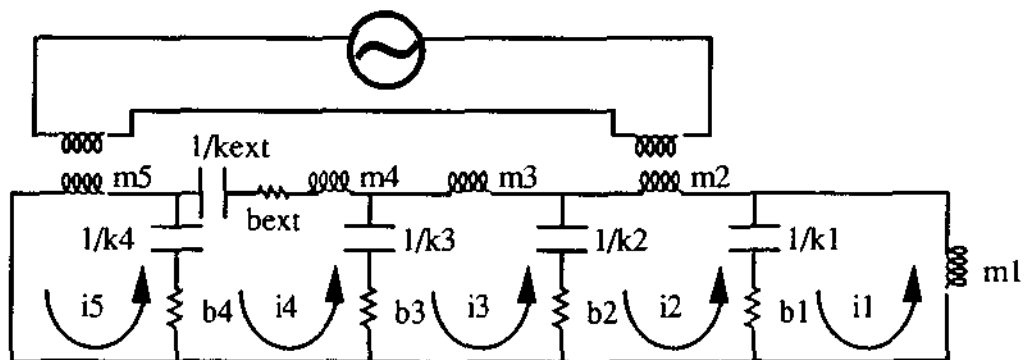
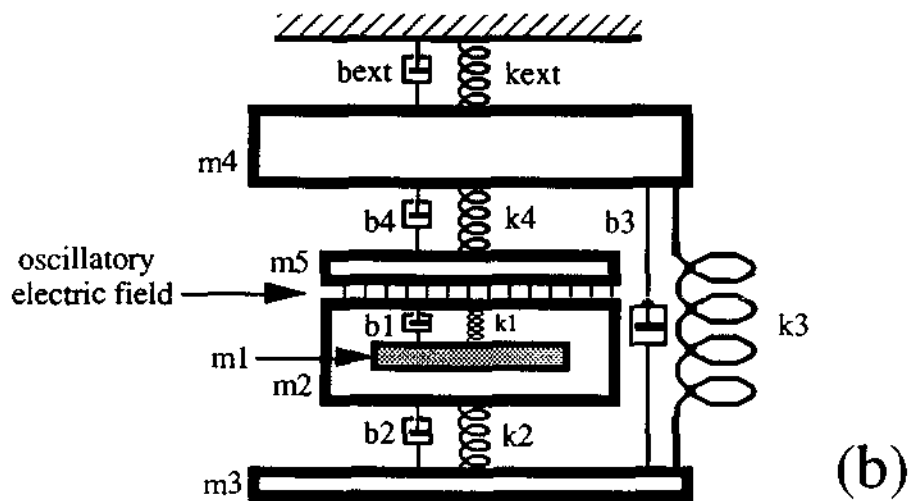
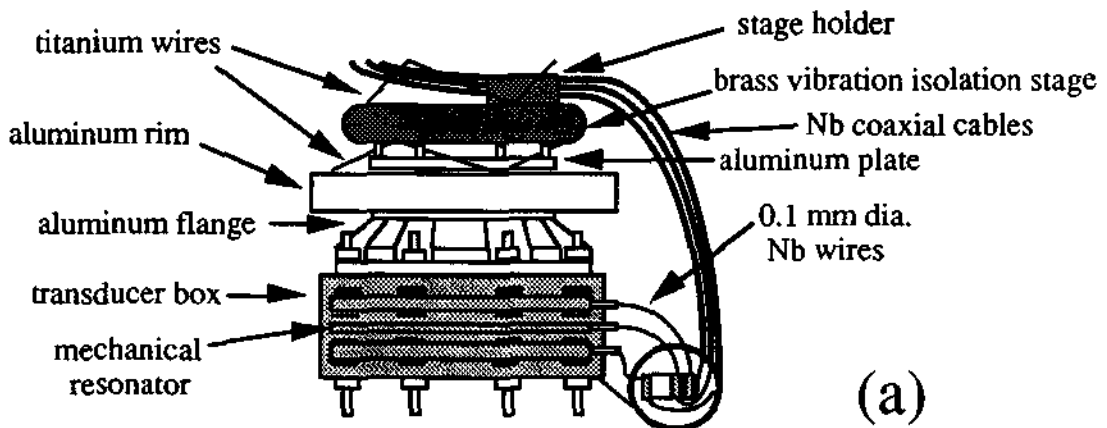


Fig. 2.2 - Transducer Calibration. (a) Detail of the hardware used for transducer calibration, (b) its mechanical schematic, and (c) electrical equivalent

The entire solution for the electrical equivalent can be found by solving the matrix equation

$$[Z][I] = [V], \quad (2.15)$$

where Z is a 5×5 square matrix with elements

$$Z_{11} = b_1 + j \omega m_1 - j k_1 / \omega,$$

$$Z_{12} = -b_1 + j k_1 / \omega,$$

$$Z_{21} = -b_1 + j k_1 / \omega,$$

$$Z_{22} = b_1 + b_2 + j \omega m_2 - j (k_1 + k_2) / \omega,$$

$$Z_{23} = -b_2 + j k_2 / \omega,$$

$$Z_{32} = -b_2 + j k_2 / \omega,$$

$$Z_{33} = b_2 + b_3 + j \omega m_3 - j (k_2 + k_3) / \omega,$$

$$Z_{34} = -b_3 + j k_3 / \omega,$$

$$Z_{43} = -b_3 + j k_3 / \omega,$$

$$Z_{44} = b_3 + b_4 + b_{ext} + j \omega m_4 - j (k_3 + k_4 + k_{ext}) / \omega,$$

$$Z_{45} = -b_4 + j k_4 / \omega,$$

$$Z_{54} = -b_4 + j k_4 / \omega,$$

$$Z_{55} = b_4 + j \omega m_5 - j k_4 / \omega,$$

all other Z elements = 0,

I is a column vector, and

V is also a column vector, but has only $V_2 = V_5 = V$ as non-null elements.

Inspection can verify that the amplitude of the resonator motion caused by the electric field force is more than four orders of magnitude larger than the resonator's amplitude of oscillations due to the mechanical forces transmitted from the aluminum plate motion via the k_4 - m_4 - k_3 - m_3 - k_2 path. Therefore, these mechanical forces can be completely neglected. Furthermore, because k_1 is much larger than k_2 , the system transducer box plus resonator can be treated as isolated. This approximation gives a

result that differs very little from the one given by the exact solution. The resonator amplitude in the approximation is only 0.4% larger than the one derived from the exact solution; and the resonant frequency in the approximation is only 0.02 Hz lower than the one calculated using the exact solution. Therefore, the resonator's steady state amplitude when the transducer box is subject to force F_{cal} along its axis can be approximated to:

$$y_m(\omega=\omega_m) = -F_{cal}(\omega_m) Q_m / \omega_m^2 M_{box}, \quad (2.16)$$

where $\omega_m / 2\pi$ is the mechanical resonant frequency, M_{box} is the transducer box mass (which is m_2 in Fig. 2.2), and Q_m is the mechanical figure of merit.

Exciting the calibrator with an a.c. voltage $V_{cal} = V_o \sin(0.5 \omega_m t)$ will cause a force (neglecting fringing fields)

$$F_{cal}(t) = - (V_o C_{cal})^2 \sin(\omega_m t) / 4 \epsilon_o A_{cal} \quad (2.17)$$

on the transducer box. In this equation, ϵ_o is the vacuum permittivity, C_{cal} is the calibrator capacitance, and A_{cal} is its area. The root mean square value (rms) of this force can be expressed as

$$F_{rms} = - (V_{rms} C_{cal})^2 / 2 \sqrt{2} \epsilon_o A_{cal}, \quad (2.18)$$

where V_{rms} is the rms capacitor voltage at half the mechanical frequency. This force acting continuously on the transducer box would set the transducer mechanical resonator into oscillations with a steady state rms amplitude

$$y_{rms} = Q_m V_{rms}^2 C_{cal}^2 / (2 \sqrt{2} \epsilon_o A_{cal} \omega_m^2 M_{box}). \quad (2.19)$$

E) Noise Analysis

a) Mechanical Noise

According to equation 2.8 there are two sources of mechanical noise acting on the transducer: thermal noise and laboratory vibrations. To these noise sources we can associate two displacement spectral densities for the resonator motion S_{Lan} and S_{vib} , respectively, in m^2 / Hz .

In order to reach the resonator the laboratory vibrations must pass all stages of vibration isolation. Then, we can treat this problem in a similar manner to the problem of calculating the transmission of the oscillations from the calibrating capacitor to the mechanical resonator. The only difference is that, in this case, all the masses of the vibration isolation system will take part. Again, the Voigt electrical equivalent can be applied to simplify the calculations by solving the problem in the frequency domain. The displacement spectral density of vibrations that reaches the resonator is the displacement spectral density of vibrations at the top of the cryostat times the square of the transfer function.²⁹

The second source of mechanical noise is the thermal noise that causes the transducer resonator to respond to the Langevin forces associated with the Brownian motion. The respective displacement spectral density S_{Lan} (Brownian) can be easily found by multiplying the mechanical resistance "force" spectrum density due to the thermal noise by the square of the Fourier transform of the mechanical resonator's transfer function.³⁰ The mechanical resistance "force" spectral density is³¹

$$S_F = 4 k_B T (\mu \omega_0 / Q_0), \quad (2.20)$$

where k_B is the Boltzmann constant, T is the temperature, μ is the transducer's reduced mass, ω_o is the mechanical angular frequency ω_m , and Q_o the unloaded Q .

The square of the mechanical resonator's transfer function, on the other hand, is

$$\left| \frac{\frac{1}{\mu}}{-\omega^2 + \omega_o^2 + j \frac{\omega \omega_o}{Q_L}} \right|^2,$$

where Q_L is the loaded Q .

Therefore, the square root of S_{Lan} becomes

$$\sqrt{S_{Lan}(\omega)} = \sqrt{\frac{4 k_B T \omega_o / (\mu Q_o)}{(\omega_o^2 - \omega^2)^2 + \omega_o^2 \omega^2 / Q_L^2}}, \quad (2.21)$$

with a peak at $\omega = \omega_o$ given by

$$\sqrt{S_{y_o}} = 6.682 \times 10^{-17} Q_L / \sqrt{Q_o} \text{ (m / } \sqrt{\text{Hz}}), \quad (2.22)$$

b) Electrical Noise

In order to explain the electrical noise measured for this transducer we use a modified version of the Bocko-Johnson¹⁹ noise model for parametric transducers. We had to modify this model slightly in order to cover the effect of both sidebands, to account for the fact that we had a slightly different parabrige circuit and we were using a different definition of imbalance. The final expression of the total electrical noise is the sum of:

- the voltage noise due to the pump phase noise, $S_{\phi_v}(\omega_+)$ and $S_{\phi_v}(\omega_-)$;
- the inner loop Johnson voltage noise, $S_{ilv}(\omega_+)$ and $S_{ilv}(\omega_-)$;
- the outer loop Johnson noise, $S_{olv}(\omega_+)$ and $S_{olv}(\omega_-)$; and
- the voltage noise due to the RF amplifier chain voltage and current noises, $S_{RFav}(\omega_+)$, $S_{RFav}(\omega_-)$, $S_{RFac}(\omega_+)$ and $S_{RFac}(\omega_-)$,

all of them calculated at some reference position such as the input of the first stage of the RF amplification or, in other words, across the read-out inductor. Then the power spectrum density of the total voltage noise (S_V), referred to this input, is the sum of the power spectrum densities of all the above noises^{32,33} plus the single sideband noise of the low frequency amplification chain (S_{LF}). The various predicted noise contributions can be expressed as:

$$S_{\phi v}(\omega_{\pm}) = (1/2 \tau_{ilr})^2 \left(\frac{|G_m(\omega_{off})|}{|J_{\pm}(\omega_{off})|} \right)^2 [(V_{cap} \text{Imb}_{\pm})^2 S_{\phi}(\omega_{\pm})], \quad (2.23)$$

$$S_{ilv}(\omega_{\pm}) = (\omega_{ilr}^2 / 2) \left(\frac{|G_m(\omega_{off})|}{|J_{\pm}(\omega_{off})|} \right)^2 [4 k_B T L_i^2 / (L_{il} \tau_{ilr})], \quad (2.24)$$

$$S_{olv}(\omega_{\pm}) = (1/2 \tau_{olr})^2 \left(\frac{|G_m(\omega_{off})|}{|J_{\pm}(\omega_{off})|} \right)^2 \text{Imb}_{\pm}^2 (4 k_B T L_{ol} / \tau_{olr}), \quad (2.25)$$

$$S_{RF}(\omega_{\pm}) = (\omega_{ilr}^2 L_i^2 / 2 L_{il})^2 \left(\frac{|G_m(\omega_{off})|}{|J_{\pm}(\omega_{off})|} \right)^2 S_{RFac}(\omega_{\pm}) + S_{RFav}(\omega_{\pm}), \quad (2.26)$$

where

$$G_m(\omega_{off}) = (j \omega_{off} m_{ec} + 1/2 \tau_m),$$

$$\omega_{off\ mec} = \omega - \omega_m,$$

$$G_{\pm}(\omega_{off}) = (j \omega_{off\ ilr} + 1/2 \tau_{ilr}),$$

$$\omega_{off\ ilr} = (\omega - \omega_m) + (\omega_+ - \omega_{ilr}) \text{ for the upper sideband,}$$

$$\omega_{off\ ilr} = (\omega - \omega_m) + (\omega_- - \omega_{ilr}) \text{ for the lower sideband,}$$

$$J_{\pm}(\omega_{off}) = G_m(\omega_{off}) G_{\pm}(\omega_{off}) \pm |f_{\pm}|^2 \beta \omega_m^2 / 16,$$

$\omega_{\pm} = \omega_p \pm \omega_m$, Imb_{\pm} is the ratio V_{Li} / V_{cap} (imbalance) at each sideband, L_i is the read-out inductance, $L_{il} \equiv 1 / [(C_l + C_r) \omega_{ilr}^2]$ is the total inner loop inductance, and $L_{ol} \equiv 4 / [(C_l + C_r) \omega_{olr}^2]$ is the total outer loop inductance; T is the temperature; and k_B is the Boltzmann constant. Note that in the expression for the Johnson noise

originated in the outer loop, the resonant frequency was supposed to be close to the pump frequency and to have a low Q , allowing us to assume a flat response in the region of interest.

The operator $(|G_m(\omega_{off})|/|J_{\pm}(\omega_{off})|)$ above is approximately constant and equal to $2\tau_{ilr}$ in the neighborhood of the mechanical resonant frequency, when f times β is zero (f given by Equation 2.11). If f times β is not zero this operator will present a depression or a peak right at the resonant frequency depending if f is positive or negative,³⁴ respectively. This means that the noise presented in the bridge inner loop due to pump phase noise or Johnson noise or amplifier current noise will have a decrease or an increase at the mechanical resonant frequency when the electromechanical coupling is not null.

The physical explanation for this result is simple. The voltage noise in one idler sideband can be represented by a narrowband random process^{35,36}

$$V_n(t) = V_N(t) \cos [\omega_i t + \phi_N(t)], \quad (2.27)$$

where $\omega_i / 2\pi$ is the idler sideband frequency,

$V_N(t) = \sqrt{u^2(t) + v^2(t)}$ is the "envelope,"

$\phi_N(t) = \tan^{-1} [u(t) / v(t)]$ is the phase, and

$u(t)$ and $v(t)$ are independent random variables with spectral densities concentrated about zero frequency. Therefore, for a few cycles of the idler sideband both the envelope and the phase will not change appreciably, and the voltage noise in the inner loop can be approximated to

$$V_n(t) = V_{N_0} \cos (\omega_i t + \phi_{N_0}). \quad (2.28)$$

Then, replacing $V_n(t)$ in Equation 2.9, we obtain an expression for the charge $q(t)$, on the center plate, proportional to $\sin (\omega_i t + \phi_{N_0})$, if $\omega_i = \omega_{ilr}$. On the other hand, from Equation 2.8, this $q(t)$ causes a displacement of the mechanical resonator as a

function of time $x(t)$ proportional to $-\sin(\omega_m t \pm \phi_{No})$, where the sign in front of ϕ_{No} is plus for the case $\omega_i = \omega_{ilr} = \omega_+$ and it is minus for the case $\omega_i = \omega_{ilr} = \omega_-$. Due to the presence of a pump signal across the capacitor plates

$$V_{cap}(t) = V_{co} \sin(\omega_p t), \quad (2.29)$$

it is apparent, from Equation 2.9, that this $x(t)$ produces a voltage "signal" in the inner loop proportional to $\cos(\omega_- t - \phi_{No}) - \cos(\omega_+ t + \phi_{No})$ for the case $\omega_i = \omega_{ilr} = \omega_+$ or proportional to $\cos(\omega_- t + \phi_{No}) - \cos(\omega_+ t - \phi_{No})$, if $\omega_i = \omega_{ilr} = \omega_-$. Therefore, there is destructive (constructive) interference between the initial noise and its "reflection" from the mechanical resonator if $\omega_i = \omega_{ilr} = \omega_+$ (ω_-), because the "reflection" is 180° out of phase (0° in phase) with respect to the initial noise. In conclusion, a decrease (increase) in the electrical noise will be found as a result of the parametric coupling between the electrical and the mechanical modes. For the case of $\omega_i = \omega_{ilr} = \omega_-$, the sign of $q(t)$ reverts in Equation 2.9 when the coupling is strong and causes the "loaded" electrical Q , as seen by the (-) interaction, to become negative. In this case also destructive interference is predicted by equations 2.23 to 2.26.

Having derived the main theoretical results to analyze the data presented in Chapter 4, we proceed to Chapter 3, where we describe the design and construction of the transducer and the experimental setup.

F) References

- ¹ E. Amaldi *et al.*, "First Gravity Coincidence Experiment Between Resonant Cryogenic Detectors: Louisiana-Rome-Stanford," *Astronomy and Astrophysics*, 216, 325 (1989).

- ² M. Bassan, E. Coccia, I. Modena, G. Pizzella, P. Rapagnani, F. Ricci, "The New Ultralow Temperature Gravitational Wave Detection Project of the Rome Group," Workshop on GW Signal Analysis and Detection (Amalfi, Italy, 1988) NATO ASI Conference Proceedings, to be published (1990).
- ³ W. W. Johnson and M. Bocko, "Approaching the Quantum Limit for Force Detection," *Physical Review Letters*, **47**, 1184 (1981).
- ⁴ V. B. Braginskii, A. B. Manukin, E. I. Popov, V. N. Rudenko, and A. A. Khorev, "An Upper Limit on the Densities of Gravitational Radiation of Extraterrestrial Origin," *Soviet Physics - JETP*, **39**, 387 (1974).
- ⁵ S. P. Boughn, W. M. Fairbank, M. S. McAshan, H. J. Paik, R. C. Taber, T. P. Bemat, D. G. Blair, and W. O. Hamilton, "The Use of Cryogenic Techniques to Achieve High Sensitivity in Gravitational Wave Detectors," in *Gravitational Radiation and Gravitational Collapse*, ed. by DeWitt-Morette (Reidel, Boston, MA, 1974).
- ⁶ W. C. Oelfke and W. O. Hamilton, "Superconducting Accelerometers for the Study of Gravitation and Gravitational Radiation," *Acta Astronautica*, **5**, 87 (1978).
- ⁷ D. G. Blair, J. Mills, and R. E. Rand, "Microwave Non-Contacting Accelerometer for Gravity Wave Antenna," *IEEE Transactions on Magnetics*, **MAG-13**, 350 (1977).
- ⁸ K. Tsubono, S. Hiramatsu, and H. Hirakawa, "Cavity Transducer for Subatomic Mechanical Vibration," *Japanese Journal of Applied Physics*, **16**, 1641 (1977).
- ⁹ V. I. Panov and J. Y. Khalili, 9th Intern. Conf. on General Relativity and Gravitation, *Abstracts 2* 397 (1980).
- ¹⁰ M. F. Bocko, L. Narici, D. H. Douglass and W. W. Johnson, "A Proposed Action Evading Read-Out for a Gravitational Wave Detector," *Physics Letters*, **97A**, 259 (1983).
- ¹¹ D. Blair, *Physics Letters*, **91A**, 197 (1982).
- ¹² W. C. Oelfke, G. Spetz and W. O. Hamilton, *Bull. Am. Phys. Soc.*, **26**, 1215 (1981).
- ¹³ K. S. Thorne, C. M. Caves, V. D. Sandberg, M. Zimmermann, and R. W. Drever, "The Quantum Limit for Gravitational-Wave Detectors and Methods of Circumventing It," in *Sources of Gravitational Radiation*, ed. L. L. Smarr (Cambridge Univ. Press, Cambridge, 1979), pp. 49-68.

- ¹⁴ W. C. Oelfke and W. O. Hamilton, *Review of Scientific Instruments*, **54**, 410 (1983).
- ¹⁵ G. Spetz, A. G. Mann, W. O. Hamilton, "Experimental Verification of a Single Transducer Back-Action Evading Measurement Scheme for Gravitational Wave Detector," *Physics Letters*, **104A**, 335 (1984).
- ¹⁶ D. G. Blair, in *Gravitational Radiation*, ed. by N. Deruelle and T. Piran (North-Holland, Amsterdam, 1983) pp. 339-385.
- ¹⁷ K. Tsubono, M. Ohashi and H. Hirakawa, "Parametric Transducer for Gravitational Radiation Detector," *Japanese Journal of Apply Physics*, **25**, 622 (1986).
- ¹⁸ M. F. Bocko and W. W. Johnson, "Phase-Sensitive Parametric Motion Transducer," *Physics Review*, **30A**, 2135 (1984).
- ¹⁹ M. F. Bocko, W. W. Johnson and V. Iafolla, "A RF Superconductive Electromechanical Transducer for Gravitational Wave Antennae," *IEEE Transactions on Magnetics*, **25**, 1358 (1989). When Equation 9 of this reference is corrected for a numerical error, it becomes Equation 2.10 above.
- ²⁰ H. H. Skilling, "Network Equations," chapter 8 in *Electrical Engineering Circuits*, 2nd ed. (John Wiley, New York, 1965).
- ²¹ W. W. Mumford, "Some Notes on the History of Parametric Transducers," *Proceedings of the IRE*, **48**, 848 (1960).
- ²² J. M. Manley and H. E. Rowe, "Some General Properties of Nonlinear Elements -- Part I. General Energy Relations," *Proc. IRE*, **44**, 904 (1956).
- ²³ Twenty years before Manley and Rowe's paper Hartley, another electrical engineer of Bell Labs., had already observed the validity of the second relation for the (-) interaction (R. V. I. Hartley, "Oscillations in Systems with Non-Linear Reactance," *Bell Sys. Tech. J.*, **15**, 424 (1936).
- ²⁴ P. Langevin, "Sur la théorie du mouvement Brownien," *Comptes Rendus Acad. Sci.*, **146**, 530 (1908).
- ²⁵ H. Nyquist, *Phys. Rev.*, **32**, 110 (1928).
- ²⁶ F. E. Terman, "Properties of Resonant Circuits," chapter 3 in *Radio Engineering*, 2nd ed. (McGraw-Hill, New York, 1932).

- ²⁷ H. H. Skilling, "Resonance," chapter 6 in *Electrical Engineering Circuits*, 2nd ed. (John Wiley, New York, 1965).
- ²⁸ O. D. Aguiar, "Computational Model for the LSU GRD Seismic Isolator Stacks," Tech. Memo. #44, Gravitational Radiation Group, LSU, Feb. 1986.
- ²⁹ D. Middleton, *An Introduction to Statistical Communication Theory* (McGraw-Hill, New York, 1960).
- ³⁰ F. Reif, *Fundamentals of Statistical and Thermal Physics* (McGraw-Hill, New York, 1965).
- ³¹ P. R. Saulson, "Thermal Noise in Mechanical Experiments," *Physical Review*, **D42**, 2437 (1990).
- ³² H. W. Ott, *Noise Reduction Techniques in Electronic Systems* (John Wiley & Sons, New York, 1976).
- ³³ M. J. Buckingham, *Noise in Electronic Devices and Systems* (Ellis Horwood Limited, New York, 1983).
- ³⁴ This operator will present a peak, if f is negative, only for small values of β . For large values of β , this operator will present a depression as in the positive f case.
- ³⁵ A. D. Whalen, *Detection of Signals in Noise* (Academic Press, San Diego, 1971).
- ³⁶ W. B. Davenport, Jr., *Probability and random processes* (McGraw-Hill, New York, NY, 1970).

CHAPTER 3 - DESIGN AND CONSTRUCTION OF A NIOBIUM CAPACITOR RF BRIDGE PARAMETRIC TRANSDUCER

This chapter describes the design and construction of the transducer as well as the hardware built to perform the experimental runs.

A) Design

The task of making a three-plate capacitor with high mechanical and electrical Q is challenging. After various designs, we arrived at the final product by following a few guidelines:

- the mechanical pick-up capacitor would be made of high purity niobium (Nb);¹
- all electrical components (inductors, capacitors, wires, coaxial cables) would be made of high purity niobium;
- the three-plate capacitor would be as symmetrical as possible, so the push-pull configuration of a springy central plate facing two equal side plates was adopted;
- the electrical insulation between all three plates would be achieved by high mechanical Q plastic washers which also would fix the distance between them;
- the bridge circuit, with the motor adjustment, would not be at the same stage as the three-plate capacitor to minimize mechanical excitations during adjustment and guarantee a good mechanical Q for the transducer;
- the niobium wiring would have a large diameter to avoid microphonics;
- because of very low dielectric loss tangent², teflon would be used for the inductor cases, transformer mounting, coaxial dielectric, and, if it is proven to have a good mechanical Q, for making the plastic washers for the three-plate capacitor;

- the entire niobium circuit would be protected from external electrical noise by niobium shielding.

In Fig. 3.1 the three-plate capacitor plus shielding box can be seen. A gap of 50 μm was provided between the middle plate and each side plate by sixteen mylar washers,³ and a 1mm gap between the side plates and the shielding box by another sixteen 1mm thick sapphire washers. Eight titanium studs 6 mm in diameter fasten the "sandwich" assembly horizontally to a 5056 aluminum alloy plate electrically accelerated for calibration purposes.

The middle plate has four built-in beams as springs. Therefore, the central circular part of this plate can oscillate if the rim is firmly attached. In order to have this mechanical oscillation in the 915-950 Hz range, a few experiments were done with aluminum plates to properly design the correct dimensions. The side plates, as mentioned before, are kept a fixed distance from the middle plate by mylar washers. These mylar washers are placed on the surface centered over each hole. A 1mm depression was provided on the side plates just between the area where the mylar washers were placed and the central core in order to maximize the percentage of the capacitor that would act as transducer pick-up. For the present design 56.8% of the capacitance was entirely used for the transducer and 39.4% was non-variable capacitance (of which 28.4% had mylar as dielectric). The area occupied by the springs accounts for the remaining 3.8% of capacitance.

The aluminum flange, to which the transducer box is bolted, is both a vibration isolation stage and part of the calibration capacitor. It is a single piece made of 5056 aluminum alloy with two major sections: the core and the rim. The core has a base with eight holes and cavities for bolting the transducer. On the top, the core has

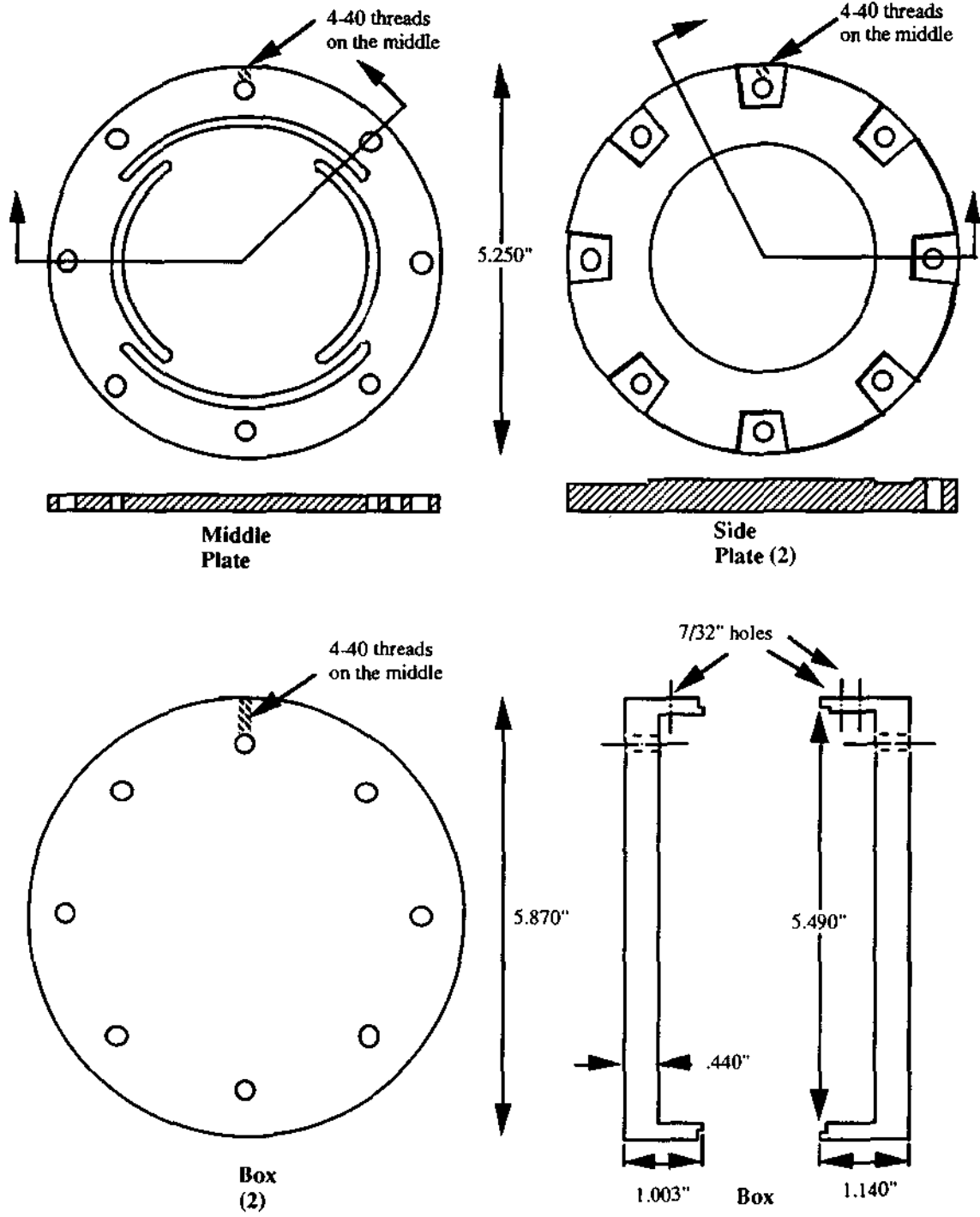


Fig. 3.1 - Three-plate capacitor and shielding box

a circular 2.75" diameter flat island and a 1.25" wide, 0.5" deep annular depression around it. This core is connected to an outside rim by springs similar to those in the transducer middle plate but much longer, and this rim is connected to the last stage of a "taber" isolation stack (see "test cryostat" section in this chapter) by titanium wires 0.030" in diameter. The stiffness of these aluminum springs were designed,^{4,5,6} so that if the rim was firmly attached, the transducer box plus aluminum flange core (a total mass of 8.2 kg) would oscillate at a frequency of about 33 Hz. The circular island on the top of the aluminum flange faces a horizontal aluminum plate, similar to the transducer middle plate, which has its rim rigidly attached by a set of nylon bolts and nuts to the last stage of the "taber" isolation stack. A distance of one-half inch is kept between the aluminum plate and the "taber" stage. The springs were machined in order to make this aluminum plate resonant in the 300 Hz vicinity, and, therefore, to be a free mass for the transducer. The gap between this plate and the flange flat island can be adjusted at the nylon bolts. The geometry is such that more than half of the entire capacitance of this plate with the outside world is just the capacitance of its "free" central portion with the aluminum flange island (a precise value of this capacitance will be given in chapter 5). This capacitor was used to mechanically excite the transducer with a known signal. There was also a PZT sensor glued to one of the flange's built-in springs. This PZT was used for non-calibrated excitations and as a vibration sensor during motor adjustment.

The bridge circuit is housed inside a niobium rectangular box which is firmly attached to the second "taber" stage above the aluminum flange (see "test cryostat" section in this chapter). This box is formed by six 3/16"- thick niobium rectangular plates 4.25" long and 2" wide. All six pieces are bolted together, forming a sandwich, by eight titanium bolts and five brass bolts. Fig. 3.2 shows the internal cavities of the box which were machined in the four central plates. The front plate has holes instead

of cavities for insertion of niobium rods, and the rear plate has two tiny holes for outside connection between the circuit's middle branch and the transformer grounding point.

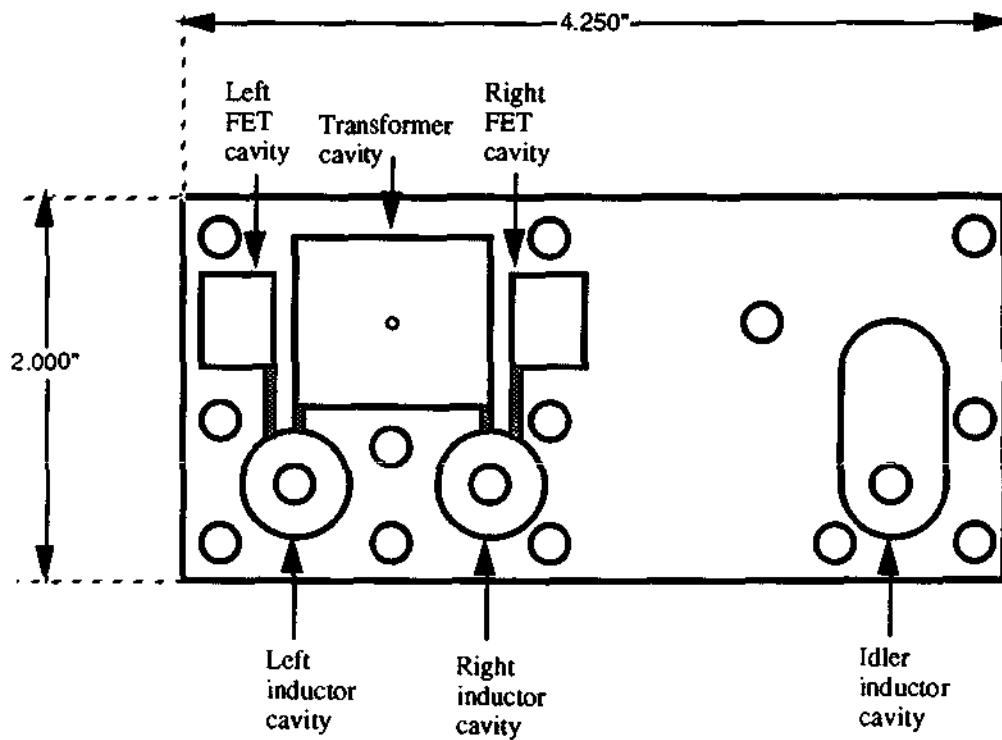


Fig. 3.2 – Bridge shielding box.

An extra niobium grounding sheet covers the grounding connection on the rear.

The transformer cavity is cubic, to house a toroidal transformer. All the other inductors are solenoids inside cylindrical cavities. These cavities have a hole at one end to let a 3/16"- diameter Nb rod penetrate in.

We designed the left, right, and idler solenoidal inductors using the following procedure:

- we built the toroidal transformer and measured, with an HP 4192A impedance analyzer, its total and partial inductances (the coupling was derived from these measurements);
- we measured the four major capacitances of the three-plate capacitor, and the inductances of the Nb coaxes linking the three-plate capacitor to the bridge box;
- using PSPICE,⁷ we tried different values for these solenoids using all the measured parameters in order to have the outer loop and inner loop resonances at 5 MHz;
- we tested different solenoids inside the bridge box until we obtained the desired inductances.

The internal radii of the solenoids for inductance adjustment were kept just a little bigger than the 3/16"- diameter Nb rods, so when they were completely inserted the solenoids would have their inductances reduced to about 60% of their maximum values.

The MESFET coils for resistance balancing were designed taking into account the minimum transistor resistance at 4.2 K, the range of values for the right and left solenoids, the estimated coupling between the coil connected to the transistor and the solenoid, and the measured resistance imbalance observed in previous runs. The transistors used for this purpose were Fujitsu FSC10FA, which presented a typical 23 Ω resistance between drain and source at 4.2 K.

The electrical continuity between the bridge box and the three-plate capacitor is made by three niobium-teflon coaxial cables. The bottom plate is connected to the left inductor, the middle plate to the idler inductor and the top plate to the right inductor (details of these connections will be given in the section B). In the original

design there was an extra adjustable capacitance linking the right branch to the idler branch inside the bridge box, but it was abandoned in favor of a fixed-value capacitor placed next to the three-plate capacitor. This second design had the advantage of simplicity and reliability, but it could not balance the bridge at all frequencies. Because we were only able to adjust the bridge inductively and resistively, a perfect balance cannot be maintained at more than one frequency.

The cryogenic amplifier circuit design was inspired by a British version used in NMR detection⁸, that had a noise temperature of (1.3 ± 0.4) K below 77 K at 5 MHz. The component values were changed to maximize power gain, to minimize noise, and to decrease power dissipation. Its circuit is shown in Fig. 3.3. The voltage gain was approximately 1 when cold, but the power gain for the 50Ω input room temperature amplifier was $\sim 2k$. The power dissipation was about 5 mW for 5.3 V bias voltage, as designed. The two FET transistors were GaAs Plessey P35-1101-101. We specifically used the characteristics of a similar device,⁹ the P35-1101-1, to design this amplifier.¹⁰

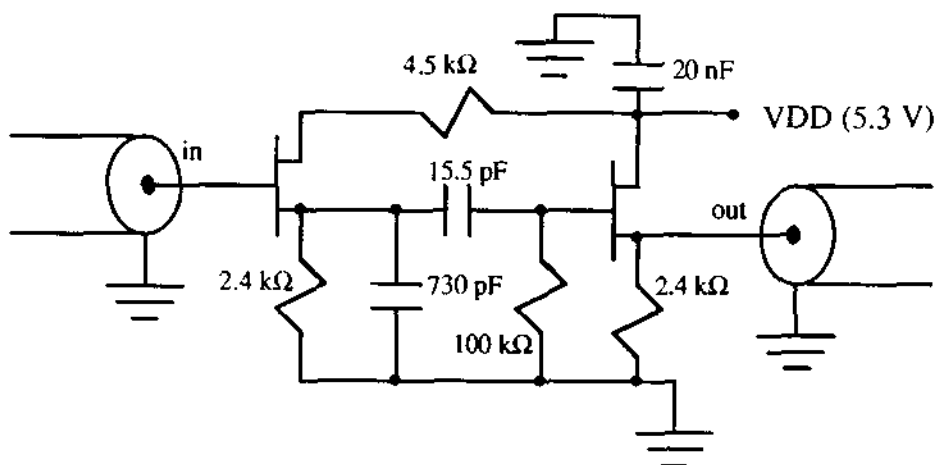


Fig. 3.3 – Cryogenic Amplifier.

B) Construction

With very few exceptions the equipment of the whole experiment was built from scratch: not only the transducer, but the experimental cryostat, the "taber" isolate system, the pump station, the cryogenic amplifier, and the calibrating capacitor. In this section we present details of the transducer construction.

Fig. 3.4 shows the schematic setup of the experiment. The experimental can is 60 cm long and 30 cm in diameter. Most of the pieces that took part in this experiment were machined in the LSU Physics Department machine shop from my blueprints. Some of them, however, were modified later or completely machined by myself in the student shop.

After having been machined, each plate of the three-plate capacitor was polished with sandpaper, starting with number 400 and going all the way to 1 μm silicon carbide-coated film from Moyco Industries (Ultralap film). Then all pieces were cleaned in ultrasound with trichloroethane 1-1-1. The transducer assembly was done in a class 100 clean bench. First, all the superconductive surfaces to be connected were immersed for about fifteen seconds in a solution of equal parts of deionized water, nitric acid at 70.6%, and hydrofluoric acid at 48%, in order to break the oxide layer. After rinsing, each wire end was pressed against one Nb disc by the head base of a 4-40 titanium screw. When this operation was completed, all discs were ready for assembling. Three especially important precautions were taken:

- the 6 mm titanium bolts could not touch any of the three internal plates;
- the presence of dust particles should be avoided on any surface, and especially inside the two 50 μm gaps;

- all washers (mylar or sapphire) should be centered to the holes of the discs and box as precisely as possible.

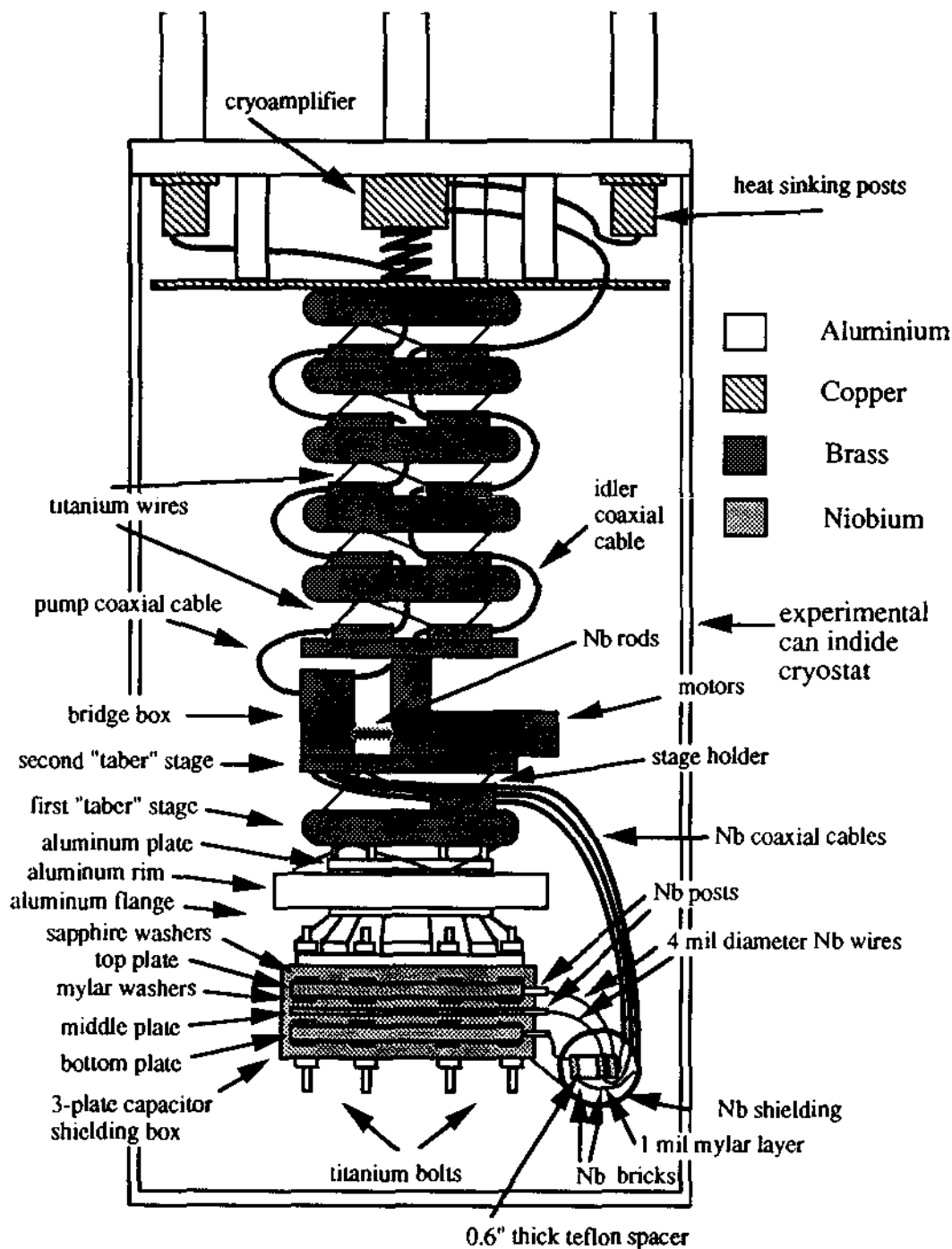


Fig. 3.4 - Setup inside the cryostat's experimental space.

The wires connected to each of the three plates went through 7/64" holes on the shielding box in order to be connected outside to the external wiring. This procedure was repeated a few times to test different thicknesses of mylar washers and a different Nb central disc. However, this configuration was abandoned after one of these wires broke inside the shielding box during the preparations for a run that was going to test the whole transducer. To redo the three-plate capacitor at this point was risky because it could ruin the already achieved 1.3×10^5 mechanical figure of merit, probably the highest we could get using mylar washers. In order to solve this problem, I decided to try a solution that would be electrically reliable, mechanically feasible, and that would avoid having to reassemble the three-plate capacitor (tpc). We increased the 7/64" holes in the shielding box to 7/32" in diameter, removed the small 4-40 titanium screws and all the machining bits from the inside, screwed one Nb post to each of the internal plates using the 4-40 threaded holes left there. This was the configuration used for all the remaining four test runs.

To each of these Nb posts a 4 mil diameter wire one inch long was connected using the above-mentioned superconductive joint procedure. The other end of these wires was screwed to Nb bricks, also by superconductive joints. Then each of the Nb coaxial cable inner conductors, which were 0.031" in diameter, were connected in the same way to the three bricks. Two of these bricks were separated by a mylar film 0.92 mil thick. This extra capacitance (~ 100 pF) was necessary to bring the two tpc capacitances closer in absolute value. The third brick was 0.6" away. A teflon block kept that distance constant. The small wire transition mentioned above was necessary to mechanically decouple the three-plate capacitor from the external wiring as much as possible.

The ground connection was made by a 4 mil diameter wire that started on the bottom half of the box, went to the top half, and then to a Nb open box that was embracing the three Nb coaxial shieldings. The interior of this Nb open box was a cylindrical 1.8" diameter internal cavity which housed the three Nb bricks and their respective wiring. This open Nb box has a pentagonal external shape whose opening faces the three-plate capacitor, but does not touch it. The function of this box is to shield the external capacitor and the weak mechanically coupled wiring leaving the three-plate capacitor. All the grounding connections were superconductive joints made by the process mentioned above. Wherever it was difficult to apply the acid solution to remove the oxide layer, an oxide free Nb blade was used to scrape it.

At two "taber" stages above the three-plate capacitor, the three Nb coaxial cables leave the base of the bridge box. A superconductive connection between the bridge box and the Nb coax outer conductor was made by peeling the outer conductor into three strips of the coax and pressing them against the outside box surface using a circular brass disc with a hole in the middle for the coaxial cable body. Three brass screws were used for each connection. Each of these screws was placed in the interval between two consecutive strips.

The transformer's secondary inside the bridge box was a toroidal coil made with a single 0.031" diameter Nb wire electrically insulated by 20-gauge teflon tubing. This wire was guided by a teflon block with one hole in the middle for the primary, 20 holes forming a circle of 0.210" radius and 20 holes forming another circle of 0.390" radius. The Nb wire used every other hole to do ten turns in the first rotation and another ten turns in the second rotation. This procedure guaranteed a very symmetrical transformer for both circuit branches and a good coupling coefficient between the two halves ($k=0.56$). The grounding point was halfway between the end

of one rotation and the beginning of the next one. First, this wire section went through a tiny hole in the box wall to meet one end of the idler inductor solenoid. There, both wires were plasma-welded together,¹¹ and this welded joint was pressed against a Nb sheet grounded to the shielding box (electrical Qs as high as 20 k at 5 MHz were observed using plasma welded joints).

The idler inductor, as well as the right and left inductors were solenoids housed inside teflon cases to keep them from springing out. Nb rods were free to move in and out of these solenoids. The mechanism used to transform the motor-gearbox rotation into a translational movement for the rods was very simple. A long brass hollow cylinder was firmly attached at one end to the gearbox axle. Its other end had a 2-56 threaded hole in which a long steel 2-56 screw was inserted. Because this screw's rotation was impeded by a pin guided in a groove parallel to the screw, the only movement allowed was the translation along its axis. Each Nb rod was attached to one of these screws, so they followed the same movement. The typical rod speed for 10 mA of current running in one motor was about 1 mm / minute.

The MESFET transistors for resistance balancing were housed in the bridge box inside teflon pads. Two five-turn 275 nH copper coils were facing the end of each side inductor (right and left ones). Each of these coils were connected to the drain and source of one transistor. The voltage control between gate and drain was sent by two copper semi-rigid coaxial cables, one for each transistor. These cables were not grounded to the bridge box.

The pump (or generator) signal was sent down to the bridge box by two twisted semi-rigid coaxial cables. In the final three runs, the inner conductor was passed through the transformer central hole four times before joining the other cable

inner conductor (for one run, we tried 13 turns for the transformer primary). The bridge box had two tiny holes to allow the cable inner conductor to penetrate the transformer. There was electrical continuity between both cables' outer conductors, but again there was no ground connection between them and the bridge box. The only ground connection was made by the copper semi-rigid coaxial cable carrying the idler signal to the cryogenic amplifier on the top of the "taber" stacks. The grounding connection between this copper coaxial cable and the bridge box was done in the same way it was done for the Nb coaxial cables.

The cryogenic amplifier shielding box was a hollow copper cylindrical box to which three soldered copper semi-rigid coaxial cables were connected. One brought the idler signal to the amplifier input, another sent the output to the top of the cryostat feedthrough, and the third was used for amplifier biasing. This copper box was pressed against the top of the experimental can by a strong spring for good thermal contact. A thermal grease, "Cry-con" from APD Cryogenics, was used for thermal contact enhancement. A paper on the top of the box and a teflon pad on the bottom prevented the box from being electrically grounded to the cryostat. The transducer grounding point was on the top of the cryostat, and only the idler coaxial cable was connecting this point to the transducer.

All the resistors used in the cryogenic amplifier were of metal film. The capacitors were silver mica, which maintained their values of capacitance at 5 MHz when cooled to 4.2 K. The circuit was soldered on a printed board with an extra ground plane. All ground regions were soldered to the copper shielding box. Both Plessey transistors were thermally grounded to this copper box with copper tape. Table 3.1 gives information about all the niobium pieces used in this experiment.

| Part | Purity (%) | Manufacturer | Type of annealing after machining | | | |
|---------------------------|---------------|---------------|---|-------|---------------|----------|
| 31 mil wire | 99.75 | Supercon | 750 °C @ 5 E-7 torr for 2 hours | | | |
| bricks | 99.83 | Wah Chang | 790 °C @ 2 E-5 torr for 2 hours | | | |
| 4 mil wire | 99.8 | Supercon | annealing not revealed (inert gas type) | | | |
| posts | 99.83 | Wah Chang | 790 °C @ 2 E-5 torr for 2 hours | | | |
| 3-plate cap. | 99.85 | Cabot | 925 °C @ 2 E-7 torr for 1 hour | | | |
| bridge box | 99.83 | Wah Chang | 790 °C @ 2 E-5 torr for 2 hours | | | |
| rods | 99.83 | Wah Chang | 790 °C @ 2 E-5 torr for 2 hours | | | |
| tubing | 99.8 | Uniform Tubes | none | | | |
| pentagon | 99.75 | Wah Chang (2) | none | | | |
| tpc box | 99.86 | Fansteel | none | | | |
| Chemical Element (in ppm) | Material from | Supercon | Wah Chang | Cabot | Wah Chang (2) | Fansteel |
| Al | | | < 20 | < 10 | < 20 | < 20 |
| B | | | < 1 | < 1 | | < 1 |
| C | | 60 | < 30 | 20 | 40 | < 10 |
| Ca | | | < 20 | < 10 | | < 20 |
| Cd | | | < 5 | | | < 5 |
| Co | | | < 10 | < 10 | | < 20 |
| Cr | | | < 20 | < 10 | < 20 | < 20 |
| Cu | | | < 40 | < 10 | < 40 | < 20 |
| Fe | | < 50 | < 50 | 45 | < 50 | < 20 |
| H | | < 5 | < 5 | < 5 | < 5 | < 5 |
| Hf | | < 50 | < 50 | | < 50 | 100 |
| Mg | | | < 20 | < 10 | | < 20 |
| Mn | | | < 20 | < 10 | | < 20 |
| Mo | | < 50 | < 50 | < 10 | < 50 | < 20 |
| N | | 36 | 8 | 20 | 23 | 36 |
| Na | | | | * | | |
| Ni | | < 20 | < 20 | < 10 | < 20 | < 20 |
| O | | < 50 | < 50 | 50 | 80 | 84 |
| P | | 28 | < 25 | | < 30 | |
| Pb | | | < 20 | | | < 20 |
| Si | | < 50 | < 50 | 10 | < 50 | < 20 |
| Sn | | | < 10 | < 10 | < 10 | < 20 |
| Ta | | 1760 | 950 | 975 | 1670 | 600 |
| Ti | | | | < 10 | < 40 | < 20 |
| Tl | | | < 40 | | | |
| V | | | < 20 | | < 20 | < 20 |
| W | | 39 | 38 | < 100 | 57 | 100 |
| Zr | | < 100 | < 100 | < 10 | < 100 | < 20 |

* not detected

Table 3.1 - Composition of niobium parts. The material from Wah Chang has a residual resistivity ratio between room temperature and 4.2 K equal to 304.

C) Test Cryostat

Fig. 3.5 gives a schematic view of the hardware arrangement. The structure supporting the test cryostat is a metal framing (Unistrut) structure composed of channels bolted together. Because this structure is attached to the ceiling, the space around the cryostat is completely free. Four aluminum channels, bolted on the base of the structure, support a set of four cylindrical air legs and four air reservoirs that, together with a 90 kg aluminum plate 1 m x 0.8 m and 5.5 cm thick, act as a vibration isolation air table for the cryostat. The total mass supported by the air table including all the experimental apparatus was about 370 kg. This air table, model 71.401 manufactured by Lansing Research Corporation, has a transmissivity of less than 1.6 at 1.1 Hz resonant frequency and a -12 dB / octave drop in transmissivity above this frequency. Vibration measurements were taken in all three floors of the Nicholson Hall extension building. The second floor, used for physics library overflow, was the quietest one as long as nobody was walking there. Attaching the experiment to this floor was, therefore, considered adequate.

On the top of the cryostat there were two sets of electrical feedthrough bases in the shape of lollipops. One side of each lollipop was free from feedthroughs and could be removed in order to repair or change an electrical connection on the other side. Due to electrical noise considerations¹² these lollipops were carefully grounded to the building's metallic structure via the channel frame. The leads going down from the lollipops to the experimental can were either a UT 85-SS (semi-rigid coaxial cable) or a twisted pair made with a 5 mil diameter high resistance wire (around $38 \Omega / \text{meter}$). They were heat sunk on the top of the experimental can before going to the "taber" isolation stack.

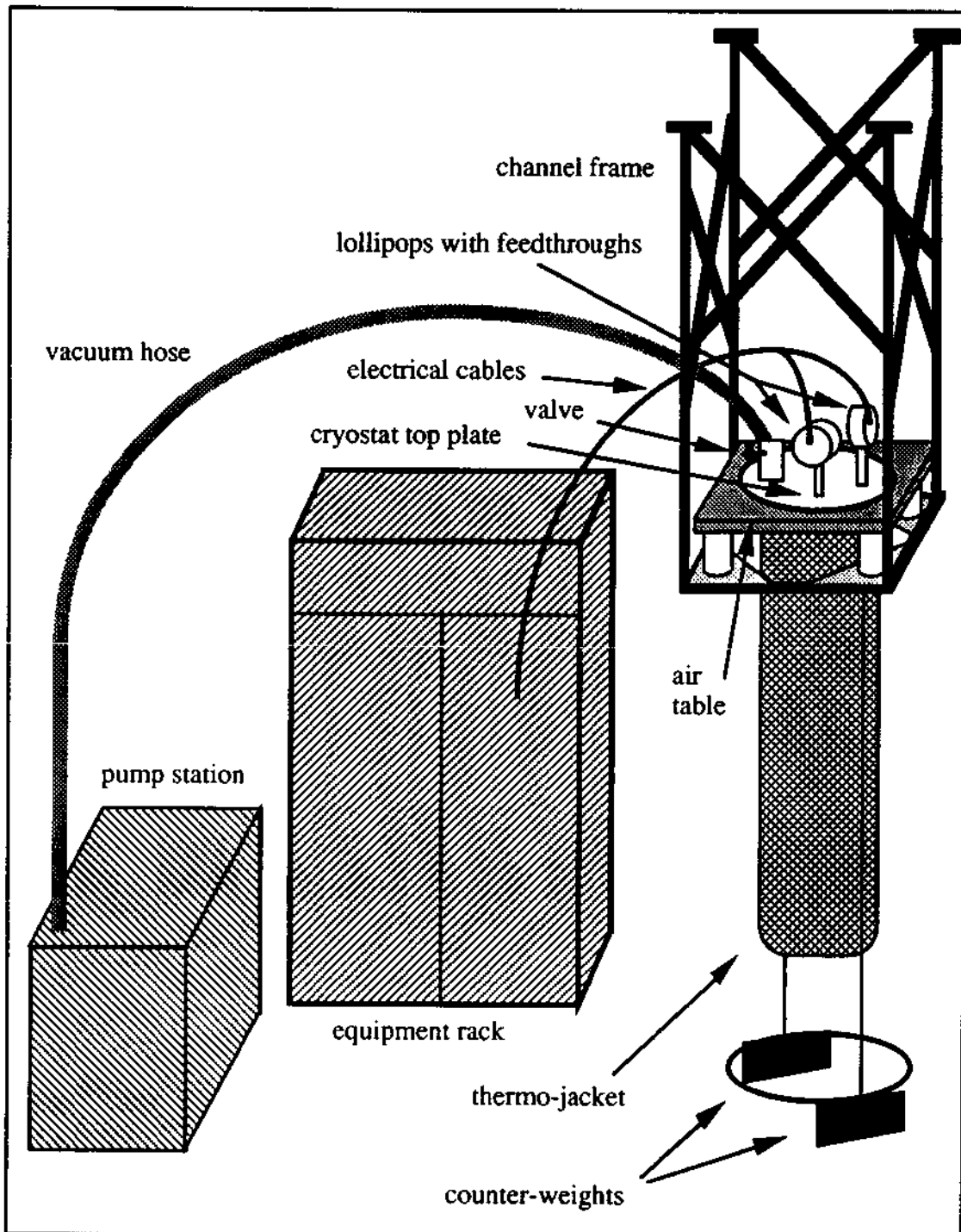


Fig. 3.5 - Hardware arrangement.

The vibration isolation system was composed of three parts. The first one, already mentioned, consisted of an air table supporting the cryostat top plate. This air table caused displacements at frequencies f above $f_0 = 1.39 \text{ Hz} (= 1.1 \text{ Hz} \times \sqrt{1.6})$ to decrease by the factor $= (f / f_0)^2$. The second part of this vibration isolation system, referred to in this text as a "taber" stack after its inventor,¹³ was a set of cylindrical brass masses connected by titanium wires and arranged in the form of a stack. All the leads going down to the transducer were mechanically grounded to each of these stages. The wire diameter was chosen, in the present design, in order to have its first transverse string resonance above 1500 Hz. This choice would still keep the tension in each wire at least 1/3 of the yield. Of course, a higher resonance could be obtained by decreasing the wire thickness, but this would compromise the safety of the apparatus by working too close to the yield strength. Furthermore, we were already using one of the toughest wires available in the market, made of a 6% Al - 4% V - Ti alloy with a minimum yield strength of 84 kg /mm². This "taber" stack, seen in Fig. 3.4, has seven stages. The maximum performance of these stages was degraded because we needed to use a total of five semi-rigid coaxial cables in order to avoid electrical noise in the MHz region. The third and last part of this vibration isolation system is the high Q aluminum flange built-in springy arms with an attenuation factor equal to $(f / f_3)^2$ (where $f_3 = 33 \text{ Hz}$ and f is any frequency above this value). Fig. 3.6 shows the theoretical total transmission expected from this vibration isolation system assuming the Voigt model discussed in Chapter 2. The actual transmission is probably a factor of 1000 or so bigger than this. Therefore, for external vibrations at the transducer mechanical resonant frequency 929 Hz, we expected a vertical attenuation of at least 280 dB, or fourteen orders of magnitude.

Every care was taken to avoid electrical ground loops inside the experimental can. The leads' heat sinking was electrically insulated.¹⁴ The 12"-diameter copper

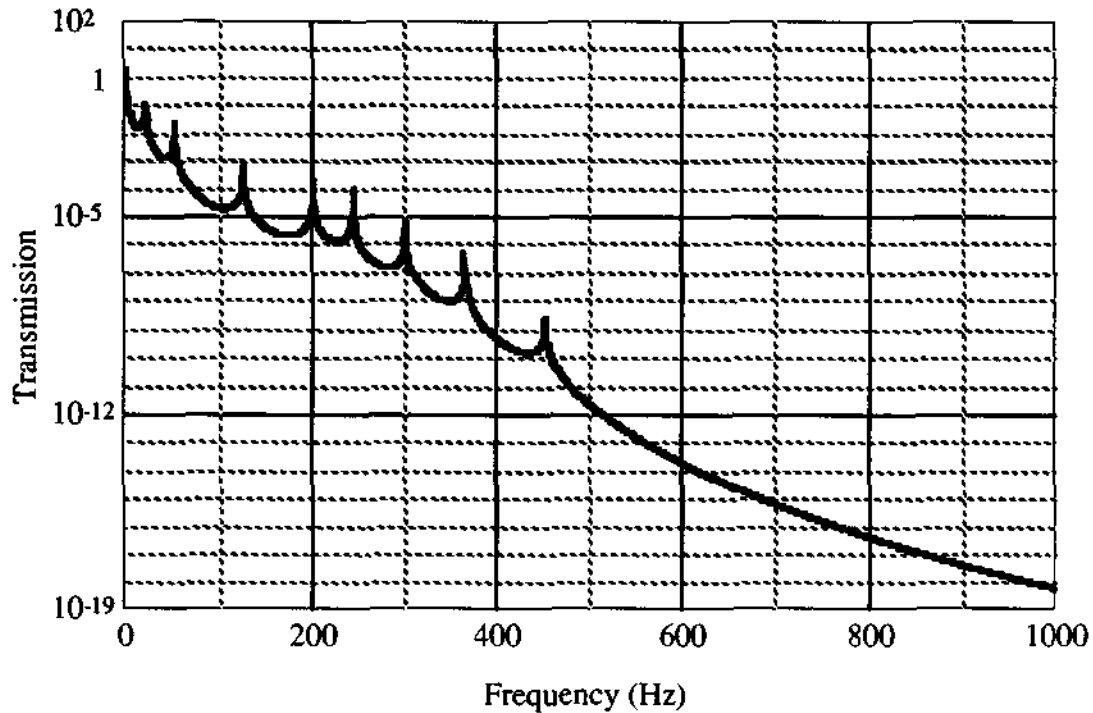


Fig. 3.6 – Vibration isolation performance (theoretical).

disc to which the "taber" stack is attached was also insulated from the cryostat. All the electrical leads were mechanically, but not electrically, grounded to each "taber" stage. In brief, the transducer was grounded to the building by and only by, the idler signal lead shielding.

The vacuum pump station for this experiment was composed of a 1402 Welch rough mechanical pump and a Varian HSA-150 type 159 diffusion pump equipped with a 3 liter liquid nitrogen cold trap and a 1400 Welch foreline mechanical pump.

Having described the design and construction of the transducer and test hardware we now move to Chapter 4 where we will discuss the experimental results and compare them with theoretical models.

D) References

- ¹ We did some experiments with vanadium to measure its mechanical quality factor (see appendix C). We did not observe a higher Q for a vanadium piece we tested in comparison with typical Qs for niobium.
- ² W. Meyer, in *Proceedings of the Sixth International Cryogenics Engineering Conference*, edited by K. Mendelssohn (IPC, Guildford, England, 1976).
- ³ A set of experiments (see Chapter four) testing different plastics for mechanical Q performance made the choice of mylar the most appropriate one.
- ⁴ W. C. Young, *Roark's Formulas for Stress and Strain* (McGraw-Hill, New York, 6th ed., 1989).
- ⁵ R. D. Blevins, *Formulas for Natural Frequency and Mode Shape* (Robert E. Krieger, Malabar, FL, 1986) (reprint).
- ⁶ W. E. Baker, "Vibration Frequencies for Uniform Beams with Central Masses," *Journal of Applied Mechanics*, **31**, 335 (1964).
- ⁷ PSPICE is an electronic circuit simulation software, and we used it in a Macintosh II computer.
- ⁸ M. G. Richards, A. R. Andrews, C. P. Lusher, and J. Schratter, "Cryogenic GaAs FET amplifiers and their use in NMR detection," *Review of Scientific Instruments*, **57**, 404 (1986).
- ⁹ D. V. Camin, G. Pessina, E. Previtali and G. Ranucci, "Low-Noise Preamplifiers for 1K Operation Using Gallium Arsenide MESFETs of Very Low 1/f Noise," *Cryogenics*, **29**, 857 (1989).
- ¹⁰ C. J. Savant Jr., M. S. Roden, G. L. Carpenter, *Electronic Circuit Design, An Engineering Approach* (Benjamin-Cummings, Menlo Park, 1987).
- ¹¹ With a PWM-6 plasma needle-arc welding machine from L-TEC in a closed chamber with inert gases.
- ¹² H. W. Ott, *Noise Reduction Techniques in Electronic Systems* (John Wiley, New York, 1976).
- ¹³ R.C. Taber, "Attenuation of Mechanical Vibrations in Wires," Tech. Memo., Stanford University, 1979.
- ¹⁴ In addition to the use of tiny spacers, the "Cry-con" high thermal conductive grease used in all heat sinks was tested and proved to be non-electrically conductive even at 5 MHz.

CHAPTER 4 - PERFORMANCE OF THE TRANSDUCER

In this chapter all the experimental results are presented, analyzed, and compared with theoretical models.

A) Runs

All the runs related to this experiment used either a small cryostat provided with a 57 cm long 18 cm diameter can or the cryostat described in Chapter 3 (upstairs cryostat), which has a 60 cm long 30 cm diameter experimental space. These runs were performed over a period of three years and three months.

The first liquid helium (LHe) run was done in the small cryostat to test an aluminum replica of the three-plate-capacitor. In this experiment we used kapton plastic washers and achieved a mechanical Q of 40 k. This run was followed by many tests of aluminum middle plates at room temperature. These experiments also showed that the chosen middle plate geometry (Fig. 3.1) always presented three fundamental resonances for the central core movement associated with its out-of-the-plate three degrees of freedom, a pure up-down oscillation plus two torsion oscillations. The lowest in frequency was the up-down oscillation or the so-called transducer mode, and the highest in frequency was the one associated with torsion around the axis to which the core presented the smaller moment of inertia.

The second overall run down to liquid helium temperatures was done in the upstairs cryostat. I wanted to measure the mechanical Q of different plastics. First I tried at room temperature six strips about 4-5" long and 0.1-0.15" wide. Two of them

were made of teflon FEP and PTFE, 10 mils and 5 mils thick respectively, one of kapton (5 mils), one of clear polycarbonate (20 mils), and two of different types of mylar. All strips were supporting weights to keep them under tension. The first fundamental string resonance was chosen in order to calculate mechanical Qs. I decided to start the run with the strongest samples, which were two 5 mil thick strips, one of mylar and the other of kapton. Each of them was supporting a 1.14 Kg weight. A PZT piezoelectric crystal was glued to an upside down 5056 aluminum T supporting the strings in order to detect the string resonances. The mylar strip was found to have a mechanical Q, in its first string mode at liquid helium temperature, of 6k, about four times the mechanical Q measured for kapton. The string mode frequencies were 958 Hz and 929 Hz respectively, and the only efficient way to excite them was to hit the top of the cryostat (no vibration isolation system was implemented for this run). In conjunction with this experiment, I measured the mechanical Q of a vanadium disc at 4.2 K; results for the vanadium disc can be found in Appendix A.

Four unsuccessful attempts to measure the mechanical Q of a niobium middle plate transducer mode at 4.2 K followed the second run. The reason for this failure was that the upstairs cryostat thermo jacket sprang a leak on the bottom of the inside space. The liquid (helium or nitrogen) was going into the evacuated space and degrading the vacuum. This caused an increase in the flux of heat from the laboratory to the liquid space, making it impossible to keep the experimental space at 4.2 K for a sufficient time to complete the measurements. An epoxy was tried to close the leak, but with no success. Finally a fifth run was carried out using a thin layer of frozen water on the bottom. It worked amazingly well in plugging the leak, allowing us to measure the niobium middle plate Qs. The three out-of-plane resonances were at frequencies 805.26 Hz (transducer mode), 911.74 Hz (high moment of inertia torsion mode), and 982.08 Hz (low moment of inertia torsion mode). The transducer mode had

a Q of only 2.8×10^5 , raising the possibility of energy dissipation in the wire suspension. In all these five runs we were using the previously established resonances of the vanadium disc as a temperature indicator. A 6"x6"x2" 5456 aluminum alloy bloc suspended by a 0.03" dia. 5056 Al wire was also inserted in the can for Q measurements. The best mechanical Q measured for this 5456 aluminum bloc was 6.8 M for the (i,j)=(2,2) mode¹ at 8514.62 Hz.

Nine runs were carried out in order to complete the three-plate-capacitor plus shielding box final assembly. All of them were executed in the small cryostat during a total period of four months. We tried different types of spacers (alumina, sapphire, and different types of mylar) and niobium middle plates. In eight of the runs the three-plate-capacitor was vertically suspended by two steel music wires around the ends of one of the 6 mm dia. titanium bolts used for transducer assembly. In the final run, however, the transducer was bolted horizontally to an aluminum flange which was attached with titanium wires to a set of two "taber" stages. This flange together with the two "taber" stages was acting as a small vibration isolation system (for details of the flange and "taber" stages please see Chapter 3).

The three first runs went only down to liquid nitrogen temperatures. A short in the 0.002" gaps of the three-plate-capacitor prevented us from proceeding further. Because these plates were made from a rolled niobium disc bought from Cabot with no posterior annealing for stress relieving, these plates were bending when cold. In particular, the middle plate was bending enough to touch both side plates. Fourth and fifth runs using thicker spacers (1 mm sapphire and 0.005" gap) did not show any short up to 4.2 K, confirming this hypothesis. We corrected this problem by heat treating the niobium central plate in Norbert's furnace at 925 °C in a vacuum of 2×10^{-7} torr for one hour. After this was done no shorts in the capacitor were found for gaps as

small as 50 μm down to 4.2 K. However, this annealing caused a problem (see bridge balancing in this chapter) realized only when we tested the full transducer set up. The stress relieving produced a permanent bending that unbalanced the capacitances by 7.5 % (there was only about 1.5 % difference before annealing). This imbalance could be prevented if the middle plate was polished after annealing. This set of runs ended with a successful mechanical Q measurement (1.33×10^5) using 0.002" (50.8 μm) thick mylar (type EL) washers.

After having defined the transducer final form, we proceeded to the measurement of other parameters such as the circuit electrical Q, bridge balancing, etc. The upstairs cryostat was fully wired, the "taber" system was installed, and the bridge circuit was coupled to the transducer. We started this new set of runs in June of 1989 and initially we had the following major problems:

- in the first run we were unable to find at 4.2 K any resonance associated with the circuit;
- the dewar sprang the same leak that occurred in the second run (even using the ice plug);
- we replaced the thermo jacket with a new one,² but the transfer line showed a very bad heat leak, making it impossible to collect enough liquid helium inside the dewar;
- we fixed the transfer line and executed the fourth run, then learned that the bridge circuit probably had a short somewhere.

After making changes in the transducer (described in Chapter 3), such as

- using a fixed capacitor next to the t-p-c for capacitance balancing,
- screwing three posts to each t-p-c plate, and
- adding a pentagon shape niobium open box shielding the external t-p-c connections,

we started to obtain very good results. The four runs that followed these changes supplied us with all the significant data that is worth publishing.

This last four-run set was carried out from March 27 to August 1, 1990. They basically differ from each other only by the number of turns in the primary circuit, by the replacement of bad resistance balancing FETs-coil units, and by the reinforcement of a superconductive joint with the use of plasma welding. The first of these runs used thirteen turns in the transformer primary; all the others used only four turns. In the last run we replaced the resistance balancing FETs-coil units, and also enhanced the transformer middle branch connection with an inert gas plasma welding joint. The final results of these four successful runs are presented, analyzed, and compared with theory in the next few sections of this chapter.

B) Experimental Results

a) Bridge Tuning and Balancing

We measured the voltage across the parabrige's idler inductor as a function of frequency for different conditions of tuning and balancing, and compared these results with the theoretical calculations derived from the equations of the electrical bridge circuit. Finally, we examined the theoretical conditions for bridge balance and tried to implement them in practice. Results were again compared with theory, and the residual capacitance imbalance and the noise leakage from the outer loop were determined.

The transducer circuitry has two electrical resonances: the outer and inner loop resonances. They were used to enhance the pump and idler signals, respectively. Fig. 4.1 shows these two resonances (b) and the equipment diagram to measure them (a). The dots are the voltages, measured with a PAR 5202 lock-in amplifier, divided by the amplification chain and by the generator voltage, and the solid line is the best fit using the loop equations 2.3 and 2.5 of the circuit shown in Fig. 2.1 with expected values for the electrical components. Notice the two resonance circles in the complex plane plot. The higher frequency resonance in this figure, which is the inner loop resonance, had an electrical Q of about 2 k. The motor adjustment of the idler inductor allowed us to tune the inner loop resonance between 4.9 MHz and 5.1 MHz; unfortunately, we were not able to do the same with the outer loop resonance. The motor adjustment of the side inductors could balance the bridge, but not tune the outer loop resonance above 4.98 MHz, which prevented our fully pumping the capacitor when we were using the 5 MHz extremely low phase noise crystal oscillator.

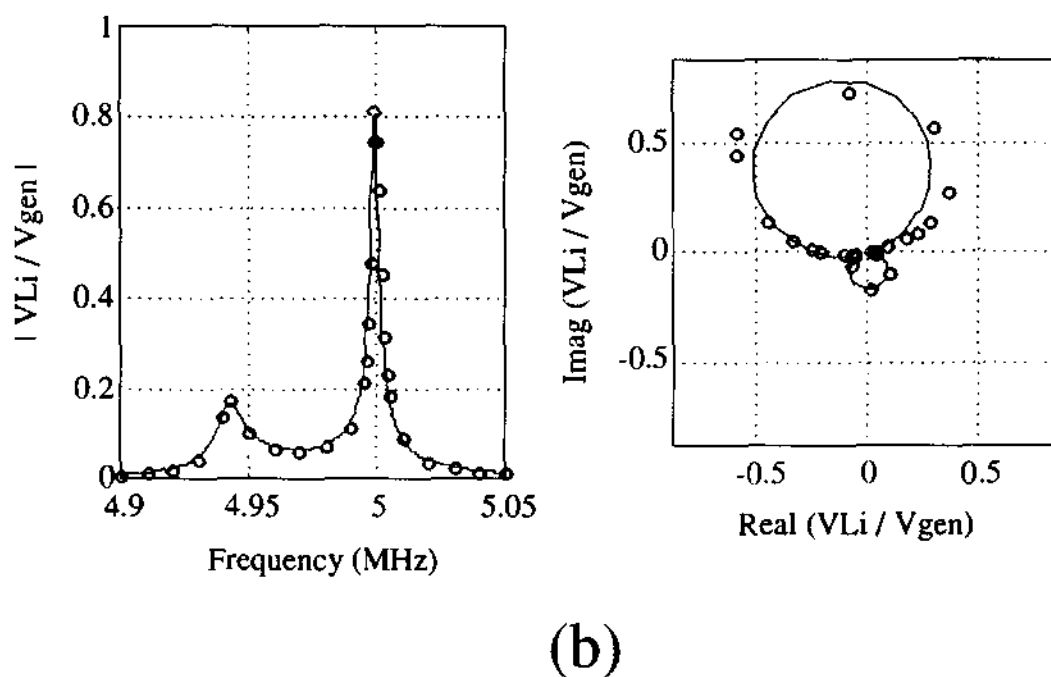
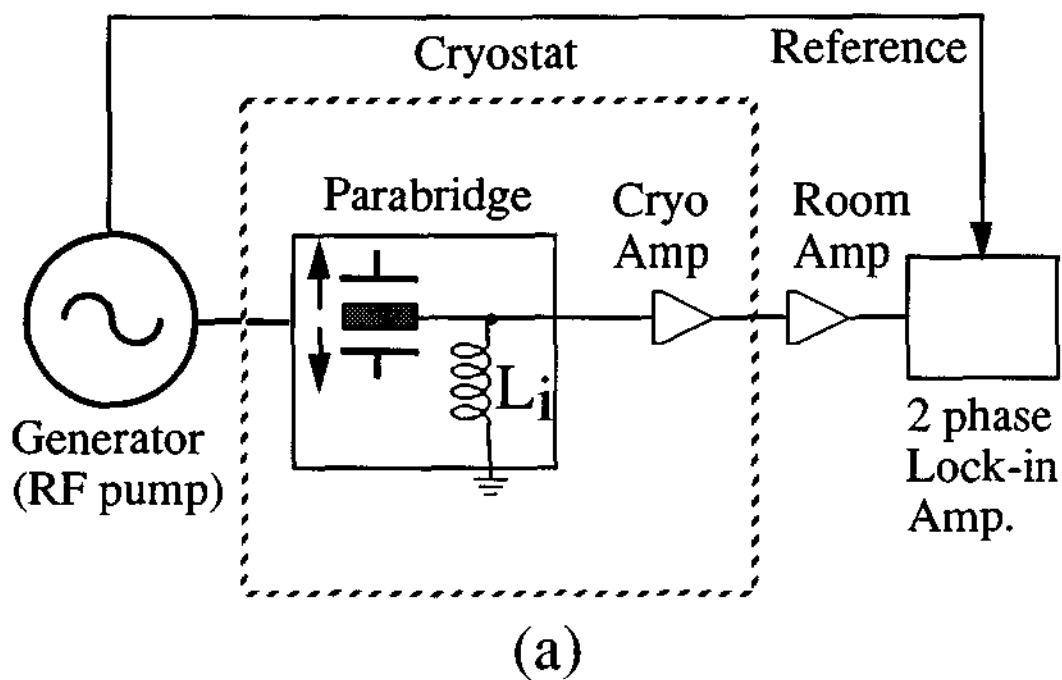


Fig. 4.1 - Parabridge Resonances. (a) The equipment diagram used to take bridge imbalance data, and (b) data showing the two electrical resonances of the bridge.

The transducer can achieve its best performance when the bridge is balanced. Balancing the bridge at the idler frequency impedes the noise generated in the outer loop at this frequency from entering the middle branch where the read-out inductor is located. Furthermore, balancing the bridge at the pump frequency minimizes the idler inductor excitation at the pump (generator) frequency, because this excitation can saturate the amplification chain.

In order to balance the bridge *both* at the idler and pump frequencies, the two side branches of the bridge must be fully balanced; this means that they must be balanced resistively, inductively, and capacitively. Because we were only able to balance the bridge resistively and inductively, we could not balance it at more than one frequency. Therefore, we had to make a choice among three possibilities: balancing the bridge at the idler frequency, at the pump frequency, or somewhere in between.

Fig. 4.2 shows the ratio V_{Li} / V_{gen} when the balancing point was chosen some 400 Hz below the inner loop resonant frequency. The dots are derived from measurements, and the solid line from theory. In this particular case, the balancing point was between pump and upper sideband idler. At the balancing point there was still some resistance imbalance due to the difficulty to visual adjustment when varying the FET gate voltage pot. The shape of the balancing achieved as a function of frequency was in agreement with a 4.2 % residual capacitance imbalance. The worst imbalance in the vicinity of the operation region corresponded to ratio V_{Li} / V_{gen} of 0.025. This ratio divided by 11, which was how many times the voltage across one of the capacitors (V_{cap}) was bigger than the generator voltage (V_{gen}), gave the maximum imbalance ($I_{mb} = V_{Li} / V_{cap}$), three parts in a thousand. From this maximum imbalance, we would expect a noise leakage from the outer loop to the read-out inductor smaller than three parts in a thousand at any frequency in the neighborhood of

the balancing point. On other hand, the best (minimum) measured imbalance at the balancing point, derived from other set of data, was 12 ppm.

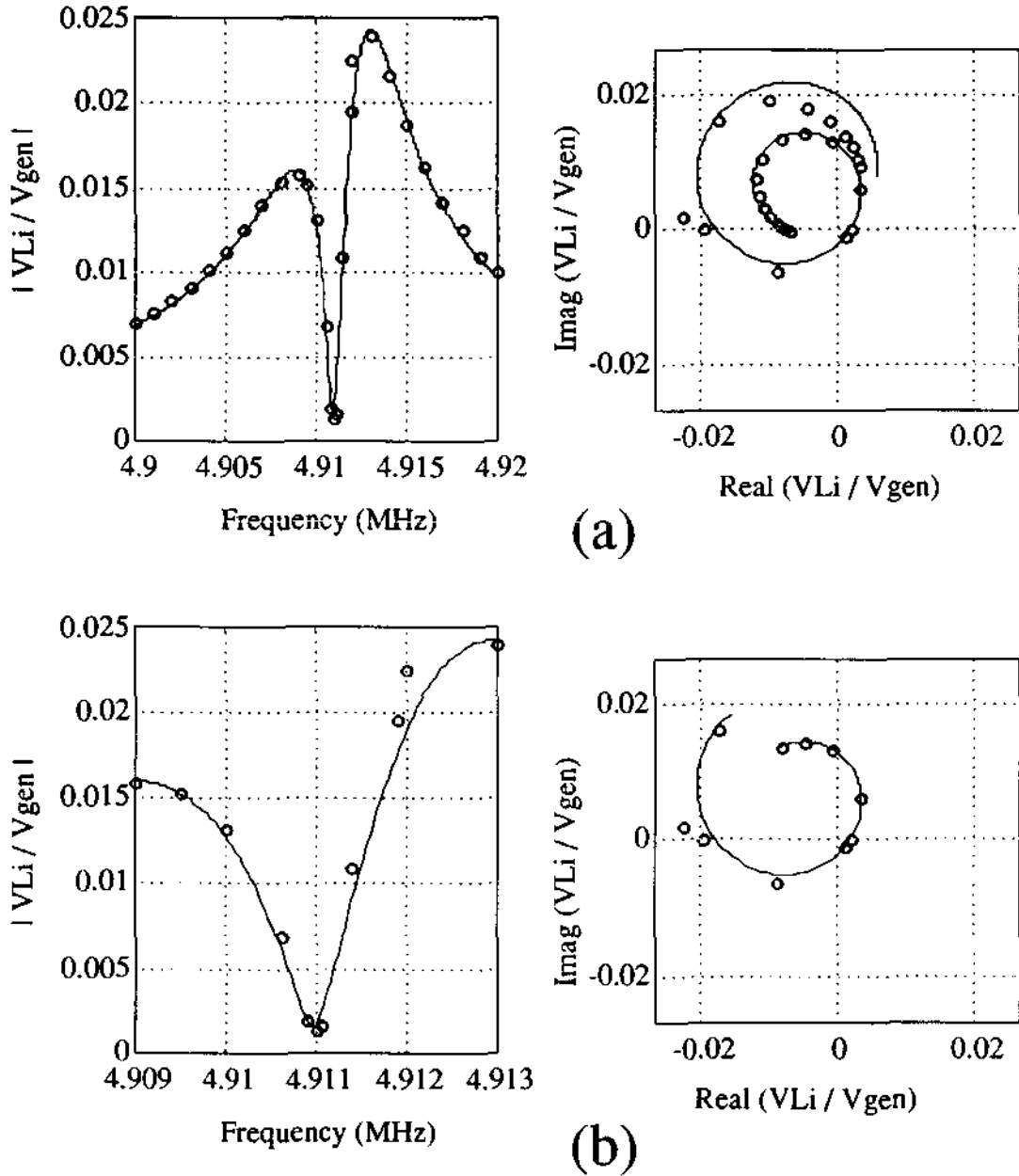


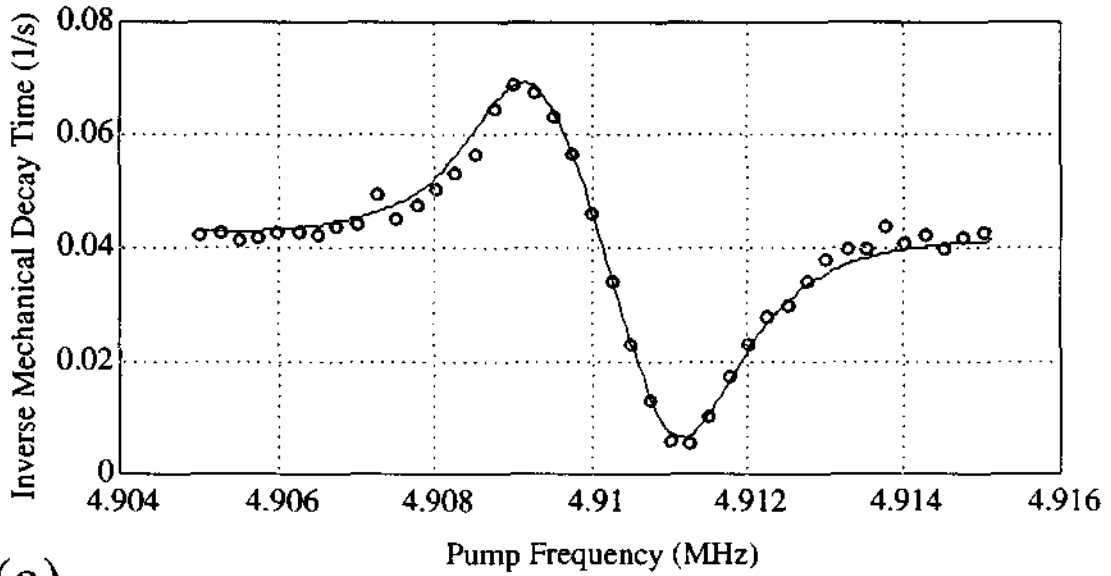
Fig. 4.2 - Balancing point inside the inner loop resonance. a) The response, for the arrangement of Figure 4.1, when the bridge had good tune and balance. b) The same data with an expanded scale.

b) Verification of the Parametric Feedback

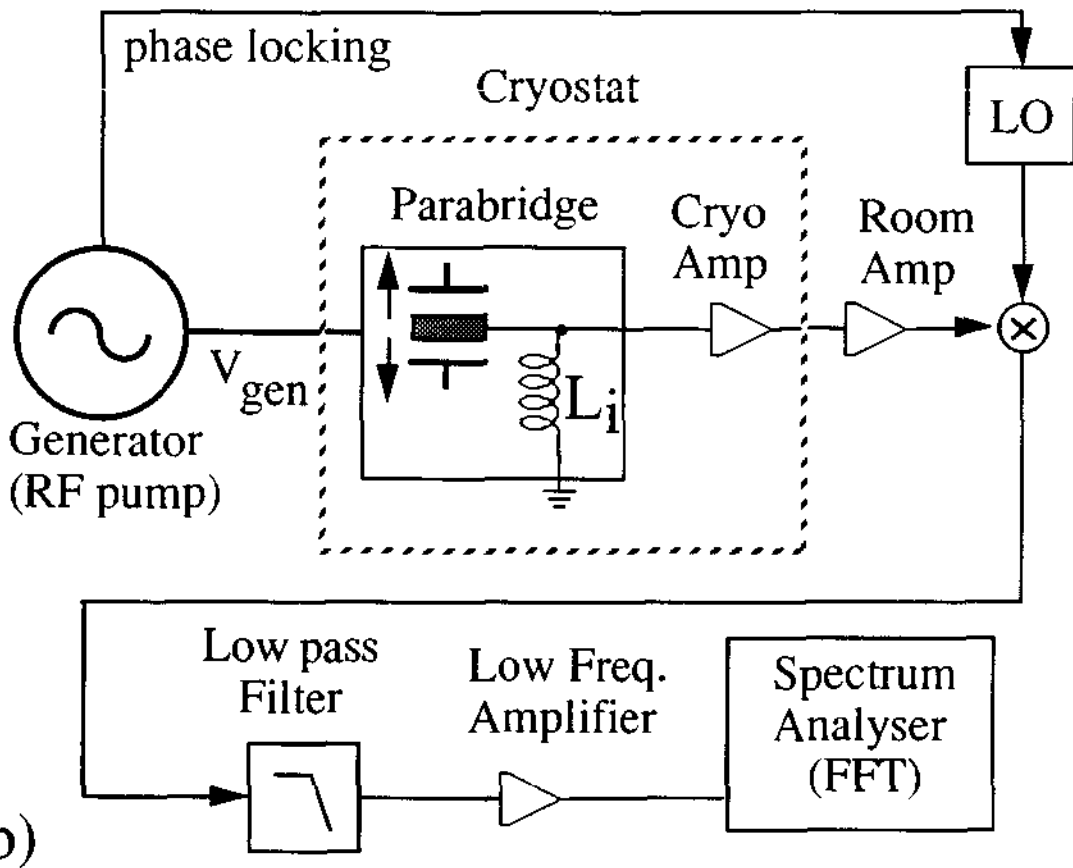
The inverse mechanical decay time was measured for various conditions of pump voltage and frequency. We analyzed these results with a modified equation previously derived for a similar case, and from them we calculated the strength of the coupling this transducer was able to achieve.

One of the characteristics of a parametric transducer is its ability to convert pump energy into energy of an electrical signal with frequency equal to the pump plus or minus the mechanical frequency, and that carries the information of the mechanical oscillator motion. This phenomenon of power transfer from one frequency to another is called the parametric effect. Although it was first discussed in 1831 by Faraday and has been studied by him and other eminent physicists such as Melde and Lord Rayleigh,³ it was not before the middle of the 1950's that Manley and Rowe derived the relations governing the parametric feedback.⁴ Here we report experimental results that show how this parametric feedback manifests in our transducer. We vary both the pump voltage and frequency and compare the results with theory (Eq. 2.10).

Fig. 4.3a shows the inverse mechanical decay time for a pump signal of 350 mVrms across a single side of the three-plate capacitor (V_{cap}) when this pump signal varies in frequency about the inner loop resonance, and Fig. 4.3b presents the equipment diagram used to measure this data. The Q_{ilr} was 2.2 k, implying a bandwidth of about 2.3 kHz. Therefore, both sidebands had to be considered. For pump frequencies below (above) the inner loop resonance, the mechanical loaded Q assumed values smaller (bigger) than the unloaded Q . The equality of the two Q s was only possible exactly at the inner loop resonant frequency. The solid line is given by



(a)



(b)

Fig. 4.3 - Parabridge damping and anti-damping. (a) Inverse mechanical decay time as function of pump frequency, and (b) equipment diagram used to measure it.

the expression above, and the dots are measured values taken with a 9000 series HP computer connected to a 3561A HP dynamic signal analyzer. This case corresponds to: $V_{\text{cap}} = 350 \text{ mVrms}$, $Q_m = 138 \text{ k}$, $Q_{\text{ilr}} = 2.2 \text{ k}$, $Q_{\text{olr}} = 600$, $f_m = 929.14 \text{ Hz}$, $f_{\text{ilr}} = 4.910100 \text{ MHz}$, and $f_{\text{olr}} = 4.911400 \text{ MHz}$. The fitting parameters were V_{cap} and f_{olr} , but V_{cap} was in the expected range given by equations 2.4 and 2.5.

Fig. 4.4a shows similar curves, now for different voltages across the capacitor, from highest to lowest: 291 mVrms, 206 mVrms, and 130 mVrms. Again the dots are measurements (there are 201 of them for each curve) and the solid line theory. The case here is for: $Q_m = 133 \text{ k}$, $Q_{\text{ilr}} = 2.1 \text{ k}$, $Q_{\text{olr}} = 651$, $f_m = 929.14 \text{ Hz}$, $f_{\text{ilr}} = 4.911350 \text{ MHz}$, and $f_{\text{olr}} = 4.913100 \text{ MHz}$. Again the fitting parameters were V_{cap} and f_{olr} (and V_{cap} was in the expected range given by equations 2.4 and 2.5).

We notice that the maximum and minimum always occur at the same frequencies above and below the inner loop resonance, which are, for the present electrical Q , about $\pm 1 \text{ kHz}$ from it. They become close to $\pm 929 \text{ Hz}$ only for very high Q s. The predicted effect of higher Q s can be seen from the theoretical curves in Fig.4.4b. In the extreme case (very high Q s) there would be only two very narrow peaks, at the sum and difference frequencies. At any other pump frequency the coupling would be essentially zero. The parameters for these cases are: $V_{\text{cap}} = 5 \text{ Vrms}$, $Q_m = 138 \text{ k}$, $Q_{\text{olr}} = 600$, $f_m = 930 \text{ Hz}$, and $f_{\text{olr}} = f_{\text{ilr}} - f_m$.

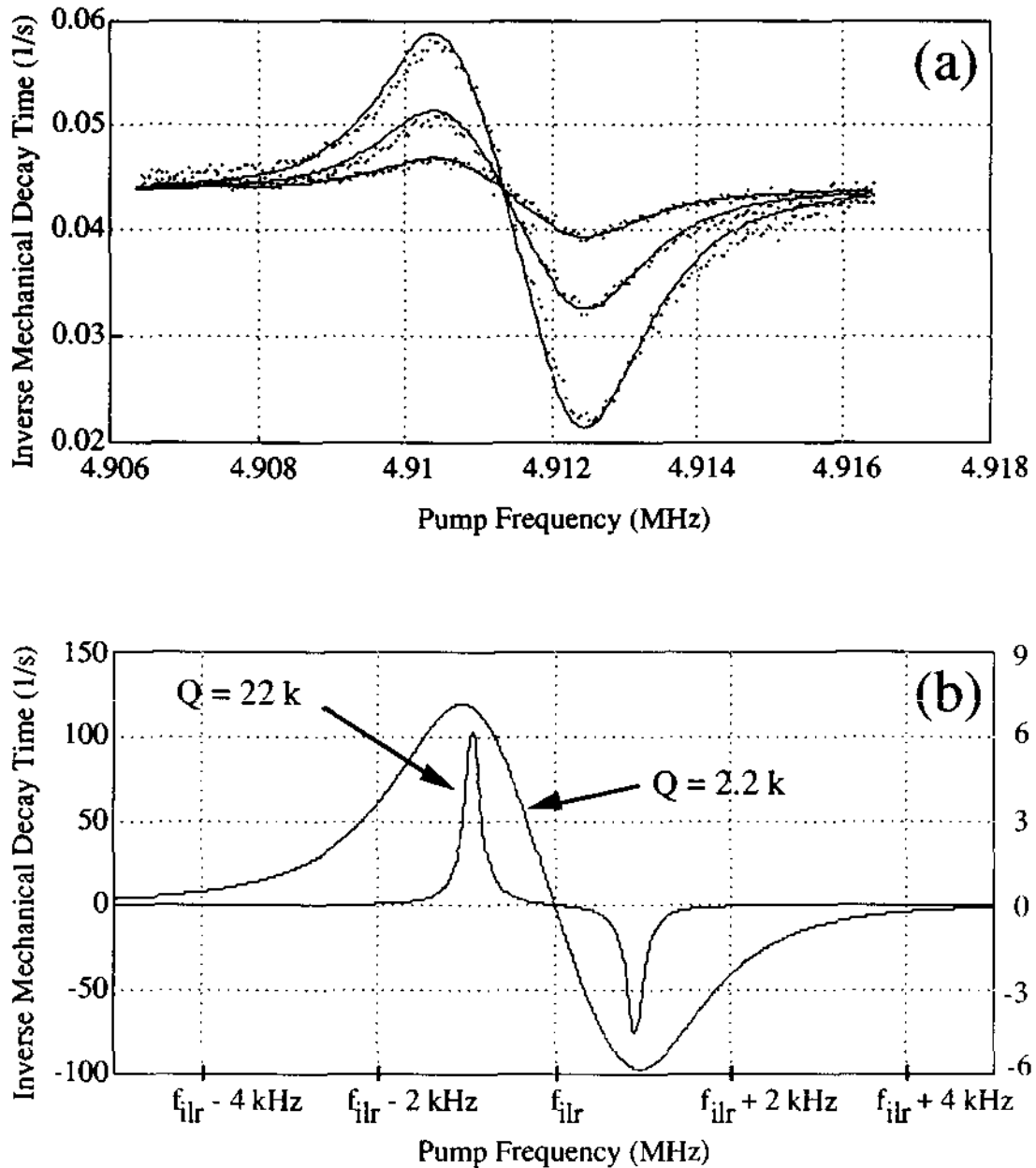


Fig. 4.4 - Parabridge damping and anti-damping as a function of pump voltage and Q_{ilr} . (a) Inverse mechanical decay time as a function of the pump frequency about the inner loop resonance for three different values of the pump voltage. (b) Comparison between two theoretical predictions of Equation 2.10 for different Q_{ilr} s. One is the measured value for the present experiment, and the other a value 10 times bigger. The vertical scale on the right side corresponds to the lower $Q (=2.2$ k).

It is interesting to observe the case when the voltage across the capacitor plates is high and we try to pump at frequencies above the inner loop resonance. The system becomes unstable and the loaded mechanical Q goes to negative values, meaning the presence of parametric oscillations. Fig.4.5 shows this behavior. Negative decay times were difficult to measure, and except for a few close to the inner loop resonance (small values of negative decay time), they were not measured (the oscillations were growing too fast and saturating the amplifiers).

We did not move the outer loop resonance from its position as recorded in Fig. 4.3; therefore, the only fitting parameter was V_{cap} , which closely agreed with equations 2.4 and 2.5. All the Q s were the same ones supposed in Fig. 4.3. The only difference (besides V_{cap}) was $f_{ilr} = 4.911533$ MHz. Notice the value of maximum inverse of decay time (measured when there was 8.94 V_{rms} across the capacitor): 22.2 sec⁻¹, corresponding to a loaded Q of 263. This value is the result of a coupling (β) of 0.054, which is the highest measured so far for this class of transducers. Actually we could have pumped even harder by using a 3325A HP synthesizer instead of a VDS-15 synthesizer. We would have reached a $\beta \sim 1$, but at the expense of degrading the phase noise from -144 dBc / Hz presented by the VDS-15 to about 115-120 dBc / Hz.

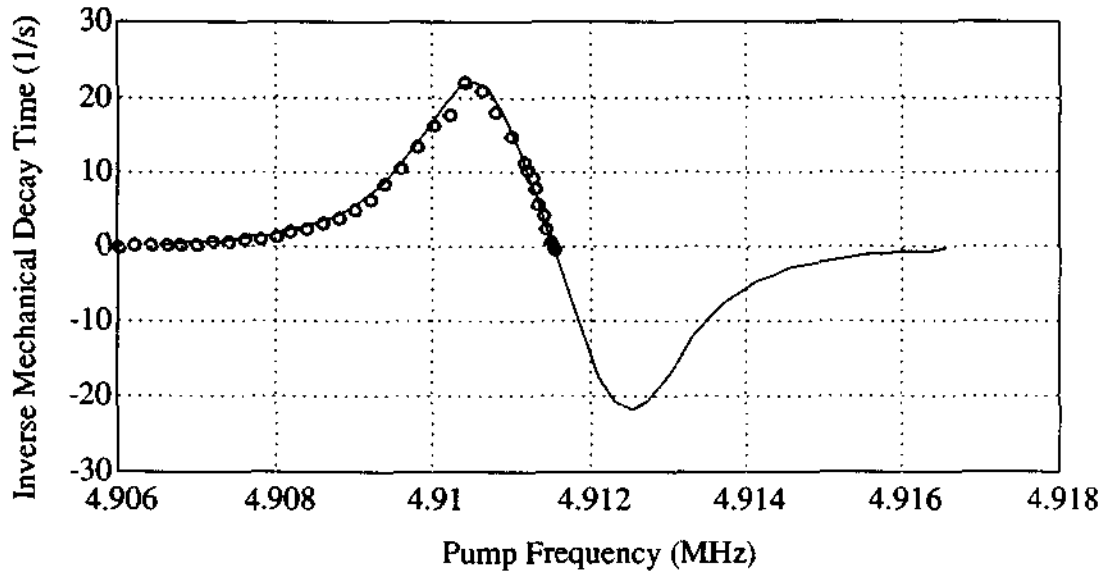


Fig. 4.5 - Inverse mechanical decay time using high coupling.

All the measurements in Figs. 4.3, 4.4 and 4.5 were taken with the outer loop resonance in the region of measurement (4.906 to 4.944 MHz), causing a strong enhancement of pump signal across the capacitor plates. We could not do the same at 5 MHz. Fig. 4.6 shows the strength of the parametric effect around 5 Mhz. The dots are measurements and the Equation 2.10 is the solid curve. We used a VDS-15 at the same level of output pumping as in Fig. 4.5 to take this measurement, and we kept the outer loop resonance at that same frequency. A much smaller β was achieved in this case: 7.7×10^{-5} , because the voltage across the capacitor (V_{cap}) was only 337 mVrms.

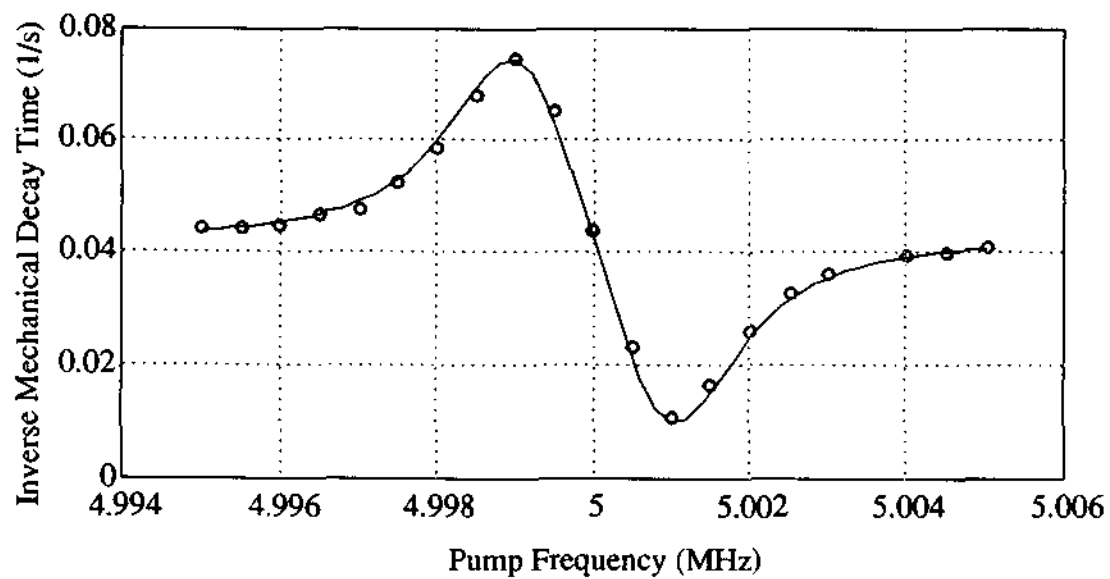


Fig. 4.6 - Inverse mechanical decay time as a function of the pump frequency about 5 MHz.

c) Sensitivity and Noise

We measured the transducer response to a calibrated force, using a capacitor plate facing the transducer body. From these measurements we calculated the total transducer gain (including amplifier chain) and the transducer sensitivity. Finally, we analyzed the noise presented in the system and tried to determine its various origins.

Calibration of ultra-high sensitive transducers such as the ones designed for gravitational wave antennas is not an easy task.^{5, 6} The experimental setup must isolate the transducer from laboratory vibrations as much as possible; otherwise, a very sensitive transducer plus amplification chain may be over excited and not allow any sort of measurement. The calibration itself is another significant problem because it must be done in a manner that minimizes the degradation of the transducer performance. Fortunately, because we constructed the cryostat with high vibration isolation characteristics, and because we simplified considerably the calibration setup, we were able not only to measure a high sensitivity for this transducer, but also to observe the transducer excitation due almost exclusively to the mechanical Langevin forces from the Brownian motion.

The calibrating capacitor was composed of an aluminum disc facing an aluminum flange to which the transducer was rigidly bolted. We carefully measured the calibrating capacitor gap at room temperature. We found a value of 0.023" for this gap at room temperature. At 4.2 K, contraction of the nylon bolts was expected to increase this gap by 5.5 mils; and the differential contraction between the titanium wires, the brass vibration isolation stage, and the aluminum flange rim should have increased the gap by another 34.2 mils.^{7,8} Therefore, the calculated distance between

the disc and flange was 1.45 mm (0.0572") corresponding to a capacitance of 28.2 pF, and the uncertainty in this value was less than 5%. The transducer was set into oscillation by driving a voltage difference between aluminum disc and flange. There was a leakage of mechanical energy from the disc oscillations to the transducer, but it was very small compared to the energy transferred through the electric coupling. Taking into account the equation of motion of the vibration isolation stages between the aluminum disc and transducer, we calculated that the amplitude of oscillations on the transducer due to mechanical forces was more than four orders of magnitude smaller than the amplitude caused by the electrical force.

To avoid any problems of miscalibrations caused by a direct pickup of the calibrating signal coming from the wave generator, we chose to excite the calibrating capacitor with an electrical signal at half the mechanical resonant frequency. Thus any direct pickup reaching the spectrum analyzer (FFT) would be at half frequency. The second harmonic produced by the wave generator was 84 dB smaller than the fundamental, and because we did not bias the calibrating capacitor with any d.c. voltage, we did not need to worry about this harmonic.

During calibration, the equipment configuration was similar to the one in Fig. 4.3b with the addition of a generator for calibration signals and electrical coaxial cables connecting it to the calibrating capacitor. The rms steady state response on the FFT screen was recorded, and the equivalent voltage divided by the rms amplitude calculated by Equation 2.19. This result was the total transducer-amplification gain in units of Volts / meter. Table 4.1 shows two cases studied:

- the VDS-15, a very low noise synthesizer⁹ (-144 dBc @ single sideband 930 Hz from carrier), in its maximum pump level (813 mV_{rms}) and at the frequency of

- 4.910604 MHz, in order to have the outer loop resonance strongly enhancing the voltage across the bridge capacitor; and
- the extremely low noise fixed frequency crystal oscillator from Austron (-182 dBc @ single sideband 930 Hz from carrier) sending a 490 mV_{rms} pump signal at 5 MHz to the bridge transformer, but with very little enhancement in the outer loop (26.5 times smaller than in the previous case) due to the impossibility of moving the outer loop resonance above 4.98 MHz.

| RF generator | VDS-15 | Crystal Osc. |
|---|------------------------|------------------------|
| phase noise @ ssb 929 Hz away from carrier | - 144 dBc | - 182 dBc |
| generator voltage | 813 mV _{rms} | 490 mV _{rms} |
| pump frequency | 4,910,604 Hz | 5,000,000 Hz |
| inner loop resonant frequency | 4,911,533 Hz | 5,000,015 Hz |
| outer loop resonant frequency | 4,911,400 Hz | 4,911,400 Hz |
| loaded mechanical quality factor | 263 | 138 k |
| electromechanical coupling | 0.054 | 2.8×10^{-5} |
| electric field strength | 1.79×10^5 V/m | 4.07×10^3 V/m |
| amplification used | 100 | 53.3×100 |
| transducer-amplifier total gain @ FFT input | 2.73×10^9 V/m | 3.46×10^9 V/m |

Table 4.1 - Transducer-amplifier total gain at the spectrum analyzer input for two different pump generators. Less room temperature amplification was used in the VDS-15 case to avoid saturation of the low frequency amplifier chain.

From the results shown in Table 4.1, we notice that if we divide the transducer-amplifier total gain at FFT input by the amplification used and by the electric field strength across the transducer capacitor, we obtain approximately the

same dimensionless result: 156. This number is a measure of transducer quality and is independent of the voltage across the transducer capacitor. We named this dimensionless number *transducer quality figure*, and it can be easily shown to be approximately equal to $(\sqrt{2}/4) Q_{ilr} (L_i / L_{il})$, where Q_{ilr} is the inner loop quality factor and (L_i / L_{il}) is the ratio between the read-out (or idler) inductor and the total inductance in the inner loop. The factor four in the denominator comes from the product of two one-halves, one from the parametric mixing between the mechanical and pump signals and the other from the demodulation mixing. The precise expression of the voltage at output of the mixer is given by Eq. 2.14.

For an inner loop quality factor of 2.2 k, the mixer output is strongly dependent on the phase difference between local oscillator and pump signal, and care should be taken to adjust this phase in order to maximize the transducer sensitivity. The optimum phase for each relative position between the pump frequency and the inner loop resonance can be found experimentally by slowly varying the phase of the local oscillator relative to the pump oscillator while continually exciting the transducer. The relative phase that obtains the maximum response on the FFT analyzer is the ideal one.

After calibrating the transducer we measured its response to pure noise sources and compared the results with a modified version of the Bocko-Johnson¹⁰ noise model for parametric transducers. The various predicted noise contributions are given by equations 2.23, 2.24, 2.25, and 2.26. Because the cryogenic amplifier was an excellent current amplifier¹¹ ($G_c \sim 2$ k) and a poor voltage amplifier ($G_v \sim 1$), the only noise in S_{LF} to be considered is the voltage noise; and in $S_{RFac}(\omega_+)$ and $S_{RFac}(\omega_-)$, we can neglect any RF current noise other than the cryoamplifier current noise.

Another noise present in the output of the bridge is the "signal" due to the transducer resonator response to the Langevin forces, associated with the Brownian motion, and the transducer response to laboratory vibrations not filtered by the isolation system. To these noise sources we can associate two displacement spectral densities for the resonator motion S_{Lan} and S_{vib} , respectively, in m^2 / Hz . The expression for S_{Lan} (Brownian) can be easily obtained by multiplying the mechanical resistance "force" spectrum density due to the thermal noise by the square of the Fourier transform of the mechanical resonator transfer function.^{12,13} The square root of this result is shown in Eq. 2.21.

Now we can add the total electrical noise spectral density to this mechanical spectral density. The way to do this is to divide the total voltage spectral density (S_V) by the square of the product between the "transducer quality figure" and the electric field strength, or equivalently, to multiply that voltage spectral density by the square of the ratio of the total amplification gain between the bridge output and the FFT to the transducer-amplifier total gain. The square root of this result is shown in Fig. 4.7 (solid line) compared with the total measured noise at the FFT divided by the transducer-amplifier total gain (stepped curve). In this case the pump frequency was almost on the top of the inner loop resonance, so the loaded mechanical Q was equal to the unloaded one, 138 k. The agreement between theory and measurement is very good, making us believe that the transducer response was due mainly to the Brownian motion of the mechanical resonator when not submitted to calibrating pulses.

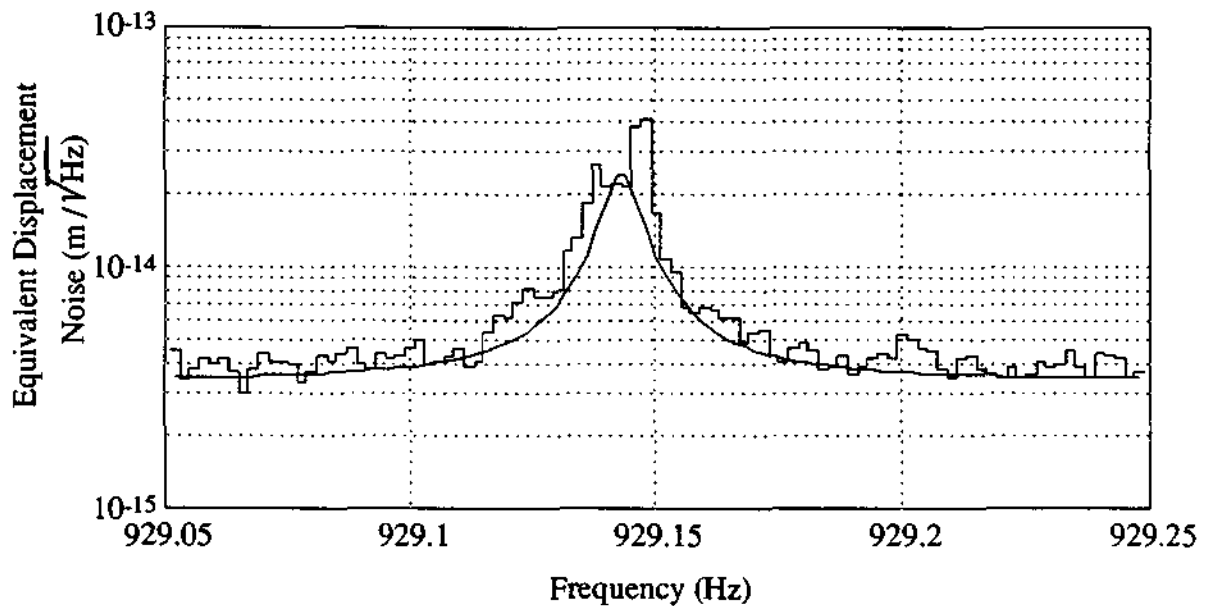


Fig. 4.7 - Equivalent displacement noise of the transducer using the 5 Mhz crystal oscillator.

We were puzzled by the presence of the two excess peaks on each side of the Brownian peak. Fortunately, we had the signal that was going to the FFT input also connected to the input of a PAR 129 low frequency lock-in amplifier with a local oscillator at the mechanical frequency. The output of this lock-in amplifier was sampled every 50 ms and converted to a digital signal that was recorded by a VAX station 3500, a procedure always used to record data from the LSU gravitational wave detector. We had more than 10 hours recorded in this way, allowing us to analyze the data taken at the same time as the one for FFT spectrum and at different times. We used a computer software to restore the spectrum as it was before entering the lock-in and being "folded" by the local oscillator. Except by the effect produced by the lock-in output filters the spectrum was identical to the three-hour integration using the FFT machine, and we could observe that the peak on the left was coming and going in a random way, consistent with statistical fluctuations. These extra peaks are probably excess mechanical noise over the Brownian due either to vibrations that managed to

pass through the isolation system or to vibrations produced there by some up conversion process, which transfers energy from very low frequency oscillations, poorly isolated by the system, to the mechanical resonator mode.

In Fig. 4.7 the total RF amplifier chain voltage noise at the input of the cryogenic amplifier, previously measured to be $1.45 \times 10^{-9} \text{ V} / \sqrt{\text{Hz}}$ for a single sideband, was the dominant source of wideband noise in this case, accounting for 87% of the total wideband power spectrum density, followed by the Johnson noise generated in the inner loop resistance (12.7%). Phase noise here was completely negligible, as was the effect of the cryoamplifier current noise. The low frequency amplification noise referred to the input of the cryoamplifier was responsible for most of the remaining 0.4% wideband noise. Considering the Brownian as a "signal," the transducer reached an equivalent displacement noise of $4 \times 10^{-15} \text{ m} / \sqrt{\text{Hz}}$, with a systematic error of less than 10%, in the case that we were using the crystal oscillator.

Fig. 4.8 shows the equivalent displacement noise using the VDS-15 frequency synthesizer. As in the previous figure, the smooth curve corresponds to the theoretical model, and the stepped curve to the measured data. Here, the phase noise was believed to be the dominant one, with 84% of the total power spectrum density. The low frequency amplification chain voltage noise at the input of the cryogenic amplifier, previously measured to be $7.5 \times 10^{-9} \text{ V} / \sqrt{\text{Hz}}$ for this case, was responsible for 14.5% of the total. Because the phase noise was the most probable major source of noise in this case, and because we could not know the read-out inductor to capacitor ratio of voltages for each sideband, we had to look in the model for an Imb_+ and Imb_- that could reproduce the noise floor observed and the shape of the dip. The values of these imbalance factors that fit with data were 3 and 1.5 parts in a hundred, respectively --

ten times the expected values. There was still some remaining discrepancy between experimental data and the theoretical model. Curiously, the agreement would be almost perfect if we had considered $1.0 \times 10^{-8} \text{ V} / \sqrt{\text{Hz}}$ as the actual low frequency amplification chain voltage noise.

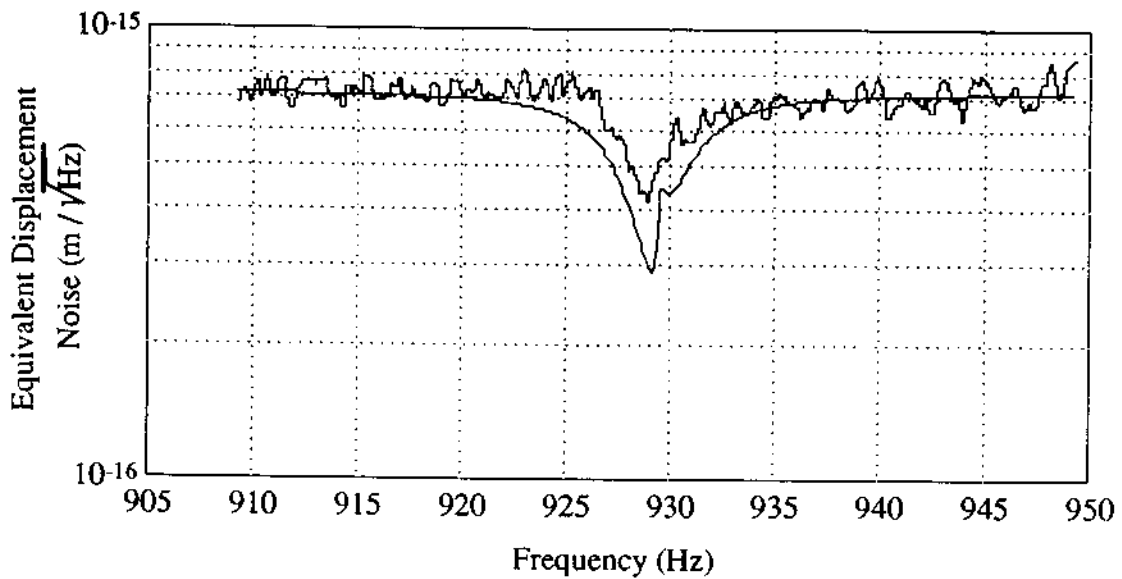


Fig. 4.8 - Equivalent displacement noise of the transducer using a VDS-15 generator.

We do not know yet why the total noise measured was about one order of magnitude higher in voltage than the total noise expected. One of the possibilities we still cannot exclude completely is an extra phase noise leakage due to additional imbalance caused by the presence of low frequency oscillations at the resonator. These low frequency vibrations coming from the laboratory were poorly filtered by the vibration isolation system, which was designed with the purpose of cutting mechanical vibrations higher than 500 Hz. The effect of these low frequency vibrations (<100 Hz) could cause a momentary bridge excess imbalance allowing, in this particular case, ten times more phase noise to leak to the read-out inductor than the leakage expected from measured average imbalances.

In any case, we were able to confirm the interesting noise behavior when the frequency was close to the mechanical resonance. Thanks to the small loaded Q, the Brownian peak was one order of magnitude below the bottom of the dip, so the shape of the wideband noise could be fully appreciated. The dip is a result of the parametric coupling between the electrical and the mechanical modes. In the presence of coupling, the noise at each sideband mixes across the capacitor plates with the pump signal to produce a force acting on the mechanical resonator at its resonant frequency; on the other hand, the resonator subjected to this motion generates a "signal" at each sideband because of the presence of the pump signal across the capacitor. The expression for this "signal" reflected back can be easily derived from the initial noise injected in the circuit. The interesting fact is that this "signal" or "reflected noise" is 180° out of phase with the initial noise if the upper sideband happens to be at the inner loop resonant frequency. In this case, there is a tendency of destructive interference -- exactly what we observed for this synthesizer case when a high beta was used and the upper sideband was set on top of the inner loop resonance. For different relative positions of this sideband, the phase difference is no longer 180° , the minus sideband contributes with in phase "reflected noise," and in some cases even constructive interference could be predicted by the model. This partial reduction of noise about the mechanical resonance allowed the transducer to achieve a measured equivalent displacement noise of $\sim 4 \times 10^{-16} \text{ m} / \sqrt{\text{Hz}}$ (error < 10%) at the bottom of the dip.

C) References

¹ R. Blevins, *Formulas for Natural Frequency and Mode Shape* (Krieger Publishing, Malabar, FL, 1979).

² The new thermo jacket was manufactured by Precision Cryogenics Systems and presented 0.66 l/h and 0.10 l/h boil off rates for liquid helium and nitrogen respectively.

- ³ W. W. Mumford, "Some Notes on the History of Parametric Transducers," *Proceedings of the IRE*, **48**, 848 (1960).
- ⁴ J. M. Manley and h. E. Rowe, "Some General Properties of Nonlinear Elements -- Part I. General Energy Relations," *Proc. IRE*, **44**, 904 (1956).
- ⁵ K. Kuroda, k. Tsubono and H. Hirakawa, "Calibration of Vibration Transducer," *Japanese Journal of Applied Physics*, **23**, L415 (1984).
- ⁶ B.X. Xu, "Calibration of a Resonant Gravity Wave Detector," Tech. Memo. #53, Gravitational Radiation Group, Louisiana State University (Feb. 1989).
- ⁷ R. B. Scott, *Cryogenic Engineering* (D. Van Nostrand, Princeton, NJ, 1959).
- ⁸ D. A. Wigley, *Materials for Low-Temperature Use* (BAS Printers Limited, Over Wallop, Hampshire, 1978).
- ⁹ The VDS-15 is a synthesizer manufactured by Sciteq Electronics, Inc., 8401 Aero Drive, San Diego, CA 92123.
- ¹⁰ M. F. Bocko, W. W. Johnson and V. Iafolla, "A RF Superconductive Electromechanical Transducer for Gravitational Wave Antennae," *IEEE Transactions on Magnetics*, **25**, 1358 (1989).
- ¹¹ M. G. Richards, A. R. Andrews, C. P. Lusher, and J. Schratte, "Cryogenic GaAs FET Amplifiers and their use in NMR Detection," *Review of Scientific Instruments*, **57**, 404 (1986).
- ¹² F. Reif, *Fundamentals of Statistical and Thermal Physics* (McGraw-Hill, New York, 1965).
- ¹³ D. Middleton, *An Introduction to Statistical Communication Theory* (McGraw-Hill, New York, 1960).

CHAPTER 5 - CONCLUSIONS

We designed, constructed, and tested at 4.2 K a capacitive parametric motion transducer made out of superconductive niobium. The experimental results agreed well with the theoretical models, allowing us to determine the most important parameters of this transducer and its best performance using two different low phase noise electrical pump generators. Table 5.1 shows a summary of the transducer fundamental parameters.

| | | | |
|--------------------|---|------------|---------------|
| T | physical temperature | 4.2 | K |
| M | transducer's reduced mass | 0.261 | kg |
| m | resonator's mass | 0.27 | kg |
| f_m | mechanical resonant frequency | 929.143 | Hz |
| f_{itr} | inner loop resonant frequency | 4.9 - 5.2 | MHz |
| f_{otr} | outer loop resonant frequency | 4.9 - 4.98 | MHz |
| Q_m | mechanical quality factor | 138 k | |
| Q_{itr} | inner loop resonance quality factor | 2.2 k | |
| Q_{otr} | outer loop resonance quality factor | 650 | |
| D | capacitor gap | 50 | μm |
| C | capacitance | 1.45 | nF |
| L_{il} | total inner loop inductance | 0.35 | μH |
| L_i | idler (read-out) inductance | 0.075 | μH |
| V_{Li} / V_{cap} | bridge imbalance (best measured) | 12 | ppm |
| β | coupling coefficient (highest measured) | 0.054 | |

Table 5.1. Fundamental parameters of the present parabridge transducer.

From measurements of the inverse mechanical decay time for various conditions of pump voltage and frequency, we were able to calculate the strength of the coupling between the mechanical and electrical modes. The maximum coupling (β) achieved was 0.054. This high coupling, corresponding to an electric field strength across the capacitor plates of 1.79×10^5 V/m, is the highest measured so far for this class of transducers, and it was obtained due to the capability of this transducer to have the two electrical bridge resonant frequencies adjusted on top of each other at the generator frequency.

In agreement with the model, we observed a continuous and smooth variation of the loaded inverse decay time as a function of the relative position of the pump frequency to the inner loop resonance. In agreement with the model, the loaded inverse decay time changed significantly, and symmetrically, from the unloaded value for a pump frequency in the range of ± 5 kHz away from the inner loop resonance. When the pump frequency was exactly at the inner loop resonant frequency, the loaded mechanical Q was identical to the unloaded Q; below (above) this frequency, damping (anti-damping) occurred. In order to correctly explain this result, the theoretical model had to be modified to account for the effect of two idler sidebands, which were present because the inner loop resonance bandwidth was large enough to generate them. According to this modified model, an electrical Q ten times higher than the measured 2.2 k would be enough to suppress the second sideband. Correctly predicted by the model, it was observed that for pump frequencies above the inner loop resonance and high coupling, the mechanical resonator went to parametric oscillation (negative Qs), and at the conditions of maximum damping we observed the mechanical Q to fall from the original 138 k to values as low as 263.

Because we were only able to balance the bridge resistively and inductively but not capacitively, we could not balance it at more than one frequency. This result was experimentally observed and theoretically confirmed. It was observed experimentally by determining the ratio of the read-out inductor voltage to the generator voltage. This ratio, divided by the pump voltage gain between generator and capacitor, found by the inverse decay time measurements, was the imbalance. The model could shape correctly the balancing achieved as a function of frequency (transfer function), indicating a 4.2 % residual capacitance imbalance.

From this imbalance, we would expect, from theory, a noise leakage from the outer loop to the read-out inductor smaller than three parts in a thousand at any frequency in the neighborhood of the balancing point. However, we observed a wideband phase noise contribution ten times higher than expected, corresponding to an imbalance of three parts in a hundred.

Our hypothesis to explain the excess noise is that there was some extra phase noise leakage due to an additional time varying imbalance caused by low frequency motions of the transducer components. The vibration isolation system was designed to filter frequencies close to 929 Hz, but for frequencies below 100 Hz its performance was poor. These low frequency vibrations could cause an additional momentary bridge imbalance, which would lead to a higher phase noise leakage and explain the electrical excess noise observed.

We also measured the transducer's response for continuous mechanical excitation of known amplitudes as well as its response for pure noise sources. From these measurements we calculated the *transducer quality figure* and the transducer equivalent displacement noise for two different pump signal generators. Thanks to a

very effective vibration isolation system built for filtering the mechanical vibrations close to the resonator frequency, we were also able to measure, in one case, the transducer mechanical resonator's Brownian motion.

We found it very important, due to the presence of two idler sidebands, to adjust the phase difference between the pump generator signal and the local oscillator signal carefully in order to maximize the transducer sensitivity. This optimum phase difference could be experimentally found by varying the phase of the local oscillator relative to the pump oscillator slowly while continually exciting the transducer. The optimum phase was the one that would achieve the maximum response on the FFT analyzer.

In one case, when the Brownian noise was negligible and the phase noise was the dominant, we observed a *dip* in the noise spectrum. This dip was found to be a result of a destructive interference between the electrical noise in the circuit and its "reflection" from the mechanical resonator. When the upper idler sideband is on top of the inner loop resonance, the "reflected" noise is 180° out of phase compared to the initial electrical noise, and destructive interference occurs. On the other hand, when the lower idler sideband is on top of the inner loop resonance, and the regime of parametric oscillations has not been reached, the "reflected" noise is in phase with the initial electrical noise, and constructive interference occurs.

We could observe the shape of the total electrical noise for this VDS-15 case because the coupling between the mechanical and electrical modes was high ($\beta=0.054$); one of the sidebands was exactly on top of the inner loop resonance; the loaded Q was very small (263), causing a negligible Brownian noise contribution; and the flat amplifier chain voltage noise was not dominant.

The maximum transducer sensitivity was achieved at the bottom of the dip, corresponding to an equivalent displacement noise of $4 \times 10^{-16} \text{ m} / \sqrt{\text{Hz}}$ at the mechanical resonant frequency. This displacement noise was not better due to the low frequency amplification chain voltage noise limiting the deepness of the dip.

For the other pump generator, an Austron 5 MHz crystal oscillator, phase noise was negligible, and even though the final voltage across the capacitor plates was 44 times smaller than when we used the synthesizer, corresponding to a coupling 2k smaller, the equivalent displacement noise measured was $4 \times 10^{-15} \text{ m} / \sqrt{\text{Hz}}$, only one order of magnitude smaller. This good performance was due to two additional low noise RF amplification stages¹ between the cryogenic amplifier and the low frequency amplification chain, causing a decrease of the total wideband amplification chain voltage noise referred to the input of the cryogenic pre-amplifier.

For this crystal oscillator case, the narrowband noise was dominated by the Langevin forces of the transducer resonator's Brownian motion. Here, the theoretical model correctly predicted the shape and height of the resonator's Brownian peak as well as the wideband noise floor. No fitting parameters were used in this case. Some excess noise was observed on top of the predicted Brownian that may be due to the vibration isolation system's failure either to completely filter the laboratory vibrations around 929 Hz or to avoid upper conversion processes generating mechanical noise, at the mechanical resonator frequency, from lower frequency mechanical oscillations.

With the measured equivalent displacement noise of $4 \times 10^{-16} \text{ m} / \sqrt{\text{Hz}}$ this parametric transducer system can measure accelerations of $1.4 \times 10^{-8} \text{ m} / \text{s}^2$ at 929 Hz in a one Hz bandwidth; if coupled to the LSU gravitational wave antenna, a

2.3×10^3 kg aluminum bar, this transducer resonator of .27 kg would allow strain sensitivities as small as 6×10^{-18} to be measured. Evidently, much improvement is still possible, and it is clear from the experimental results, and from the present models, that the right way to proceed, in order to significantly improve transducer performance, is to increase the electric field strength across the capacitor plates. The model shows that a pump generator of phase noise as small as the Austron oscillator operating in the frequency range of our transducer's outer loop resonance would allow the transducer to reach an equivalent displacement noise of $2 \times 10^{-17} \text{ m} / \sqrt{\text{Hz}}$ as long as $50 \text{ V}_{\text{peak}}$ were achieved across the capacitor plates, a very easy task for a $5 \text{ V}_{\text{peak}}$ generator. This improved sensitivity corresponds to a gravitational wave strain detectability of approximately 3×10^{-19} . Notice that we would still be using the same amplification chain employed in the set of experiments with the crystal oscillator. Because this amplification chain would continue to be the major source of noise, it is apparent that additional improvement would occur with the use of a lower noise amplification chain, one that would include, for example, a DC SQUID.

¹ An Anzac AM-107 amplifier of 1.4 dB noise figure and 11.1 dB gain, plus an Aercom AT 1601 amplifier of 23.4 dB gain and 1.81 dB measured noise figure.

APPENDIX A

High Purity Vanadium Mechanical Quality Factor

Introduction

In the physics field of very weak force measurement such as gravitational radiation detection it is crucial to use very low loss materials. For that purpose acoustic losses of many pure metals and alloys have already been investigated.^{1,2,3,4} Here we present some results for Vanadium because of its desirable superconducting properties and commercial availability.

The Sample

Vanadium belongs to the Niobium family. Some properties of Vanadium are: superconductivity below 5.43 K,⁵ 4.6 km/sec. speed of sound (35% higher than the speed of sound in Niobium); density of 5.96 g/cm³; body-centered cubic crystalline structure at room temperature; and melting point of 1890°C. The recrystallization temperature⁶ is 700-900°C, slightly lower than that of Niobium.

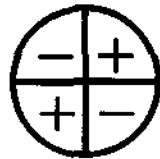
The Vanadium piece tested was a five-inch disc 0.2" thick purchased from Teledyne Wah Chang Albany. The chemical composition for that particular piece is in ppm: Al (290), B(3), C(<30), Cr(<20), Fe(100), H(<5), Hf(<100), Mo(150), N(31), Nb(<250), Ni(<20), O(310), P(<30), S(<20), Si(240), Ta(<300), Ti(<50), U(<2), Zr(180). It was annealed for two hours at 1066°C and 2×10^{-5} Torr (standard annealing for Nb in Wah Chang).

Suspension and Pick-up

The disc was suspended by a .025" thick 5056 Al wire glued with Araldite inside a .028" diameter hole made through the center of disc. The aluminum wire was 12.5" long. The oscillation amplitude for the fundamental modes of the disc was sensed by a small piezo-electric crystal (PZT), which was also glued with Araldite very close to the center of the disc. The electrical connections were made with a very fine wire to avoid loading down the mechanical Q of the disc.

Results

Figures A1 and A2 show the results at room temperature (~294 K), liquid nitrogen temperature (77.4 K), and liquid helium temperature (4.2 K) for the five modes investigated. There are two almost degenerate frequencies for the two nodal diameter mode below



one at 1507 Hz and another at 1521 Hz. The node pattern for the three nodal diameter mode, which is at 3502 Hz, is



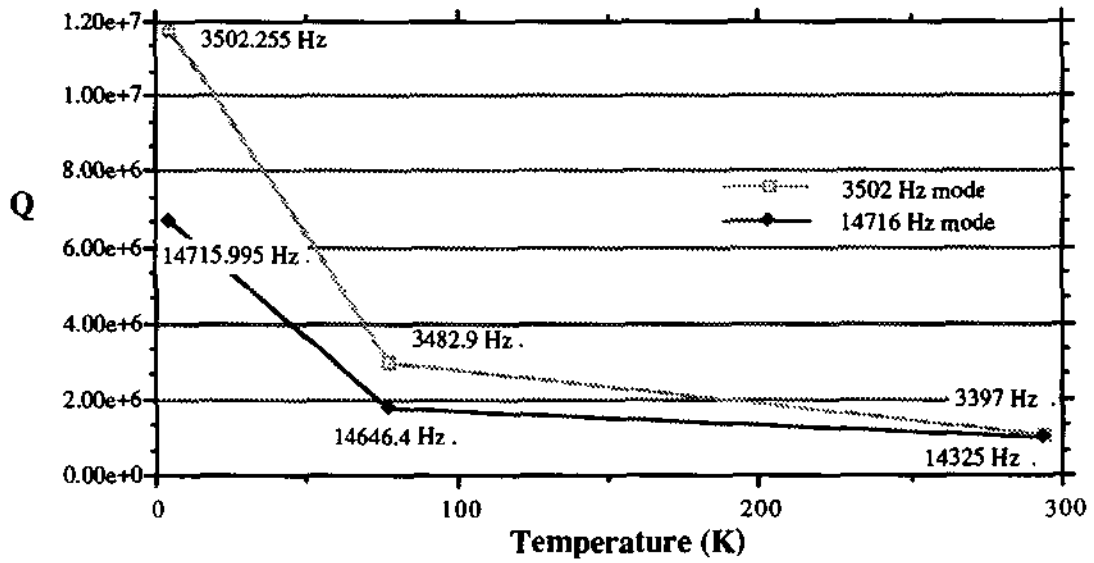


Fig. A1 - Quality factors for the 3502 Hz and 14716 Hz modes.

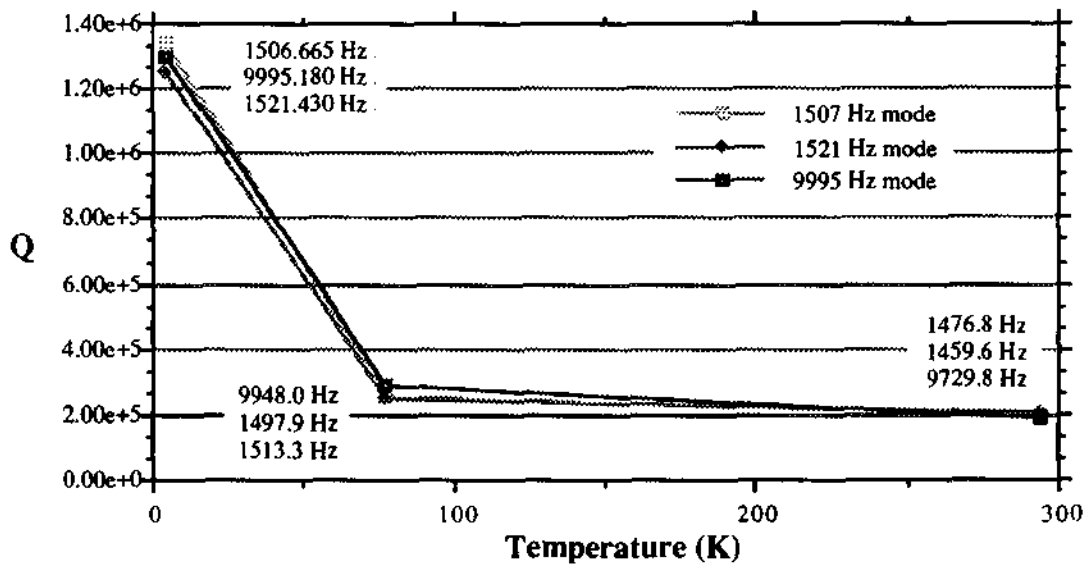


Fig. A2 - Quality factors for the 1507 Hz, 1521 Hz, and 9995 Hz modes.

All the modes presented a maximum frequency at the transition temperature. The highest Q , 12.4×10^6 , was achieved by the 3502 Hz mode around the Vanadium transition temperature. This same mode presented a $Q = 11.8 \times 10^6$ at 4.2 K. Figure A3 shows the mechanical figure of merit (Q) around the transition temperature. The numbers one to seven represent the sample at different temperatures starting at 4.2 K (number one) and going up. Number four is the measurement for the disc at the transition temperature.

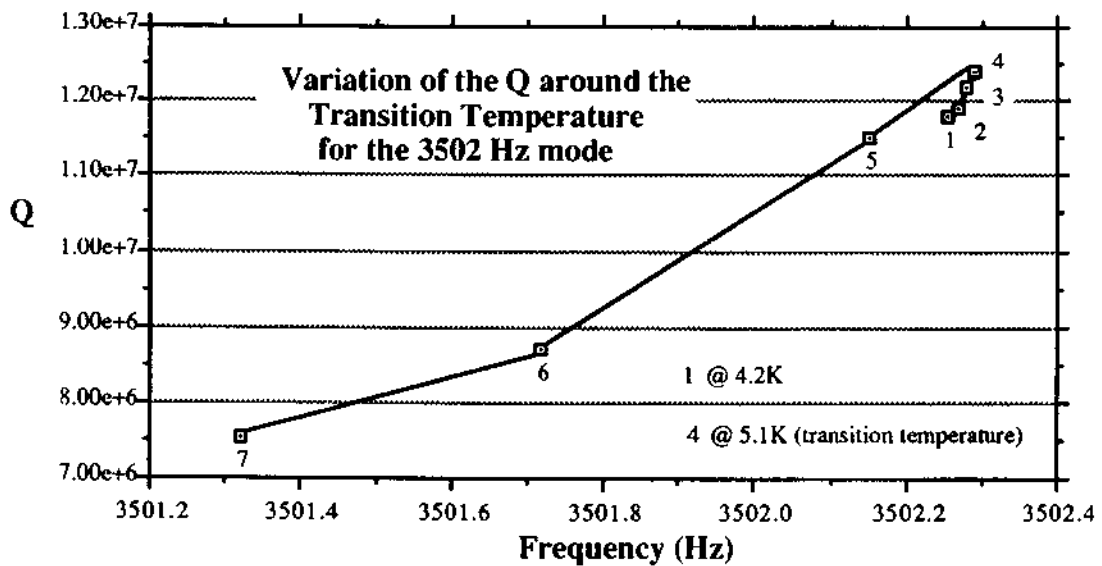


Fig. A3 - Variation of quality factor around the transition temperature for the 3502 Hz mode.

The sample had two more runs down to liquid nitrogen temperature and one to liquid helium temperature; all Q 's were reproducible.

References

- 1 "Quality Factor of Vibration of Aluminum Alloy Disks," T. Suzuki, K. Tsubono and H. Hirakawa, *Phys. Lett.*, **67A**, 2 (1978).
- 2 *Study of Internal Friction in Aluminum-Magnesium Alloys*, James Randolph Marsden, Ph.D. Thesis, University of Rochester, 1984.
- 3 *Low Temperature Internal Friction in Niobium*, John Ferreirinho, Ph.D. Thesis, University of Western Australia, 1986.
- 4 "Cryogenic Acoustic Loss of Molybdenum," Norbert Solomonson and A.G. Mann, *Cryogenics*, **27**, 588 (1987).
- 5 "Magnetic Properties of Superconducting Vanadium," S.T. Sekula and R.H. Kernohan, *Phys. Rev.*, **B5**, 904 (1972).
- 6 "Vanadium," H.E. Dunn and D.L. Edlund, In: *Rare Metals Handbook*, Ed. Clifford A. Hampel, Reinhold Publishing, London, p. 629-52, 1961.

APPENDIX B

Technical Memoranda Written for the Experimental Gravitation Group

Tech. Memo. # 44 - "Computational Model for the LSU GRD Seismic Isolator Stacks,"
February 1986.

Tech. Memo. # 46 - "Intermediate H-Mass Density Measurements," May 1987.

Tech. Memo. # 48 - "Contact Between Solid Metal Surfaces - Up Conversion and
Energy Loss," August 1987.

Tech. Memo. # 49 - "Coincidence Analysis between the LSU, Stanford, Rome, and
Guangzhou Bar Detectors," August 1987.

Tech. Memo. # 52 - "High Purity Vanadium Mechanical Quality Factor," December
1988.

Tech. Memo. # 58 - "Where Should We Point our Bar Antennas," November 1989.

VITA

Odylio Denys de Aguiar was born on December 27, 1953 in Rio de Janeiro, Brazil, to Gilda Denys and Gabriel de Aguiar. He attended Colégio Militar do Rio de Janeiro and Curso Bahiense high schools, both in Rio.

He attended the Instituto Tecnológico de Aeronáutica, in São José dos Campos, São Paulo state, Brazil, from 1973 to 1978, where he earned a Bachelor of Science degree in Electronic Engineering.

In 1979 he began graduate studies in the Instituto Nacional de Pesquisas Espaciais, in São José dos Campos, where he worked in gamma ray astronomy under Prof. Daniel J. R. Nordemann, receiving his Master's degree in Space Physics in 1983. A year later he started his doctoral program in relativity at Centro Brasileiro de Pesquisas Físicas, in Rio de Janeiro, continuing this program at Louisiana State University.

At LSU, he began research in gravitational wave detection in the spring of 1985 under Prof. William O. Hamilton and Prof. Warren W. Johnson, successively. He expects to complete his Doctor of Philosophy degree in December 1990.

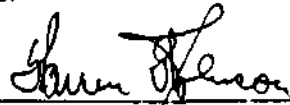
DOCTORAL EXAMINATION AND DISSERTATION REPORT

Candidate: Odylio Denys de Aguiar

Major Field: Physics

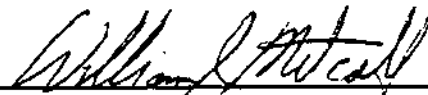
Title of Dissertation: Parametric Motion Transducer for Gravitational Wave Detectors

Approved:


Major Professor and Chairman

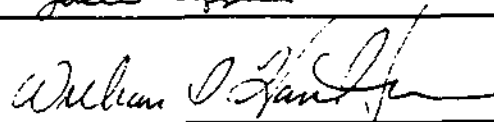
Dean of the Graduate School

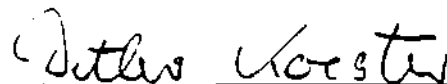
EXAMINING COMMITTEE:











Date of Examination:

November 27, 1990



AUTORIZAÇÃO PARA PUBLICAÇÃO

| | | | | | |
|---|---|------------------------------------|--|---|------------------------------|
| TÍTULO | | | | | |
| PARAMETRIC MOTION TRANSDUCER FOR GRAVITATIONAL WAVE DETECTORS | | | | | |
| AUTOR | | | | | |
| Odylio Denys de Aguiar | | | | | |
| TRADUTOR | | | | | |
| | | | | | |
| EDITOR | | | | | |
| Faculty of the Louisiana State University and Agricultural and Mechanical College | | | | | |
| ORIGEM | PROJETO | SÉRIE | Nº DE PÁGINAS | Nº DE FOTOS | Nº DE MAPAS |
| DAS | ASTRO | | 111 | - | - |
| TIPO | | | | | |
| <input type="checkbox"/> RPQ | <input type="checkbox"/> PRE | <input type="checkbox"/> NTC | <input type="checkbox"/> PRP | <input type="checkbox"/> MAN | <input type="checkbox"/> PUD |
| | | | | <input checked="" type="checkbox"/> TAE | <input type="checkbox"/> — |
| DIVULGAÇÃO | | | | | |
| <input type="checkbox"/> EXTERNA | <input checked="" type="checkbox"/> INTERNA | <input type="checkbox"/> RESERVADA | <input type="checkbox"/> LISTA DE DISTRIBUIÇÃO ANEXA | | |
| PERIÓDICO/EVENTO | | | | | |
| | | | | | |
| CONVÊNIO | | | | | |
| | | | | | |
| AUTORIZAÇÃO PRELIMINAR | | | | | |
| ___/___/___ | | | _____ | | |
| | | | ASSINATURA | | |
| REVISÃO TÉCNICA | | | | | |
| <input type="checkbox"/> SOLICITADA | <input type="checkbox"/> DISPENSADA | | | | |
| | | | _____ | | |
| | | | ASSINATURA | | |
| RECEBIDA ___/___/___ | DEVOLVIDA ___/___/___ | | _____ | | |
| | | | ASSINATURA DO REVISOR | | |
| REVISÃO DE LINGUAGEM | | | | | |
| <input type="checkbox"/> SOLICITADA | <input type="checkbox"/> DISPENSADA | | | | |
| | | | _____ | | |
| | | | ASSINATURA | | |
| Nº _____ | | | | | |
| RECEBIDA ___/___/___ | DEVOLVIDA ___/___/___ | | _____ | | |
| | | | ASSINATURA DO REVISOR | | |
| PROCESSAMENTO/DATILOGRAFIA | | | | | |
| RECEBIDA ___/___/___ | DEVOLVIDA ___/___/___ | | _____ | | |
| | | | ASSINATURA | | |
| REVISÃO TIPOGRÁFICA | | | | | |
| RECEBIDA ___/___/___ | DEVOLVIDA ___/___/___ | | _____ | | |
| | | | ASSINATURA | | |
| AUTORIZAÇÃO FINAL | | | | | |
| 03, 04, 91 | | V.W.J.H. Kirchhoff | | | |
| | | Coordenador-CEA | | ASSINATURA | |
| PALAVRAS-CHAVE | | | | | |
| GRAVITATIONAL WAVES; TRANSDUCERS; GRAVITATIONAL WAVES; SUPERCONDUCTIVITY; | | | | | |
| PARAMETRIC TRANSDUCERS | | | | | |